

Electrical Energy Storage

Bernhard Arndt

Faculty Electrical Engineering

University of Applied Sciences Würzburg-Schweinfurt FHWS

Schweinfurt, Germany

bernhard.arndt@fhws.de

Abstract—In today’s trend to power generation from renewable sources it is necessary to store electricity. An overview is given for the different means from directly storing in the electric or magnetic field and indirect storage by chemical means, like accumulators, and mechanical like flywheel, pumped hydro and compressed air.

An overview about the cost is finally given.

Index Terms—electricity storage, cost of electricity storage, battery technologies

I. INTRODUCTION

This document is a model and instructions for L^AT_EX. Please observe the conference page limits.

II. ELECTRICITY STORAGE

Several storage options are suitable for power supply:

- 1) direct electric storage
- 2) indirect storage
 - a) chemical
 - b) mechanical
 - c) other

The following options apply to direct electric storage:

A. In the electric field -> capacitor, SuperCAP

$$W = \frac{1}{2} C \cdot V^2 \quad (1)$$

Technical specifications of a SuperCAP:

Rated capacitance	3500 F
Nominal voltage	2.5 V
Maximum voltage	2.7 V
Minimum Voltage	0 V (1.0 V for practical purposes)
Resistance HFR	< 0.5 mΩ (1 kHz or 2 s pulse)
ESR	< 1 mΩ (0.01 Hz)
Dimensions (diameter * height)	55 * 220 mm
Volume	0.5 l
Weight	0.65 kg
Maximum current	1000 A (750 A repetitive)
Maximum specific power	3225 W/kg at 500 A
Operating temperature range	-40°C to +60°C
Transport and storage temperature	-40°C to +70°C

Price: approx. 65.- € per unit in 2011

The stored energy is

$$W = C \cdot V^2 = 3,500 \cdot 2.5^2 \text{ Ws} = 0.003 \text{ kWh}$$

This amounts to:

Price per kWh: approx. 300 * 65.- € = 20,000 €/kWh

Weight per kWh: approx. 300 * 0.65 kg = 200 kg/kWh

or: 5 Wh/kg

B. In the magnetic field -> large (superconducting) coils

These systems are referred to as

Superconducting Magnetic Energy Storage (SMES)

Stored energy:

$$W = \frac{1}{2} L \cdot I^2 \quad (2)$$

The first European SMES was developed by the Forschungszentrum Karlsruhe in cooperation with the University of Karlsruhe and installed in a saw mill in Fischweier/Albtal in the low voltage grid of the Badenwerk. It has a maximum storage capacity of 250 kJ and an output of 80 kVA. The SMES consists of 6 magnetic modules in a solenoid coil. Each magnetic module comprises 1,000 turns of the 1.3 mm thick NbTi superconductor and has a diameter of 36 cm. Thus, the overall design has an inductance of 4.37 H and only uses a current of 300 A to store the required energy.

The price is unknown; the stored energy of 250 kJ is 0.069 kWh!

This may be 23 times more than in a SuperCAP, but the expenses are also much higher, not to mention the issue of cooling.

The industrial-scale storage of electrical energy in either the electric or magnetic field will not be achieved in the near future.

III. INDIRECT STORAGE OF ELECTRICAL ENERGY AS CHEMICAL ENERGY

A. Classic: Battery and rechargeable battery

Comparison battery and SuperCAP

	Accumulators	SuperCAPs
Energy storage method	Faradaic reactions mass transfer between the electrodes	mostly electrostatic interactions ionic charge accumulation at the active material
discharge curve		
cycle life	depending on cycling profile	>> 1,000,000 (100%DoD)
energy level	60 Wh/kg (alkaline) 140 Wh/kg (Li-ion)	1 - 10 Wh/kg
power level	0.4 - 0.8 kW/kg (alkal.) 0.3 - 1.5 kW/kg (Li-ion)	1 - 6 kW/kg

Typical data of different battery types:

Type	Energy (¹) Wh/kg	Output (²) W/kg
Lead-acid battery	50	200
Nickel-cadmium battery	53	160
Nickel-metal hydride battery	70	175
Sodium-sulfur battery battery	85	115
Lithium iron sulfide battery	95	104
Lithium polymer battery	130	140
Lithium iron phosphate battery	120	180
Zinc-bromine battery	75	45
Medium-term goals in the development of batteries	80-130	150-200

(¹) 3 hours discharge cycle

(²) Peak power to a depth of discharge (DoD) of 80 %

B. Some prices

1) Lead-acid battery

13.8 V /100 Ah approx. 60.- € (wholesale, 2015), that is 1.38 kWh.

Problems in long-term use: number of cycles

2) Li-polymer battery

22.2 V /20 Ah approx. 120.- € (wholesale, 2015), that is 0.44 kWh

Same here: finite number of charge and discharge cycles as well as finite service life (typically about 500 cycles and 2-3 years, except batteries used in the field of space operations: here, up to 60,000 cycles with 20 % DOD for LEO or 18 years with 80 % DOD for GEO)

IV. ALTERNATIVE: FUEL CELL

The basic principle of storage is electrolysis: water is split into hydrogen and oxygen before the hydrogen is conventionally stored in tanks.

The fuel cell then uses the hydrogen to generate electricity.

A. Electrolysis

Hydrogen has been produced with tried and tested methods for over 100 years. One of these methods is the alkaline water electrolysis. This versatile method has many applications, such as the supply of hydrogen to cool generators in power plants. The conventional alkaline electrolysis has further been developed, e.g. concentrating the electrode material and separator (diaphragm or membrane) on the anode and cathode side as well as its positioning towards the electrodes. These developments have improved the efficiency. Efficiency is currently from 50 - 60%.

There are systems with an output of 100 Nm³/h (normal cubic meter per hour), equal to an output of about 90 MW.

Another method is the PEM electrolysis: Due to its less attractive price-performance ratio, it is only suitable for smaller systems of up to 50 kW. Efficiency currently varies from 55 - 70%.

Tanks are used for storage, an unproblematic and tried and tested method.

By the way, the hydrogen can also be used differently. For example, rotary piston engines (Wankel engines) can directly run on hydrogen due to their otherwise impractically low compression.

B. Converting hydrogen into electricity using fuel cells

Fuel cells (FC) use a source of fuel (usually hydrogen, but also methane etc.) and oxygen (air is often sufficient) to directly generate electricity.

The following applies if gas is used as fuel: Fuel cells reach conversion efficiencies of up to 60 % (with H₂) or 40 % (with CH₄) (that is, they are actually unacceptable as rechargeable batteries!)

Their good scalability is a further advantage: Fuel cells can be produced for various power classes, from a few milliwatts up to several megawatts.

If applicable, the waste heat (more than 40 %) can be used in cogeneration.

Of course, it can also be used to generate electricity with gas from other sources.

Hydrogen ions are carried through the central membrane, the electrons travel through an external circuit.

A fuel cell stack consists of several individual fuel cells. In PEM fuel cells (Proton Exchange Membrane), each cell has two lattice electrodes separated by a membrane. Hydrogen is on one side (image left), oxygen on the other. The external electricity is generated as hydrogen is split on the hydrogen side. Each hydrogen molecule is split into two electrons and two protons. The protons are conducted to the oxygen side through the membrane. The electrons travel there through the

external circuit. The reason for this is the lack of electrons on the oxygen side. Here, water is produced from protons, electrons and oxygen. The main product of the fuel cell is electricity, but waste heat is also produced. This can be used in small cogeneration plants.

Which fuels can be used?

There is not just one fuel cell. In fact, five or six different types exist. All of them are modern interpretations of the idea formed by the English physicist Sir William Grove, who wrote about *cold combustion* as early as 1839. The following list provides an overview of the different types of fuel cells.

1) *The PEM fuel cell:*

PEMFC	Proton Exchange Membrane Fuel Cell		
Electrolyte	Polymer membrane	Efficiency	60 % (H ₂) 40 % (CH ₄)
Anode gases	Hydrogen (Methanol)* (Methane)*		
Temperature	0-80 C		
Output	up to 250 kW	Note	CO sensitive

2) *The Solid Oxide Fuel Cell:*

SOFC	Solid Oxide Fuel Cell		
Electrolyte	Zr(Y)O ₂	Efficiency	50-65 %
Anode gases	Hydrogen Methane Coal gas		
Temperature	800-1,000 C		
Output	10-25 kW	Note	Reforming of fuel gases unnecessary

3) *The alkaline fuel cell (AFC):*

AFC	Alkaline Fuel Cell		
Electrolyte	Potassium hydroxide (KOH)	Efficiency	60 %
Anode gases	ultrapure hydrogen		
Temperature	60-90 C		
Output	20 kW	Note	CO ₂ sensitive

4) *The molten carbonate fuel cell (MCFC):*

MCFC	Molten Carbonate Fuel Cell		
Electrolyte	Molten alkali carbonate	Efficiency	48-60 %
Anode gases	Hydrogen Methane Coal gas		
Temperature	650 C		
Output	2.2 MW	Note	CO ₂ needs to be present in the cell cycle

5) *The direct methanol fuel cell (DMFC):*

DMFC	Direct Methanol Fuel Cell		
Electrolyte	Polymer membrane	Efficiency	40 %
Anode gases	Methanol		
Temperature	60-130 C		
Output	up to 250 kW	Note	promising since there is no H ₂ production required

6) *The phosphoric acid fuel cell (PAFC):*

PAFC	Phosphoric Acid Fuel Cell		
Electrolyte	concentrated H ₃ PO ₄	Efficiency	40 %
Anode gases	Hydrogen (Methane)*		
Temperature	130-220 C		
Output	11 MW	Note	weak CO sensitive

* Hydrogen is produced via reforming

Each principle has specific advantages and disadvantages. Not only are fuel cells still very expensive, their actual service life is also often too short. And there is one essential problem: Where does the fuel used in fuel cells come from? As long as fossil energy sources such as natural gas are used, there is nothing to gain. The reason for the popularity of the fuel cell is the fact that it works well with hydrogen, which can be produced from renewable energies.

V. ALTERNATIVE SUPPLY WITH HYDROGEN?

When it comes to the future of the fuel cell, hydrogen economy is often talked about, such as the production of hydrogen in giant solar farms in the desert. From there, the hydrogen produced via electrolysis is supposed to be transported to Central Europe in large tankers or through pipelines. Apart from the fact that conversion and transport would generate major losses, there are other reasons why this is still a long way off. Today, industrial-scale fuel cells are powered with two other fuels: Methanol or methane gas (natural gas). Depending on the type of fuel cell, these fuels can be processed directly or via a so-called reformer. Reformers separate hydrogen from

methane or methanol, which can then be used for the actual fuel cell.

Another concept is a *hybrid* hydrogen economy. Hydrogen produced via electrolysis (e.g. 5 %) is added to regular natural gas. In this way, the giant natural gas storage facilities that already exist can be utilized and this mixture of gases can be used as before. Natural gas consists of 85 - 98% methane, 4 - 1% alkanes and 11 - 1% inert gases.

The former town gas consisted of 51% hydrogen, 21% methane and 15% nitrogen plus 9% carbon monoxide.

VI. REDOX FLOW BATTERY

Advantages:

- Highest number of full cycles of all battery systems (> 10,000), proven without capacity and efficiency loss
- 100% chargeable and dischargeable without disadvantages on the lifetime (Li ions only approx. 80%, lead only approx. 50%)
- Can be configured as required: power and capacity can be configured separately
- Ideal for longer storage periods: From approx. 3 hours on, the most economical battery technology for very high energies/performances
- Storage of high capacities is comparatively simple, since only a few subsystems are required. In contrast, a 100kWh Li-Ion system already consists of thousands of single batteries, which all have to be constantly monitored and adjusted to each other regarding the charge state.
- Very low self-discharge with battery switched off, approx. 2% per year
- Safe: No fire hazard due to design principle

Disadvantages:

- Efficiency AC/AC 65-75% (LiIon 85%, Pb 80%)
- Maintenance of process engineering necessary (pumps, valves,...)
- Limited use in water protection areas
- Costs reasonable only with larger systems up from approx. 100 kWh
- For applications with a low number of cycles and/or a short storage period, it is not feasible
- only suitable for stationary applications

VII. MECHANICAL STORAGE

Type	State of development	Potential output	Actual output
Compressed air	Comm.	50 - 300 MW	100 - 300 MW
Pumped storage plant	Comm.	250 - 2,000 MW	5 - 2,100 MW
Flywheel	Demos	1 - 1,000 MW	< 1 MW (1 kW for 2 hours in a telecom application)

All three versions have an efficiency of about 80%

VIII. COMPRESSED AIR ENERGY STORAGE (CAES) IN SALT DOMES

IX. PUMPED STORAGE PLANTS

Kopswerk II in Vorarlberg/Austria built 2004-2008 – 175 MW

X. FLYWHEEL ENERGY STORAGE

XI. COMPARATIVE COST ESTIMATION OF INDUSTRIAL-SCALE PLANTS

Cost of construction €/kW	Ditto €/kWh	Storage time in h	Total €/kW (if h = 6)
Compressed air storage (100 MW)	390	1	396
Pumped storage plant (1,000 MW)	110	10	170
Battery (100 MW)	120	170	1,140
SMES (1,000 MW)	120	300	1,920
Flywheel energy storage (100 MW)	150	300	1,950

XII. COST EXAMPLE OF THE LOW-POWER SECTOR:

An electrolyzer with an equivalent power of 2 kW, a storage device with an equivalent capacity of 10 kWh and a fuel cell of 1.5 kW 130,000 € (actual price 2012).

In 2015, the prices of fuel cells went down and remained stable in the case of electrolyzers. In contrast, tanks have become more expensive:

Current prices SOFC fuel cell 1.5 kW 29,000 € net, electrolyzer 1 kW 27,000 €

A Gradient Descent Based Efficiency Calculation Method With Learning Rate Adaption

Felix Oberdorf¹, Kevin McFall², Joachim Kempkes³

1) Felix.Oberdorf@fhws.de, University of Applied Sciences Würzburg-Schweinfurt, Ignaz-Schön-Straße 11, 97421 Schweinfurt, Germany

2) KMcFall@Kennesaw.edu, Kennesaw State University, 1000 Chastain Road, 30144 Kennesaw, USA

3) Joachim.Kempkes@fhws.de, University of Applied Sciences Würzburg-Schweinfurt, Ignaz-Schön-Straße 11, 97421 Schweinfurt, Germany

This paper presents a gradient descent based calculation method with an adaptive learning rate for the maximum efficiency calculation of an electrical machine. The method is applied to a permanent magnet synchronous machine, thus the machine equations are described. Of course the method could be applied to other machine types as well. The presented method reduces some problems, which occur while the usage of a gradient descent based method without learning rate adaption. The results are presented and conspicuous features are discussed.

Keywords: Efficiency, gradient descent, learning rate adaption, optimization

1 Introduction

Because of the increasing integration and thus the limited possibilities for heat dissipation the importance of efficiency calculation of electrical machines is growing. Therefore the power losses and the resulting efficiency have to be studied. The principle calculation of efficiency maps is a well known topic [1], [2], [3], even with saturation effects [4]. The calculations are mainly based on curve- and surface fitting methods to obtain an algebraic equation describing e.g. the dependency of flux linkage and current in direct and quadrature axis $\psi(I_d, I_q)$.

As an alternative approach in comparison to an exhaustive search a method is presented in [5]. It is based on a gradient descent (GD) optimization function. The

main objective is a tuning of the input parameters torque T and rotational speed n of an electrical machine to find the maximum efficiency. The presented method shows good results, with little problems in the optimization process. Because of the chosen learning rate an overtuning for $T_0 = 150$ Nm and $n_0 = 1000$ rpm (Figure 1 yellow dotted ellipse) can be observed. The yellow arrows mark the evolution of the predicted efficiency. There was stated, that a fixed learning rate of $\alpha_f = 5 \cdot 10^4$ was chosen, because learning rates of $\alpha \geq 8 \cdot 10^4$ led to convergence problems.

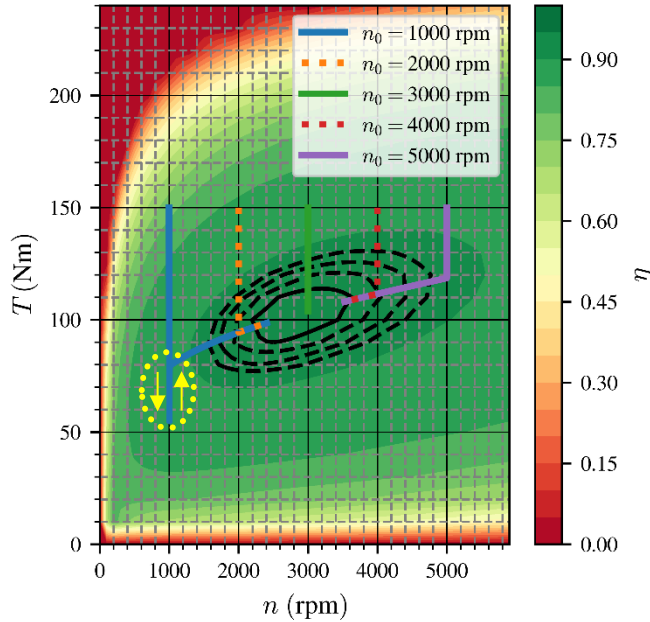


Figure 1

Efficiency map with a comparison of the evolution of η during the optimization process for $T_0 = 150$ Nm and different rotational speed starting values n_0 [5]. The overtuning for $n_0 = 1000$ rpm is marked with an yellow dotted ellipse.

As a solution this paper presents an improved GD method with a learning rate adaption, which is further called the GDa (a for alpha – learning rate) method. Therefore in section 2 the machine and loss models are presented. Section 3 includes an overview of the optimization process and the learning rate adaption. In section 4 the results are shown and conspicuous features are discussed.

2 Machine Model

2.1 Main equations

The Torque T of a permanent-magnet synchronous-machine (PMSM) can be described using (1), based on flux linkage and currents in direct and quadrature axis directions as well as the number of pole pairs p [5].

$$T = \frac{3}{2} \cdot p \cdot (\psi_d \cdot I_q + \psi_q \cdot I_d) \quad (1)$$

The electromagnetic power P_{em} is further calculated by T and the mechanical angular speed ω_{Mech} .

$$P_{em} = T \cdot \omega_{Mech} \quad (2)$$

2.2 Power loss calculation

An electrical machine's power losses can be divided into copper, iron, eddy current, windage and bearing losses. The copper losses are calculated by (3) with R_{ph} as the phase resistance and I_S as the stator phase current.

$$P_{l,Cu} = 3 \cdot I_S^2 \cdot R_{ph} \quad (3)$$

The iron losses are calculated with default settings in ANSYS Maxwell® and described as a 3D surface depending on the torque T and the rotational speed n . The mechanical losses are adapted from [1] and [6], where measurements with a dummy rotor were performed, including bearing and windage losses. As a simplification the eddy current losses in magnets are neglected. The total losses P_1 can be calculated by (4).

$$P_1 = P_{l,Cu} + P_{l,Fe} + P_{l,Mech} \quad (4)$$

The efficiency η is calculated by (5) from the electromagnetic power P_{em} and the total power loss P_1 .

$$\eta = \frac{P_{em}}{P_{em} + P_1} \quad (5)$$

Based on (5) the efficiency for a given operating point can be calculated. In Figure 2 the efficiency map of the machine is shown with an ellipse highlighting an area with $\eta \approx 90.8\%$. This area is further called the area of maximum efficiency. The target of the optimization (section 3) is to find results within this area. This simplification is assumed on the basis of the calculation effort and further described in section 3.

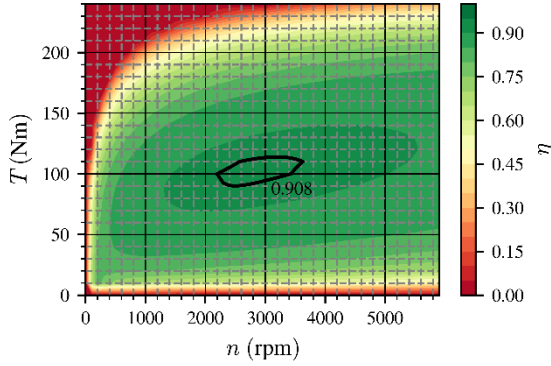


Figure 2
Efficiency map of the electrical machine

3 Optimization

3.1 Gradient Descent Method

The gradient descent optimization function is described in [7]. The main purpose of this function is the reaching of a minimum. To apply this to the problem of finding the maximum efficiency a (optimization) loss function is necessary. A common loss function is the Mean Squared Error (MSE) function (6) [7].

$$l(\mathbf{w}) = \frac{1}{N} \cdot \sum_{j=1}^N (\eta_{\text{pred}}(\mathbf{w}, x_j) - \eta_{\text{tar},j})^2 \quad (6)$$

The calculated loss is used for the weight update process. Therefore the update rule (7) [8] is applied.

$$\mathbf{w}_t = \mathbf{w}_{t-1} - \alpha \cdot \nabla l(\mathbf{w}_{t-1}) \quad (7)$$

Equation 7 includes the learning rate α with the purpose of an adaption of the gradient's slope. Like mentioned in [5] there is a large effect on the behaviour of the optimization process. Hence there are more details in section 3.2.

Within the iterative process the (optimization) loss is calculated and the weights are updated. To avoid protracted calculation times, a specific stop criteria has to be defined. It is calculated by the change of loss (8) and compared to the stop criteria of $\Delta l < 1e^{-12}$. This realizes an applicable trade-off between accuracy and optimization time.

$$\Delta l = |l_{t-1} - l_t| \quad (8)$$

3.2 Learning Rate Adaption

During some research about the GD method there was pointed out, that the stability problems as well as the so called overtuning strongly depends on the learning rate. Especially for learning rate of $\alpha \geq 8 \cdot 10^4$ there occurred problems e. g. no convergence of the calculated efficiency. Further there could be detected the mentioned overtuning. It was assumed that this behaviour of the GD method is mainly depending on the chosen learning rate, especially within the first epochs. Thus the GDa method with a learning rate adaption was implemented.

To explain the GDa method a comparison with the GD method is presented. Therefore the GD method with a fixed learning rate $\alpha_f = 15 \cdot 10^4$ is applied. The results can be seen in Figure 3 a) and Figure 4 a) for different start values of torque T_0 and rotational speed n_0 . During the optimization the learning rate α_f is constant.

While the optimization process with the GDa method the learning rate α_a is adapted and defined by (9). For the example α_a depends on the number of the actual epoch while optimization process N_{epoch} .

$$\alpha_a(N_{\text{epoch}}) = \begin{cases} 5000, & N_{\text{epoch}} < 200 \\ 150000, & N_{\text{epoch}} \geq 200 \end{cases} \quad (9)$$

As defined by (9) the learning rate for the first 199 epochs is $\alpha_a = 5 \cdot 10^3$, within epoch 200 the learning rate is adapted to $\alpha_a = 15 \cdot 10^4$. Beside the chosen definition of α_a there could be applied functional dependencies like linear, quadratic or exponential equations. Further an adaptive learning rate method like ADADELTA [9] could be implemented. The results of the GDa method with the discrete learning rate change (9) are presented in section 4 in comparison to the original GD method.

4 Results

In Figure 3 and Figure 4 the evolutions of η are shown for different starting values. The results are shown for a) a fixed learning rate (GD method) and b) an adaptive learning rate (GDa method) respectively.

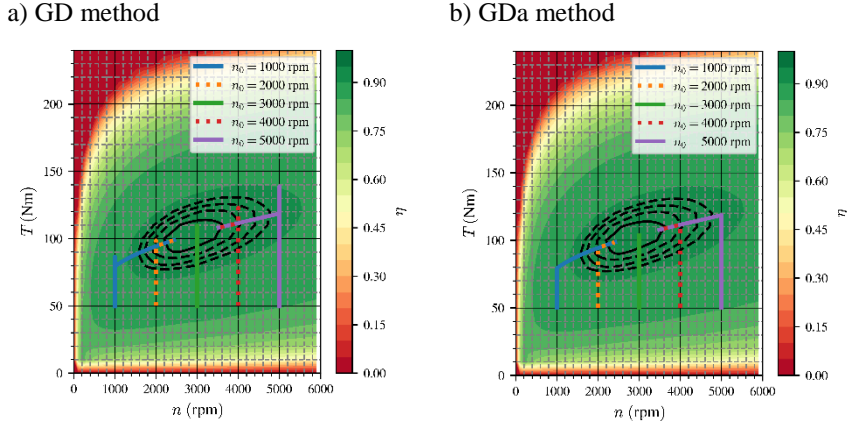


Figure 3

Efficiency map with a comparison of the evolution of η during the optimization process for $T_0 = 50$ Nm and different rotational speed starting values n_0 . With a) GD and b) GDa method defined by (9).

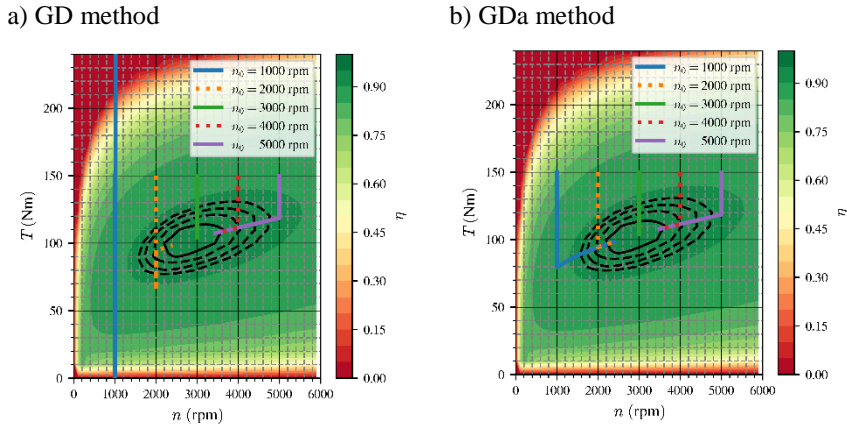


Figure 4

Efficiency map with a comparison of the evolution of η during the optimization process for $T_0 = 150$ Nm and different rotational speed starting values n_0 . With a) GD and b) GDa defined by (9).

In Table 1 the optimization results are compared for different starting values and both methods. There are shown the maximum predicted efficiency $\eta_{\text{pred,max}}$, the torque $T_{\eta_{\text{max}}}$ and rotational speed $n_{\eta_{\text{max}}}$ at maximum predicted efficiency as well as the number of epochs N_{epochs} until fulfilment of the stop criteria.

Table 1

Comparison of the optimization results for different starting values for the GD method and the GDa method

T_0	n_0	GD method				GDa method			
		$\eta_{\text{pred,max}}$	$T_{\eta_{\text{max}}}$	$n_{\eta_{\text{max}}}$	N_{epochs}	$\eta_{\text{pred,max}}$	$T_{\eta_{\text{max}}}$	$n_{\eta_{\text{max}}}$	N_{epochs}
50	1000	0.9091	98.8	2437	7804	0.9091	98.6	2414	7887
150	1000	-	-	-	-	0.9090	98.5	2397	7691
50	2000	0.9091	98.7	2428	4639	0.9090	98.6	2409	4730
150	2000	0.9090	98.5	2399	4142	0.9090	98.5	2405	4421
50	3000	0.9094	103.8	2999	11	0.9094	103.8	2999	207
150	3000	0.9094	103.9	3000	10	0.9094	103.8	3000	208
50	4000	0.9086	107.8	3503	6304	0.9087	107.7	3488	6740
150	4000	0.9087	107.7	3493	6474	0.9086	107.9	3524	6616
50	5000	0.9086	107.9	3519	14470	0.9087	107.7	3489	15132
150	5000	0.9087	107.5	3458	15449	0.9087	107.8	3492	15595

As shown in Figure 3 a) the GD method with constant $\alpha_f = 15 \cdot 10^4$ leads to an overtuning of the evolution of η_{pred} . Further in Figure 4 a) can be seen that for $T_0 = 150$ Nm not just an overtuning exist, but also for $n_0 = 1000$ rpm η_{pred} does not convergence. This approves the statement in [5] and the limitation of $\alpha_f < 8 \cdot 10^4$.

The results of the GDa method are presented in Figure 3 b) and Figure 4 b) as well as in Table 1. At first it is obvious that all the evolutions of η_{pred} result in the area of maximum efficiency $\eta_{\text{max}} > 0.9086$. Thus the GDa method is approved. Further it can be seen that the overtuning is reduced.

A comparison of the resulting values for $T_{\eta_{\text{max}}}$ and $n_{\eta_{\text{max}}}$ (Table 1) shows that the values vary in a little range, which is presumed admissible. The number of epochs until fulfilment of the stop criteria N_{epochs} is increasing with the GDa method, which is the consequence of the reduced learning rate for the first 200 epochs. Nevertheless it has to be mentioned that the difference of N_{epochs} GD and GDa method is not exactly the chosen number of 200 epochs. This results from the optimization

process, which leads to results with a small variation. Thus the calculations were repeated multiple times and the presented results could be proved.

5 Discussion

Usually while an optimization process at first a high learning rate is chosen and at a certain point the learning rate is reduced to fine tune the results. The application within the GDa method is different. The GDa method starts with a small learning rate which further is increased. This mainly depends on the equations (7) and (8) and the chosen stop criteria. The loss between the actual epoch and the previous one is calculated by (8). The result is compared with the stop criteria. If the absolute difference in the loss between two epochs is too small, the stop criteria is fulfilled and the optimization process is finished. Actually this should happen in the area of maximum efficiency, since the gradient in this area is small.

Especially around the path of maximum gradient [5], where the evolutions of η_{pred} are located on, the gradient is high. Based on the gradient calculation in (7) the weights are updated strongly. This actually leads to the described overtuning or even no convergence. The reduced learning rate for the first 199 epochs compensates the high gradient calculation and prevents overtuning as well as no convergence. Afterwards the high learning rate allows a computational efficient reaching of the area of maximum efficiency, without a premature finish of the evolution because of the chosen stop criteria.

Conclusions

In this paper the application of the GDa method for calculating the maximum efficiency area η_{max} of an electrical machine was presented. It is a further development of the GD method and has the main benefit of an adaptive learning rate. The GDa method is applied to a PMSM, nevertheless it could be applied to other machine types as well. The power and power loss calculations are based on the equations in section 2. The gradient descent optimization function, the (optimization) loss function and the learning rate adaption are presented in section 3. The GDa optimization results show, that the area of maximum efficiency $\eta_{\text{max}} > 0.9086$ can be found. The described overtuning or not converging evolutions are reduced. Further the results are discussed and features of the GDa method are explained.

Within further research the presented method could be applied to other machine types. Further additional power losses e. g. eddy current losses in magnets should be considered. The method could also be applied to electrical drive systems including power electronics.

References

- [1] J. Goss, P. H. Mellor, R. Wrobel, D. A. Staton and M. Popescu, “The design of AC permanent magnet motors for electric vehicles: a computationally efficient model of the operational envelope,” in 6th IET International Conference on Power Electronics, Machines and Drives (PEMD), March 2012.
- [2] L. Song, Z. Li, Z. Cui and G. Yang, “Efficiency map calculation for surface-mounted permanent-magnet in-wheel motor based on design parameters and control strategy,” in IEEE Conference and Expo Transportation Electrification Asia-Pacific (ITEC Asia-Pacific), Beijing, November 2014.
- [3] R. Bojoi, E. Armando, M. Pastorelli and K. Lang, “Efficiency and loss mapping of AC motors using advanced testing tools,” in XXII International Conference on Electrical Machines (ICEM) , Lausanne, September 2016.
- [4] S. Stipetic and J. Goss, “Calculation of efficiency maps using scalable saturated flux-linkage and loss model of a synchronous motor,” in XXII International Conference on Electrical Machines (ICEM) , Lausanne, September 2016.
- [5] F. Oberdorf, K. McFall, S. Moros and J. Kempkes ., “A Gradient Descent Based Method For Maximum Efficiency Calculation” in International IEEE Conference AND workshop in Óbuda on Electrical and Power Engineering (IEEE CANDO EPE 2018), Budapest, November 2018.
- [6] J. S. Jsu, C. W. Ayers, C. L. Coomer and R. H. Wiles, “Report on Toyota/Prius Motor Torque Capability, Torque Property, No-Load Back EMF and Mechanical losses,” Oak Ridge National Laboratory, Rep. ORNL/TM-2004/185, September 2004.
- [7] I. Goodfellow, Y. Bengio and A. Courville, “Deep learning,” in MIT Press , 2016.
- [8] B. Widrow and M. A. Lehr, “30 years of adaptive neural networks: perceptron, Madaline, and backpropagation,” in Proceedings of IEEE, September 1990.
- [9] M. D. Zeiller, “ADADELTA: AN ADAPTIVE LEARNING RATE METHOD”, in Cornell University Library, December 2012.

Platform for Anomaly Detection in Time-Series

Gheorghe Sebestyen, Anca Hangan, György Kovács, Zoltán Czakó

Technical University of Cluj-Napoca
Memorandumului 28, 400114, Cluj-Napoca, Romania
{gheorghe.sebestyen, anca.hangan, gyorgy.kovacs, zoltan.czako}@cs.utcluj.ro

Abstract: This paper presents a platform that integrates a number of functionalities necessary in the process of anomaly detection, from preprocessing towards various anomaly detection techniques and visualization methods. The purpose of this tool is to allow a developer to test, select and fine tune different algorithms that best fit anomaly detection in a given domain. To demonstrate the utility of the platform, we present a series of experiments done with different methods for anomaly detection on time-series and evaluate their results.

Keywords: anomaly detection, time-series, tools, data processing

1 Introduction

Monitoring of complex cyber-physical systems generates large amounts of data in the form of time series. Unfortunately, collected data may contain erroneous values, caused by various events (e.g. device defects, communication errors, environmental changes, etc.), which may affect the stability and controllability of the system. Therefore, a variety of methods were developed in order to identify and eliminate this so called “anomalies” [1] [2].

Anomaly detection in time series uses various methods [3] such as basic ones inspired from signal processing, methods that are based on time, space or functional correlations, methods based on system theory, or on pattern recognition. These methods perform differently on different data sets and for different types of anomalies. There is no “universal recipe” that works in all cases. Data analysts must choose the right approach for anomaly detection, taking into consideration the characteristics of data, the characteristics of the monitored system and the type of anomaly.

In this paper we propose a platform containing a set of tools that can aid in deciding which anomaly detection algorithm works best for a particular problem, by allowing the data analyst to try different anomaly detection approaches and then compare their results. Furthermore, we present a set of experiments in which we focus on anomaly detection techniques for time series data that contain different types of anomalies.

For the rest of this paper, we consider that analyzed data has the following form: $X = \{x_t \in \mathbb{R} : \forall t \geq 0\}$. Moreover, we will use the following functional definition

of an anomaly: “An anomaly is a data point or set of data, which is significantly different from all other data points or sets.” This means that in order to define an anomaly, one must first have a notion of nominal (or normal) data. The term anomaly is relative and can not be applied to a data-point independently of any dataset.

The following chapters are structured as follows: In Section 2 we describe related work on the subject. Next, in Section 3 we give a brief description of the developed platform and its features. In Section 4 we describe the types of anomaly detection methods provided by our platform. We will test these methods in Section 5. This will be followed by conclusions and discussion on the future research directions.

2 Related Work

Most methods for anomaly detection are developed for a given field or have a specific application. In [4] and [5] the authors developed methods to detect anomalies in airplane data. In [6] similar methods were developed for IoT. In [7] methods for detecting anomalies in Big Data are presented. In [8] methods are used to detect anomalies in industrial machinery.

In [3] a group of algorithms and techniques are described and categorized. The authors found that while some algorithms in different fields are very similar, most algorithms are hard to generalize. They also note, that numerous formulations of anomaly detection problems are not sufficiently explored, i.e. it is not known how well some algorithms perform in a field that was not intended for that algorithm.

Efforts to bundle up different anomaly detection algorithms have already begun. In [9] the authors introduced an open source, generic framework for detecting anomalies in large scale time-series data.

In [10] a platform is proposed, that offers tools for data visualization, filtering and classification for a variety of data formats, including but not limited to time series data.

We believe that there is a real advantage in a platform that offers a variety of anomaly detection methods to the user. One can test the performance of a number of anomaly detection algorithms for some given test data. By having as many implementations of these algorithms as possible, the user can easily test as many algorithms as she wants with minimal effort and cost.

3 The Platform

Our platform includes a set of tools for data acquisition, preprocessing, anomaly detection and plotting. We envision the anomaly detection process as a workflow with configurable and interchangeable nodes in which the user has access to intermediate results. Figure 1 shows the envisioned workflow. The workflow has several types of nodes that the user includes in the custom anomaly detection process as follows:

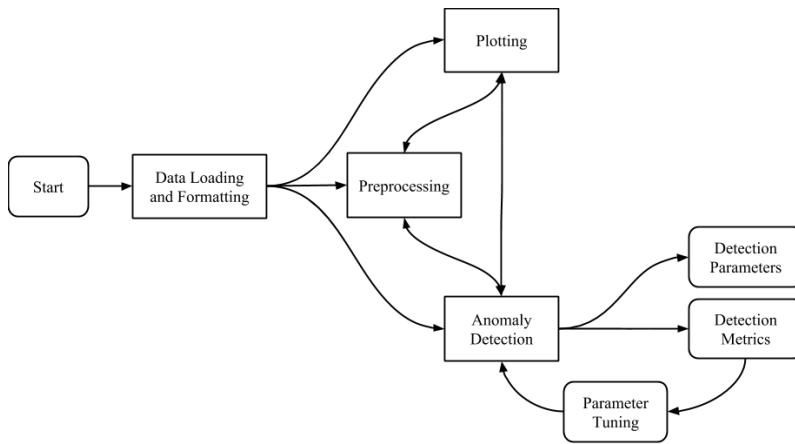


Figure 1
Workflow of the classification process.

- **Data Loading:** The user starts by loading in some data that she wishes to analyze. Because data can be stored in many different formats, the platform was designed to work with excel, Comma Separated Values (CSV) and Attribute-Relation File Format (ARFF) files, alongside MAT files.
- **Plotting:** The user can choose to visualize the data using the visualization tools provided by the platform. We provide tools both for time-series and non time-series data. For time-series data we provide tools for plotting, histograms and Fourier decomposition.
- **Preprocessing:** The user can apply transformations to the dataset either to smooth out the data or to emphasize some of its characteristics in an attempt to improve the classification results. For this we provide high-pass, low-pass and band-pass filters.
- **Anomaly Detection:** Next, a user can try out an anomaly detection algorithm from a collection of algorithms. Each one will have a set of parameters. These can be fine tuned to improve the classification quality. The quality of the classification can be measured using classification metrics. The confusion matrix can be generated as well as some derived metrics such as precision and recall.

When the user is satisfied with the classification, she can use the parameters of the classification method either for future tests or to implement a specialized system for monitoring anomalies.

4 Anomaly Detection Techniques

In this section we give short descriptions of some of the possible anomaly types. For each anomaly type we present some methods for detecting it.

In principle, anomaly detection may be derived from more classical methods such as system identification or classification. In the first case the methods try to identify a “nominal” behavior model for a system (or dataset) and detect anomalies as points or value sequences that don’t fit with the model. In the second case a given classification method (from artificial intelligence field) is applied in order to label points as nominal or anomalous. Anomaly detection is slightly different from these at least in one regard: anomalies are generally rare, and comprise a very small percent of the data. Therefore the process of training the classifiers is sometimes difficult or even impossible.

Some datasets do not even contain anomalies, and algorithms are expected to learn the nominal functioning of the system from “clean data”. We call a dataset that doesn’t contain anomalies a clean dataset.

Depending on the moment when the detection is performed we can distinguish between on-line and off-line methods. Offline methods work on prerecorded datasets; usually they perform better, since for each data point we can use both past and future values and the processing time is not limited by the sampling period. The on-line methods are used for real-time detection, when only the past values are available and the detection algorithm must be performed in the interval between to samples. Sometimes the detection is delayed a few sampling periods in order to have values before and after the considered sample.

Next, a number of anomaly types are presented and also some techniques used for their detection.

4.1 Outliers

Given a dataset an outlier is a singular value (sample) that does not fit with its neighbours, because the value breaks somehow a given correlation with the neighbouring values. For this purpose, we define a function *label* that labels a data-point $x \in X$ either as anomalous or nominal:

$$c_x = \text{label}(x, X)$$

$$c_x \in \{Nominal, Anomaly\}$$

4.1.1 Bounded Method

A very intuitive method would be to label elements as anomalies by setting global lower and upper bounds. This can be used to detect obvious anomalies such as extreme temperature levels or very high blood pressure.

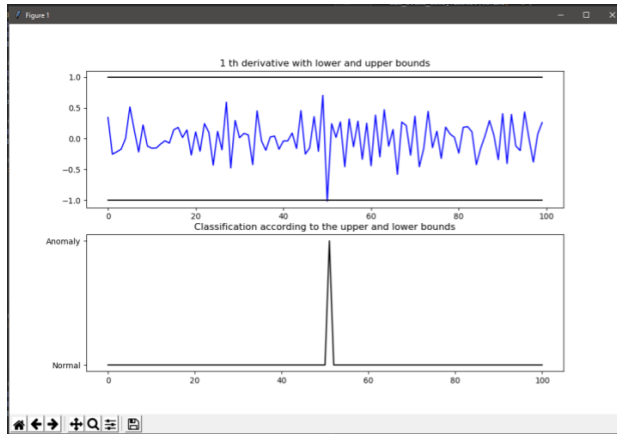


Figure 2

A signal with a higher than average disturbance in the middle is detected by the method. Forward difference is used as an approximation for the derivative.

In the platform we provide a method that classifies a point as an anomaly if it is outside certain bounds. This can be done even with any derivative of the function. We call this *Bounded Derivative Method*. BDM is defined as:

$$BDM(x) = \begin{cases} \text{Nominal} & \text{if } B^+ > f(x)^{(n)} > B^- \\ \text{Anomaly} & \text{otherwise} \end{cases}$$

where B^+ and B^- are the upper and lower bounds, and $f(x)^{(n)}$ is the n -th derivative of the signal. An example of the usage can be seen in Figure 2. The interval of “normality” may be set by the designer or it can be automatically detected using a dataset without outliers.

A more adaptive method, which can be applied for time-series with very slow or seasonal variations could set local bounds available for a given period or seasonal intervals of time. The same technique may be used for system that have multiple quasi-stationary stages.

Even though this detection is trivial, many existing real systems rely on this technique for detection.

4.1.2 Model Distance Methods

If the previous methods are not applicable, because of the complex nature of the time-series, more elaborate approaches can be used.

Since in many cases a time-series is generated by a generative process (e.g. the output of a linear system), one could accurately describe the underlying process, and create a model of the system:

$$x_t^* = f(t)$$

where x_t^* is the predicted value of x at time t .

Given such a model, the detection algorithm can label an anomaly based on the distance between an actual value and its prediction. Because the noise may influence the actual value a threshold must be established. If the distance (in absolute value) between the predicted value x_t^* and the actual value x_t is greater than some threshold d_{max} , x_t than it can be considered an anomaly:

$$p(x_t) = \begin{cases} \text{Anomaly} & \text{if } |x_t - f(t)| \geq d_{max} \\ \text{Nominal} & \text{otherwise} \end{cases}$$

The predictor of a time-series can be obtained using (auto)regression techniques or system identification methods (if the input of the system is also available). Although such a model is highly useful, sometimes in practice, in order to make a prediction, it is good enough to consider only the neighboring points.

Next we present some model distance methods implemented in our platform:

Median Distance Method This method is known as the *Double Sided Median Method* for anomaly detection [5]. By using a sliding window, we calculate the mean of the values inside the window, and if a given value is outside the allowed bounds, it is considered an anomaly.

$$DSMM(x_t) = \begin{cases} \text{Anomaly} & \text{if } |f(x_t) - \text{mean}(f(x_{t-k}), \dots, f(x_{t+k}))| > d \\ \text{Nominal} & \text{otherwise} \end{cases}$$

An example can be seen in Figure 3.

Linear Approximation Method The linear approximation method is based on the assumption that the next point will fall on or near the line made up of the previous two points. The distance function is defined as the distance from a point to the line made up from the previous two points.

Auto-regressive Method Other regressive models, that use the past values to predict the new values are also used: $x_t^* = f(x_{t-1}, x_{t-2}, \dots, x_{t-n})$, $n \geq 1$. If given that the data starts at $t = 0$ and $t - n > 0$, we use a sliding window approach, where we generate a prediction for the next value based on the actual old values. This is useful if we can model the time series using an auto-regressive model.

4.2 Change Point Detection

Change Point detection focuses on the underlying model of the process. The data is generated by a generative process $f(t, p)$, where $p \in \mathbb{R}^n$ are the parameters

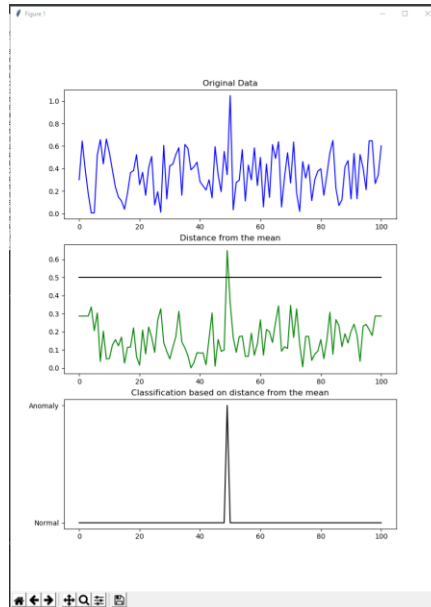


Figure 3

In the top figure, we can see the raw signal. In green we see the distance of each point from the mean of the sliding window. The black line from the middle plot is the distance limit. If the values falls outside the maximum distance, that point is considered to be an anomaly, as can be seen in the bottom plot.

of the model. That process is considered to be the nominal generative process. There is also an error $e(t)$ associated with the process. The error function is usually considered to be white noise.

$$x_t = f(t, p) - e(t)$$

This detection methods focuses on more long term changes compared to regular outlier detection methods. When a change in the system behavior is observed, it is considered an anomalous behavior. In other words, we constantly update the parameters of the process p_n , and compare it with the previous parameters p_{n-1} . p_n is considered an anomalous behavior if $|p_n - p_{n-1}| > d_p$, where $d_p \in \mathbb{R}$ is a threshold value.

An example of this is illustrated in Figure 4.

5 Experiments

In this section we will compare the results obtained with a number of anomaly detection methods.

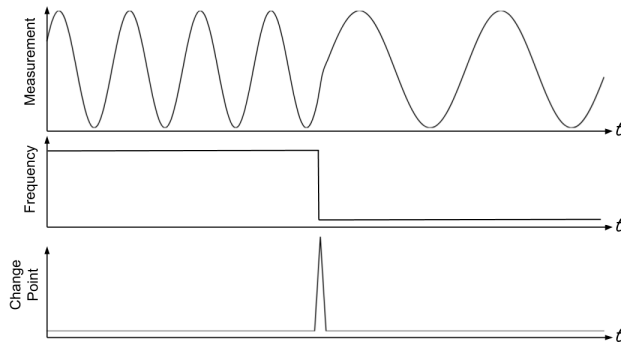


Figure 4

In the top most graph, we can see the observed process. In this case it is a pure sine wave. In the middle graphs we can see the coefficient of the model, which in this case is just a function of it's frequency, since it is enough to perfectly describe the process. We consider as anomaly either the change point, either all the points where the model is outside some bounds.

The figures presented throughout this section display the values from different datasets labeled as normal (blue dots) and outliers (red dots). The points were labelled by the authors of this paper. This may seem arbitrary, but we contend that it is a valid method for establishing ground truth because of the fact that the very definition of anomaly is vague and is difficult to express in mathematical terms, yet it can be very intuitive. This is similar to the difficulty of expressing what a cat looks like in an image, however one would have no difficulty whatsoever determining if a picture contains a cat by just looking at it. It is also important to mention that the labelling phase was completed before the experiments and the labels were not changed in any way afterwards.

In order to judge the validity of the methods, a number of metrics were used. For each method, we included the number of true positive (TP), true negative (TN), false positive (FP) and false negative (FN) labels, as well as the calculated accuracy, precision and recall.

The accuracy represents the overall quality of the classification; it is just the percentage of labels that are correct. However since by definition most anomalies are rare events, they do not influence the final score as much. This is why this metric is not a good measure for the classification.

$$accuracy = \frac{TP + TN}{TP + TN + FP + FN}$$

Precision refers to the number of relevant (anomalous) labels from the correctly identified selection.

$$precision = \frac{TP}{TP + FN}$$

Recall refers to the number of correct relevant (anomalous) points selected.

$$recall = \frac{TP}{TP + FP}$$

5.1 First Dataset - Concurrent Users

We will use the a training dataset from [9]. The dataset is a univariate time-series displayed in Figure 5. This time series is a periodic signal with a couple of extreme points that are considered anomalies. Most points are either too low, or too high. The results obtained are aggregated in Table 1.

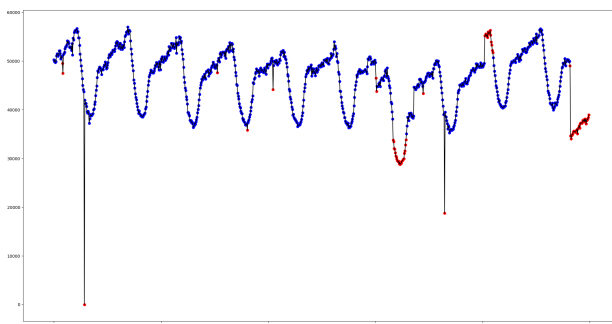


Figure 5

The x axis represents the timestamp of the measurement, and the y axis represents the number of concurrent users.

Table 1

Results of applying different methods to the first dataset.

Method	TP	TN	FP	FN	Accuracy	Precision	Recall
Bounded Derivative ($d = 0$)	32	912	0	55	0.9449	0.0339	1.0000
Bounded Derivative ($d = 1$)	6	908	4	81	0.9149	0.0066	0.6000
Median Method	8	896	16	79	0.9049	0.0088	0.3333
Linear Approximation	3	903	16	79	0.9069	0.0033	0.2500
First Order AR	1	904	8	86	0.9059	0.0011	0.1111

5.2 Second Dataset - Concurrent Users

The next dataset is also from [9]. For the second dataset we used a second univariate-time series similar to the previous one. This new one has clear change-point anoma-

lies, as well as the extreme values from the previous dataset. The shape of the graph and the labelled points are visible in Figure 6.

One could consider the first third of the data as anomalous behavior right until the change point. That is a valid interpretation of the data. However we decided not to go on that route, instead considering only the change point as an anomaly. The results are given in Table 2.

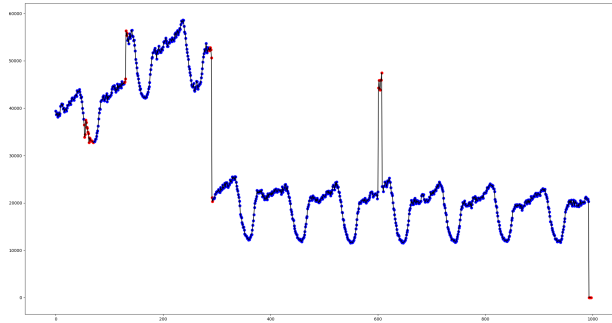


Figure 6

The x axis represents the timestamp of the measurement, and the y axis represents the number of concurrent users.

Table 2

Results of applying different methods to the second dataset.

Method	TP	TN	FP	FN	Accuracy	Precision	Recall
Bounded Derivative ($d = 0$)	42	692	261	3	0.7355	0.0572	0.1386
Bounded Derivative ($d = 1$)	7	952	1	38	0.9609	0.0073	0.8750
Median Method	20	944	9	25	0.9659	0.0207	0.6897
Linear Approximation	9	951	2	36	0.9619	0.0094	0.8182
First Order AR	1	947	6	44	0.9499	0.0011	0.1429

5.3 Third Dataset - Synthetic Data

The third dataset is a synthetic one and was generated by adding a white noise on top of a sine wave. Two points have been added that are outside the “normal” range of the signal. These two are considered anomalies, while the others are considered nominal points. The graph with the labels can be seen in Figure 7, and the result of the different methodologies can be seen in Table 3.

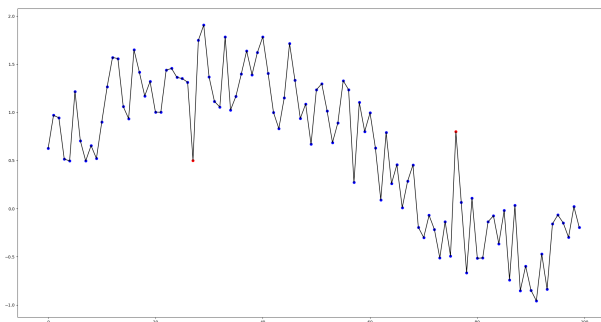


Figure 7

The axes have no real significance since this is just synthetic data that is obtained by adding together a signal with white noise and one with a sine wave.

Table 3

Results of applying different methods to the third dataset.

Method	TP	TN	FP	FN	Accuracy	Precision	Recall
Bounded Derivative ($d = 0$)	0	98	0	2	0.9800	0.0000	—
Bounded Derivative ($d = 1$)	1	97	1	1	0.9800	0.0102	0.5000
Median Method	0	96	2	2	0.9600	0.0000	0.0000
Linear Approximation	0	97	1	2	0.9700	0.0000	0.0000
First Order AR	0	96	2	2	0.9600	0.0000	0.0000

5.4 Fourth Dataset - CO2 emission

The last dataset is from [11]. It represents the CO₂ (ppm) emitted by the Mauna Loa volcano between the years 1965 and 1980. The ground truth classification can be seen in Figure 8. We observed that most neighbouring points have a certain distance between them, while a small number of neighboring points are more closely bunched. We considered these points as anomalous. The classification metrics are aggregated in Table 4.

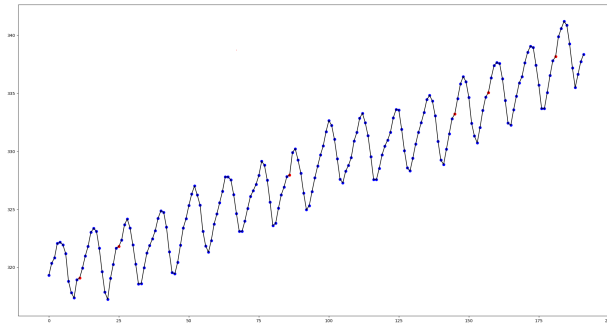


Figure 8

The x axis represents the months between 1965 and 1980, while the y axis represents the emitted CO₂.

Table 4
Results of applying different methods to the fourth dataset.

Method	TP	TN	FP	FN	Accuracy	Precision	Recall
Bounded Derivative ($d = 0$)	0	186	0	6	0.9688	0.0000	—
Bounded Derivative ($d = 1$)	0	182	4	6	0.9479	0.0000	0.0000
Median Method	0	182	4	6	0.9479	0.0000	0.0000
Linear Approximation	0	181	5	6	0.9427	0.0000	0.0000
First Order AR	0	183	3	6	0.9531	0.0000	0.0000

Conclusions

This paper presents an anomaly detection platform that incorporates a number of methods needed in the process of anomaly detection. The platform is useful for finding the best method that fits for a given dataset. This tool will allow a designer to decide which anomaly detection technique should be integrated in a given real-world application.

The experiments showed that in some cases less complex methods (with less execution time requirements) can generate results that are similar to more complex and more time consuming methods. The platform was designed in a modular manner in order to allow easy integration of new methods. The detection process is built up as a sequence of modules which may be combined by the user in order to get the best results.

In the future we intend to add more complex detection techniques which use artificial intelligence methods for pattern recognition.

Another point of interest are the classification metrics themselves. While the traditional confusion matrix is useful, we noticed that most errors were “off by one” classifications. Many times we have seen algorithms detect an anomaly, but placed

it with one time-stamp before or after the ground truth. Since the detection of the anomaly may be more important than the exact pinpointing of it, some metrics could be devised to take this preference into account.

References

- [1] V. Chandola, A. Banerjee, and V. Kumar, “Anomaly detection: A survey”, *ACM Computing Surveys* 41,3, 2009.
- [2] M. Rassam, A. Zainal, and M. Maarof, “Advancements of data anomaly detection research in wireless sensor networks: A survey and open issues”, *Sensors*, 2013.
- [3] M. Gupta, J. Gao, C. C. Aggarwal, and J. Han, “Outlier detection for temporal data: A survey”, *IEEE Transactions on Knowledge and Data Engineering*, 2014. DOI: 10.1109/TKDE.2013.184.
- [4] G. Silvestri, F. B. Verona, M. Innocenti, and M. Napolitano, “Fault detection using neural networks”, in *IEEE World Congress on Computational Intelligence*, 1994. DOI: 10.1109/ICNN.1994.374815.
- [5] S. Basu and M. Meckesheimer, “Automatic outlier detection for time series: An application to sensor data”, *Knowledge and Information Systems*, 2006. DOI: 10.1007/s10115-006-0026-6.
- [6] T. J. Lee, J. Gottschlich, N. Tatbul, E. Metcalf, and S. Zdonik, “Greenhouse: A zero-positive machine learning system for time-series anomaly detection”, *CoRR*, vol. abs/1801.03168, 2018.
- [7] C. K. Maurya, D. Toshniwal, and V. Agarwal, “Anomaly detection via distributed sparse class-imbalance learning”, in *International Conference on Machine Learning*, 2016.
- [8] D. Dasgupta and S. Forrest, “Novelty detection in time series data using ideas from immunology”, in *International Conference on Intelligent Systems*, 1996.
- [9] N. Laptev, S. Amizadeh, and I. Flint, “Generic and scalable framework for automated time-series anomaly detection”, in *Proceedings of the 21th ACM SIGKDD International Conference on Knowledge Discovery and Data Mining*, ACM, 2015, pp. 1939–1947.
- [10] G. Sebestyén, A. Hangan, Z. Czako, and G. Kovács, “A taxonomy and platform for anomaly detection”, *2018 IEEE International Conference on Automation, Quality and Testing, Robotics (AQTR)*, pp. 1–6, 2018. DOI: 10.1109/AQTR.2018.8402710.
- [11] R. Hyndman, *Time series data library*, <https://datamarket.com/data/list/?q=provider:tsdl>, Accessed: 2018-11-12.

Ranking of Hungarian Researchers from Several Disciplines Using Google Scholar Database

Gyula Mester

Óbuda University, Doctoral School of Safety and Security Sciences, Népszínház utca 8, 1081, Budapest, Hungary, drmestergyula@gmail.

Abstract: Using the h5-index and the number of citations in natural sciences, techniques and humanities in this article the best 500 Hungarian researchers is ranked. The ranking list may be formed based on the h5-index and the number of citations, given in Web of Science, Scopus, Publish or Perish Program and Google Scholar. Data for the first 500 researchers are presented. Google Scholar is the most complete. Therefore, to define a single indicator, h5-index calculated by Google Scholar may be a good and simple one. The ranking is made based primary on h5-index and number of citation based on the database in Google Scholar. Researches ranked first by h5-index in decreasing order and then by the number of citations.

Keywords: h5-index; number of citations; ranking of Hungarian researchers; Google Scholar database

1 Introduction

Due to the requests in a variety of activities ranking researchers in different disciplines of science become very important in last decade. Ranking is possible on different criteria: number of published papers, number of citations, etc.

One of these measures is h-index which includes both the productivity and citation impact of the publications of a scientist. The h-index was suggested in 2005 by Jorge E. Hirsch [1]. h5-index is the h-index for articles published in the last 5 complete years. It is the largest number h such that h articles published in 2013-2018 have at least h citations each.

h5-index can be determined according to the different sources: Google Scholar, WOS (Web of Science), Scopus and Publish or Perish Program. In this article the

list of the 500 best Hungarian researchers is presented. List covers researchers from natural sciences, techniques and human sciences.

As a primary source Google Scholar [2] has been used [3-12]. The author chooses the Google Scholar database as it is the widest. Introduced by Google in 2004, Google Scholar has become a very popular alternative data source. Google Scholar is the most complete.

Therefore, to define a single indicator, h5-index calculated by Google Scholar may be a good and simple one. Ranking is possible to be based on h-index (primary) and number of citations.

The article is organized as follows:

- In Section 1, the Introduction is given,
- In Section 2, the Ranking list of the 500 best Hungarian researchers is considered,
- Conclusions are given in Section 3.

2 Ranking list of the 500 best Hungarian researchers

The ranking is made based primary on h5-index and number of citation based on the database in Google Scholar (accessed: 20th November, 2018). Researches ranked first by h5-index in decreasing order and then by the number of citations.

Table 1
Ranking list of the 500 best Hungarian researchers

No.	Researcher, University, Country, Orcid ID	h5-index 2013-2018	Citations 213-2018
1	Zoltán Trócsányi, University of Debrecen, Hungary	121	82493
2	Dezso Horvath, missing	119	82210
3	Gabriella Pasztor, Eötvös Loránd University	118	99400
4	József Pálinkás, Hungarian Academy of Sciences	106	63115
5	Albert-László Barabási, <i>Northeastern University</i>	104	91118
6	Gyorgy Buzsaki, <i>NYU Neuroscience Institute</i>	102	39975
7	Peter Fonagy, <i>University College London</i>	95	46356
8	Peter Levai, MTA Wigner RCP, Hungary	83	26117
9	Ferenc Jolesz, <i>Harvard Medical School</i>	78	21638
10	Ferenc Siklér, MTA Wigner RCP	76	43371
11	Tamas L. Horvath, <i>Yale University</i>	73	18484
12	A. S. Szalay, <i>Johns Hopkins University</i>	71	31203
13	Andras Nagy, <i>Lunenfeld-Tanenbaum Research Institute</i>	71	22647
14	Ferenc Krausz, <i>Max Planck Institut</i>	70	25370
15	Pal Pacher, Semmelweis University	68	19885
16	Zoltan Acs, <i>George Mason University</i>	66	22078
17	Zoltán Dörnyei, <i>University of Nottingham</i>	65	34425

18	John von Neumann, <i>Princeton University</i>	62	37446
19	Imre Bartos, <i>University of Florida</i>	62	24330
20	Tamas Revesz, <i>UCL Queen Square Institute of Neurology</i>	62	14642
21	Zsolt Frei, Eötvös Loránd University	58	22396
22	Laszlo Lovasz, Eötvös Loránd University	58	18155
23	Tamás Csörgő, Wigner Research Centre for Physics	57	14801
24	Peter Raffai, Eötvös Loránd University, Hungary	56	21596
25	Zoltán Kutalik, <i>University of Lausanne</i>	56	18575
26	Zoltan Ungvari, <i>University of Oklahoma</i>	56	9517
27	Tibor Schuster, <i>McGill University</i>	54	10838
28	Istvan Csabai, Eötvös University	51	20659
29	J.A. Fodor, <i>Rutgers University</i>	51	19628
30	Attila Szolnoki, Institute of Materials Science and Technical Physics	51	9202
31	Gergely Csibra, Central European University	50	10227
32	Adam Miklosi, Eötvös University	50	8140
33	Tamas Vicsek, Eötvös University	49	20060
34	Peter Laszlo Lakatos, Semmelweis University	49	8673
35	László Árpád Gergely, University of Szeged	48	19584
36	Mátyás Vasúth, MTA Wigner RCP	48	19139
37	Tamas Gombosi, <i>University of Michigan</i>	48	8528
38	Reka Albert, <i>Penn State</i>	47	39722
39	Zoltan Haiman, <i>Columbia University</i>	47	7812
40	Béla Merkely, Semmelweis University	46	26748
41	Zoltan Fodor, <i>University of Wuppertal</i> , Germany	45	10800
42	Attila T Lorincz, <i>Queen Mary University of London</i> , UK	45	9019
43	Sandor Batkai, Cardior Pharmaceutical GmbH	45	7514
44	Andras Kis, EPFL	44	28406
45	Peter Tompa, <i>VIB SBRC</i> , Brussels	44	10476
46	Jozsef Karger-Kocsis, Budapest University of Technology and Economics	44	8451
47	Gyorgy Hajnoczky, <i>Thomas Jefferson University</i>	44	7232
48	Tamas Dalmay, <i>University of East Anglia</i>	43	8182
49	Szekanecz Zoltán, University of Debrecen	43	7187
50	István Winkler, Hungarian Academy of Sciences	43	6855
51	Zsolt Radak, missing	43	5905
52	Sandor D Katz, Eotvos University	42	9530
53	Ferenc Nagy, Biological Research Centre	42	6255
54	Zsolt Demetrovics, Eötvös Loránd University	42	5407
55	Tamás Budavári, <i>Johns Hopkins University</i>	41	12469
56	Zoltán Molnár, missing	41	5561
57	Zoltan T. Nagy, <i>Royal Belgian Institute of Natural Sciences</i>	40	7212
58	Bardossy Andras, <i>Universität Stuttgart</i>	40	5249
59	Imre Dékány, University of Szeged	39	7729
60	Peter Csermely, Semmelweis University	39	7359
61	Csaba Szepesvari, <i>University of Alberta</i>	39	6926

62	Zoltan Takats, <i>Imperial College London</i>	39	6459
63	Michael J. Antal, <i>Hawaii Natural Energy Institute</i>	39	6294
64	Péter Ferdinandy, Semmelweis University	39	6273
65	Sandor Vajda, <i>Boston University</i>	39	6195
66	Ungar Tamas, Eötvös Loránd University, Hungary	39	5444
67	Andras Varro, University of Szeged	39	5049
68	Zoltan Szallasi, <i>Harvard Medical School</i>	38	13183
69	Janos Kertesz, Central European University	38	8416
70	Sandor Vajda, <i>Boston University</i> , missig	38	6144
71	Gabor Stepan, Budapest University of Technology and Economics	38	5598
72	John von Neumann, <i>Princeton University</i>	37	37138
73	György Gergely, Central European University, Budapest, Hungary	37	10999
74	Gabor Toth, <i>University of Michigan</i>	37	5035
75	Levente Buttyan, Budapest University of Technology and Economics	37	4976
76	Béla Pukánszky, Budapest University of Technology and Economics	37	4836
77	Laszlo Vigh, Biological Research Centre of HASc, Szeged, Hungary	37	4231
78	József Haller, missing	37	3764
79	Peter Denes, LBNL	36	6740
80	Béla Novák, <i>University of Oxford</i>	36	4764
81	Bela Suki, <i>Boston University</i>	36	4494
82	Bela Fejer, <i>Utah State University</i>	36	3836
83	Tamas Biro, University of Debrecen	36	3758
84	Laszlo Gondan, Eötvös Loránd University, Hungary	35	12490
85	Gyorgy Szabadkai, <i>University College London</i>	35	11467
86	Gabor Lugosi, <i>ICREA and Universitat Pompeu Fabra</i>	35	8077
87	László Vécsei, University of Szeged	35	6939
88	Lajos Kemény, University of Szeged	35	6198
89	Istvan Simon, Hungarian Academy of Sciences, Hungary	35	6095
90	Zoltan Dienes, <i>University of Sussex</i>	35	5658
91	János Fodor, Óbuda University	35	4996
92	Balázs Sarkadi, Hungarian Academy of Sciences,	35	4935
93	Attila G. Császár, Eötvös University	35	4774
94	Béla Novák, <i>University of Oxford</i>	35	4706
95	Zoltan Konya, University of Szeged	35	4677
96	Istvan Ulbert, Hungarian Academy of Sciences	35	4581
97	Zoltan N. Oltvai, <i>University of Pittsburgh</i>	34	12875
98	Balázs Gyórfy, Semmelweis University	34	5911
99	E. Sylvester Vizi, Hungarian Academy of Sciences	34	5753
100	Laszlo Nagy, University of Debrecen	34	5453
101	Tibor Hortobágyi, University of Szeged	34	5059
102	Gali Adám, Hungarian Academy of Sciences,	34	4830

	missing		
103	Katona Istvan, Hungarian Academy of Sciences	34	4742
104	Laszlo Otvos, <i>OLPE, LLC</i>	34	4512
105	József Burgyán, Mezőgazdasági Biotechnológiai Kutatóközpont, missing	34	4433
106	Zoltan Nusser, KOKI	34	4217
107	Judit Padisak, University of Pannonia	34	4212
108	Dániel Marx, Hungarian Academy of Sciences	34	4155
109	Adam Miklosi, Eötvös University	34	4121
110	Tibor Harkany, <i>Karolinska Institutet</i>	34	4066
111	Laszlo Virag, University of Debrecen	34	3531
112	Mihaly Hajos, <i>Yale University</i>	34	3034
113	Rudolf R. Sinkovics, <i>The University of Manchester</i>	33	8917
114	Béla Meleg, University of Pécs	33	8153
115	László Horváth, Óbuda University	33	5572
116	András Báldi, MTA Centre for Ecological Research	33	5041
117	Laszlo Peter Biro, Research Inst. for Tech. Physics and Mater. Science	33	4457
118	Béla Tóthmérész, University of Debrecen	33	4218
119	Zoltan H Endre, <i>University of Otago</i>	33	4024
120	Janos Szebeni, Semmelweis University	33	4001
121	Imre Vass, Hungarian Academy of Sciences	33	3459
122	George Szakacs, Budapest University of Technology and Economics	33	3458
123	Mihály Pósfai, University of Pannonia	33	3222
124	Andrea Petroczi, <i>Kingston University</i>	33	3155
125	Nándor Gábor Than, Hungarian Academy of Sciences	33	3028
126	Edit Buzas, missing	32	8207
127	Fulop Ferenc, missing	32	6665
128	janos kornai, Corvinus University	32	6027
129	András Falus, Semmelweis University	32	5726
130	Krisztián Bányai, MTA ATK AOTI	32	5598
131	Peter Batary, <i>Georg-August-University</i> , Germany	32	4536
132	Tamás Székely, <i>University of Bath</i> , UK	32	4474
133	Mihaly Horanyi, <i>University of Colorado</i>	32	4188
134	Prohaszka Zoltan, Semmelweis University	32	4087
135	Judit Hohmann, University of Szeged	32	3978
136	Laszlo Kiss, Hungarian Academy of Sciences	32	3902
137	Eva Kondorosí, Biological Research Centre	32	3762
138	Etelka Tombác, University of Szeged	32	3532
139	George Szakacs, Budapest University of Technology and Economics	32	3419
140	György Marosi, Budapest University of Technology and Economics	32	3276
141	Zsolt Liposits, Hungarian Academy of Sciences	32	3182
142	Endre Somorjai, MTA Atomki	32	2740
143	Tápai Márton, University of Szeged	31	14787

144	László Csiba, missing	31	6677
145	Andras Fiser, <i>Albert Einstein College of Medicine</i>	31	5902
146	Ilma R Korponay-Szabo, University of Debrecen	31	5129
147	András Schubert, Hungarian Academy of Sciences, missing	31	4778
148	István Rácz, Wigner RCP	31	4317
149	Mária A. Deli, Biological Research Centre, Szeged, Hungary	31	3731
150	József Varga, Budapest University of Technology and Economics	31	3690
151	Jeno Gubicza, Eötvös Loránd University	31	3370
152	Endre Suli, <i>University of Oxford</i>	31	3267
153	Attila Janos Mozer, <i>Intelligent Polymer Research Institute</i>	31	3204
154	Gábor Várhegyi, Hungarian Academy of Sciences	31	3191
155	Gyula Szegedi, University of Debrecen	31	2936
156	Katalin Mikecz, <i>Rush University Medical Center</i>	31	2726
157	Zoltan Ligeti, <i>Lawrence Berkely Lab</i>	30	13223
158	Istvan Edes, University of Debrecen	30	8366
159	Gyorgy Hutvagner, missing	30	6766
160	Loretta J. Mester, Federal Reserve Bank of Cleveland	30	4753
161	Csaba Pal, Biological Research Center, Hungary	30	3968
162	Antal Jakli, <i>Kent State university</i>	30	3551
163	Tamás Inspurger, Budapest University of Technology and Economics	30	3358
164	Szabolcs Kéri, Budapest University of Technology and Economics	30	3152
165	Tibor Torok, Predictive Science Inc.	30	2680
166	László Fésüs, University of Debrecen	29	8416
167	Gabor Juhasz, Hungarian Academy of Sciences	29	7910
168	Istvan Bitter, Semmelweis University	29	5622
169	Eors Szathmary, MTA Ecological Research Center	29	4778
170	Gabor Csanyi, <i>University of Cambridge</i>	29	3554
171	András Gelencsér, University of Pannonia	29	3511
172	Peter Szabó, Budapest University of Technology and Economics	29	3484
173	Jozsef Balla, University of Debrecen	29	3436
174	Peter Frankl, Hungarian Academy of Sciences	29	3250
175	Robert S. Balog, <i>Texas A&M University</i>	29	3215
176	Jozsef Timar, missing	29	3110
177	Laszlo Guzzi, Hungarian Academy of Sciences	29	2780
178	Zoltan Furedi, missing	29	2714
179	Julia Szekeres-Bartho, University of Pécs, Hungary	29	2617
180	Gyorgy Gyurky, MTA Atomki	29	2568
181	Andras Dinnyes, Szent Istvan University	29	2538
182	Barnabas Poczos, <i>Carnegie Mellon University</i>	29	2550
183	Paul Sandor, <i>University of Toronto</i>	28	10161
184	László Fésüs, University of Debrecen	28	8302

185	Endre Pap, <i>Univerzitet Singidunum</i>	28	5449
186	Tibor Palfai, missing	28	4204
187	Balázs Papp, Biological Research Centre, Szeged, Hungary	28	3904
188	Dénes Petz, Budapest University of Technology and Economics	28	3685
189	Akos Kukovecz, University of Szeged, Hungary	28	3377
190	Boldizsar Czech, University of Pécs	28	3326
191	Mihály Kállay, Budapest University of Technology and Economics	28	3117
192	Bettina Piko, University of Szeged, Hungary	28	3043
193	Peter Hegyi, University of Pécs, Hungary	28	2980
194	Beata Sperlagh, Hungarian Academy of Sciences	28	2813
195	Laszlo Bela Kish, <i>Texas A&M University</i> , missing	28	2797
196	Zoltan Furedi, missing	28	2726
197	Klivenyi Peter, University of Szeged	28	2660
198	Gabor Szabo, Institute of Experimental Medicine, Budapest, Hungary	28	2641
199	Puskas Laszlo G, HAS, Biological Research Center	28	2596
200	Vankó György, Hungarian Academy of Sciences	28	2507
201	Istvan Seri, Semmelweis University	28	2411
202	Gábor Czakó, University of Szeged	28	2178
203	Tom Gedeon, <i>Australian National University</i>	27	3053
204	Tamás Kerekes, <i>Aalborg University</i>	27	3501
205	Jozsef Baranyi, University of Debrecen	27	3498
206	János Hebling, University of Pécs	27	3304
207	György M. Keserű, Hungarian Academy of Sciences	27	3253
208	Andras Guttman, missing	27	2915
209	Balázs SÜMEGI, University of Pécs	27	2822
210	Gyozo Garab, Hungarian Academy of Sciences, Szeged, Hungary	27	2810
211	Gyula Kiss, MTA-PE Air Chemistry Research Group	27	2730
212	András Büki, University of Pécs	27	2585
213	Vankó György, Wigner Research Centre for Physics	27	2473
214	Sándor P. Fekete, <i>TU Braunschweig</i>	27	2418
215	Ilona Kovacs, Péter Pázmány Catholic University	27	2370
216	Jozsef Vinko, Hungarian Academy of Sciences	27	2276
217	Attila Szabo, Eötvös Loránd University, Hungary	27	2245
218	Elekes Zoltan, Institute for Nuclear Research (MTA Atomki)	27	2141
219	Mihály Józsi, MTA, Eötvös Loránd University	27	2022
220	Péter Gál, Hungarian Academy of Sciences	27	1938
221	Tibor Antal, <i>University of Edinburgh</i>	26	4891
222	György Csaba, Semmelweis University	26	3884
223	György Keglevich, Budapest University of Technology and Economics	26	3420
224	Jozsef Bokor, Hungarian Academy of Sciences	26	3329

225	Zsolt Tuza, University of Pannonia	26	3272
226	Sandor Szabo, missing	26	3015
227	Zoltan Mester, <i>National Research Council Canada</i>	26	2945
228	Gyorgy Csaba, Pázmány Péter Catholic University	26	2788
229	Zoltan Donko, Wigner Research Centre for Physics	26	2665
230	Komoly S, University of Pécs	26	2646
231	László Muszbek, University of Debrecen	26	2619
232	Márta Gácsi, Hungarian Academy of Sciences	26	2557
233	Szöllősi János, University of Debrecen	26	2472
234	Janos Podani, Eotvos University, missing	26	2468
235	Tamas Turanyi, Eötvös Loránd University	26	2369
236	Pál Frenger, Ericsson AB	26	2327
237	Róbert Urbán, Eötvös Loránd University	26	2240
238	László Gulácsi, Corvinus University, Hungary	26	2153
239	László Erdei, University of Szeged	26	1856
240	Erik Hrabovszky, Hungarian Academy of Sciences	26	1737
241	Gábor I. Csonka, Budapest University of Technology and Economics	25	5793
242	Botond Koszegi, Central European University	25	4985
243	Peter Lakatos, <i>Nathan Kline Institute</i>	25	4805
244	Andras Czirok, <i>Univeristy of Kansas Medical Center</i>	25	4754
245	Miklós Garami, Semmelweis University	25	4508
246	Agnes Kittel, Hungarian Academy of Sciences	25	4128
247	Attila Kovacs, <i>Smithsonian Astrophysical Observatory</i>	25	3278
248	Tamas Terlaky, <i>Lehigh University</i>	25	3026
249	Attila Sik, <i>University of Birmingham</i>	25	2876
250	Cserni Gábor, University of Szeged	25	2695
251	Attila Mekis, <i>Luxtera</i>	25	2628
252	Éva Hideg, University of Pécs	25	2612
253	Tibor Czigany, Budapest University of Technology and Economics	25	2569
254	András Berta, University of Debrecen	25	2497
255	János Török, Eötvös Loránd Tudományegyetem	25	2421
256	Andras Gruber, Semmelweis University	25	2417
257	Miklós Geiszt, Semmelweis University	25	2158
258	Imre Takac, Dynamita	25	2092
259	Eniko Kubinyi, Eötvös Loránd University	25	1871
260	Tamás Csont, University of Szeged	25	1849
261	Tamás Vértesi, MTA Atommagkutató Intézet	25	1820
262	Róbert E. Gyurcsányi, Budapest University of Technology and Economics	25	1782
263	Ilona Sarvari Horvath, <i>University of Borås</i>	25	1635
264	Gabor Banhegyi, Semmelweis University	24	7570
265	Szabolcs Borsanyi, <i>Bergische Universität Wuppertal</i>	24	4184
266	Beatrix Dienes, University of Debrecen	24	3150
267	Zoltan Kunszt, <i>Institute for Theoretical Physics,</i>	24	2920

	ETH, Zurich		
268	Peter Baranyi, Szechenyi Istvan University	24	2904
269	Karoly Heberger, Hungarian Academy of Sciences	24	2796
270	Zoltán Papp, University of Debrecen	24	2741
271	Balla György, University of Debrecen	24	2619
272	Endre Nagy, University of Pannonia	24	2604
273	György Paragh, University of Debrecen	24	2520
274	Domonkos Tikk, Gravity R&D	24	2487
275	Lajos Diósi, Wigner Research Centre for Physics, Hungary	24	2444
276	Balazs Harrach, Hungarian Academy of Sciences	24	2430
277	Jozsef Janszky, Pécsi Tudományegyetem	24	2396
278	Imre Vida, Charité – <i>Universitätsmedizin Berlin</i> , DE	24	2303
279	Andras Gyarfás, Hungarian Academy of Sciences	24	2283
280	Attila I. Gulyas, Hungarian Academy of Sciences	24	2263
281	T Doczi, missing	24	2192
282	László Gránásy, Wigner RCP	24	2174
283	Tótsaki Árpád, Debreceni Egyetem (University of Debrecen)	24	2116
284	Peter Bai, University of Debrecen	24	2115
285	Záray Gyula, Eötvös Loránd Tudományegyetem	24	2027
286	Éva Kiss, University of Szeged	24	2015
287	Eva Rajnavolgyi, University of Debrecen	24	1977
288	Peter S. Sandor, <i>Universität Zürich</i>	24	1964
289	Irma Tari, University of Szeged	24	1920
290	Gyorgy Vereb, University of Debrecen	24	1912
291	Sandor Beniczka, <i>Aarhus University</i>	24	1716
292	Joseph Najbauer, University of Pécs, Hungary	24	1684
293	Gyula Kovacs, <i>Friedrich Schiller University Jena</i>	24	1597
294	Peter J. Toth, University of Pecs	24	1543
295	Tamás Forster, University of Szeged	23	6668
296	Tibor Dunai, <i>Universität zu Köln</i>	23	2997
297	Mark Jelasić, University of Szeged	23	2711
298	Dániel Aradi, Semmelweis University, Hungary	23	2425
299	Tamas Tel, Eotvos University	23	2212
300	Attila Tarnok, <i>University Leipzig</i>	23	2103
301	Tibor Hartel, <i>Babeş-Bolyai University</i>	23	2091
302	Imre Barany, Renyi Institute, Hungary	23	1940
303	László Szunyogh, Budapest University of Technology and Economics	23	1909
304	András Hoffer, MTA-PE Air Chemistry Research Group	23	1893
305	András Liker, University of Pannonia	23	1845
306	Tibor Magura, University of Debrecen	23	1832

307	George Kaptay, University of Miskolc	23	1821
308	Zoltan Rakonczay Jr., University of Szeged	23	1814
309	Attila Molvarec, Semmelweis University, Hungary	23	1810
310	Judit Ovadi, Hungarian Academy of Sciences	23	1741
311	Laszlo Pathy, Institute of Enzymology, Budapest, Hungary	23	1690
312	Bence Kocsis, Eotvos Lorand University	23	1642
313	László Orbán, University of Pannonia	23	1593
314	Nándor Nemestóthy, University of Pannonia	23	1549
315	Dezső Boda, University of Pannonia, Hungary	23	1521
316	Tamás Pusztai, Wigner Research Centre for Physics	23	1506
317	Sándor Hornok, University of Veterinary Medicine, Budapest	23	1416
318	Mihály Braun, Atomki, Debrecen, Hungary	23	1324
319	Pál Maurovich-Horvat, Semmelweis University	22	7445
320	Pál Géher, Semmelweis University	22	3068
321	Laszlo Monostori, Computer and Automation research Institute	22	3020
322	Robert Fullér, Széchenyi István University	22	2715
323	Imre J. Rudas, Óbuda University	22	2587
324	Gábor E. Tusnády, Institute of Enzymology, RCNS, HAS	22	2286
325	Tibor A Rauch, <i>Rush University Medical Center</i>	22	2151
326	István Pócsi, University of Debrecen	22	2020
327	Pál Sümegi, University of Szeged	22	1955
328	Attila Kereszt, Biological Research Centre HAS	22	1922
329	Valentina Kutiyfa, <i>University of Rochester</i>	22	1890
330	Gabor Tardos, Hungarian Academy of Sciences	22	1866
331	Miklos Telek, Budapest University of Technology and Economics	22	1846
332	Martin Pál, Google, Inc.	22	1841
333	Ferenc Jordan, MTA Centre for Ecological Research, Budapest, Hungary	22	1805
334	Klara Hernadi, University of Szeged, missing	22	1770
335	László Kredics, University of Szeged	22	1727
336	Péter Nánási, University of Debrecen	22	1699
337	Tamás Takács, University of Szeged	22	1645
348	Salma Imre, Eötvös Loránd University	22	1622
339	Laszlo Buday, Institute of Enzymology	22	1548
340	Zoltan Giricz, Semmelweis University	22	1528
341	Tibor Valyi-Nagy, <i>University of Illinois at Chicago</i>	22	1515
342	Albert Oszkó, University of Szeged	22	1503
343	Attila Bacsi, University of Debrecen, missing	22	1480
344	Tamas Varga, <i>Pacific Northwest National Laboratory</i>	22	1428
345	Ferenc Gallyas, University of Pécs, Hungary	22	1406

346	Laszlo Orfi, Semmelweis University	22	1262
347	Beata G. Vertessy, Hungarian Academy of Sciences	21	6989
348	Tamás Nepusz, Eötvös Loránd University	21	6199
349	László Györfi, Budapest University of Technology and Economics	21	3807
350	Tamas Papp, MTA TKI	21	3719
351	Tamas Szabo, University of Szeged	21	3374
352	Miklos Maroti, University of Szeged	21	2833
353	Barnabas Bede, Óbuda University	21	2648
354	Endre Boros, <i>Rutgers University</i>	21	2429
355	Gabor L Lovei, <i>Aarhus University</i>	21	2398
356	Attila Molnar, <i>University of Edinburgh</i>	21	2352
357	Tibor Braun, Hungarian Academy of Sciences	21	2231
358	Gyuri Wolf, Wigner RCP	21	2201
359	Borbely Andras, <i>MINES Saint-Etienne</i>	21	2038
360	Peter Domokos, Wigner Research Centre	21	1952
361	Ferenc Bari, University of Szeged	21	1911
362	József Tihanyi, University of Physical Education	21	1869
363	Kacsuk Péter, MTA SZTAKI	21	1860
364	László Tiszlavicz, University of Szeged,	21	1848
365	Istvan Krizbai, Biological Research Centre	21	1776
366	Árpád Baricz, <i>Babes-Bolyai University</i>	21	1762
367	Kornel Kovacs, University of Szeged	21	1724
368	Szántó Sándor, Debreceni Egyetem	21	1705
369	Attila Gacser, University of Szeged	21	1630
370	Gábor Rákhely, University of Szeged	21	1624
371	László Virág, University of Szeged	21	1618
372	Gergely Maroti, Hungarian Academy of Sciences, Szeged, missing	21	1611
373	pal ormos, MTA SZBK, missing	21	1565
374	Tamás Martinek, University of Szeged, missing	21	1563
375	Markus J. Tamás, <i>University of Gothenburg</i> , missing	21	1543
376	Zarand Gergely, Budapest University of Technology and Economics	21	1540
377	Magda Antal, missing	21	1528
378	Dr. Mihaly Boros, University of Szeged, missing	21	1482
379	Tibor Erős, Hungarian Academy of Sciences, missing	21	1481
380	Tamas Gaal, <i>university of wisconsin</i> , missing	21	1367
381	Szabolcs Béni, Semmelweis University, missing	21	1288
382	Péter Pongrácz, Eötvös Loránd University, missing	21	1198
383	Imre Kacsokovics, Eötvös Loránd University, missing	21	1126
384	Gyula Mester, Óbuda University, Hungary, ORCID: 0000-0001-7796-2820	21	1006
385	György Panyi, University of Debrecen, Hungary	21	959
386	Tamas Korcsmaros, <i>Earlham Institute</i>	20	7145
387	Imre Derenyi, Eotvos University, Hungary	20	4881

388	László Molnár, Hungarian Academy of Sciences	20	4744
389	Janos Korner, <i>University of Rome</i>	20	4601
390	Tamas Papp, MTA TKI	20	3680
391	János Aczél, University of Debrecen	20	2921
392	Gábor Kovács, University of Pécs	20	2321
393	Tamas Belgya, Centre for Energy Research, Hungary	20	2274
394	Laszlo Huber, missing	20	2255
395	Tamas Keviczky, <i>Delft University of Technology</i> , missing	20	2036
396	Attila Horváth, missing	20	1983
397	Gábor Halmos, University of Debrecen	20	1922
398	Janos Abonyi, University of Pannonia	20	1901
399	Zoltán G. Soos, <i>Princeton University</i> , USA	20	1854
400	GS Reusz, Semmelweis University	20	1837
401	József Tózsér, University of Debrecen	20	1762
402	Sándor J Kovács, <i>Washington University</i>	20	1664
403	Szabolcs Lengyel, Hungarian Academy of Sciences	20	1662
404	Gábor Rákhely, University of Szeged	20	1598
405	Janos Nemeth, Semmelweis University	20	1587
406	Attila Szanto, missing	20	1578
407	Attila Reményi, Research Center for Natural Sciences, missing	20	1567
408	Imre Sovago, University of Debrecen	20	1559
409	Antus Sándor, University of Debrecen	20	1555
410	János Timár, MTA Atomki	20	1537
411	Endre Horvath, <i>Ecole Polytechnique Federale de Lausanne</i>	20	1499
412	Biró Tamás Sándor, Wigner Research Centre for Physics	20	1423
413	A. Marcell Szasz, missing	20	1382
414	Karlo Penc, Wigner Research Centre for Physics	20	1380
415	István Ráth, Budapest University of Technology and Economics	20	1361
416	Anna Erdei, Eötvös Loránd University, Hungary	20	1292
417	László Biczók, Hungarian Academy of Sciences, Hungary	20	1284
418	Isván Kézsmárki, Budapest University of Technology and Economics	20	1278
419	Tamas Banyasz, University of Debrecen	20	1271
420	János A. Bergou, University of Pécs	20	1229
421	Gábor Borics, MTA Centre for Ecological Research	20	1226
422	László Poppe, Budapest University of Technology and Economics	20	1214
423	Péter Bakonyi, University of Pannonia, Hungary	20	1211
424	Bence Béky, <i>Harvard University</i>	20	1207
425	Tibor Macko, <i>Scientist at Fraunhofer Institute LBF</i>	20	1185
426	George Horvai, Budapest University of Technology	20	1170

	and Economics		
427	József Kaszaki, University of Szeged	20	1155
428	Jozsef Halasz, Obuda University	20	1148
429	Valeria Guzsvany, <i>University of Novi Sad</i>	20	1133
430	Balazs Deak, University of Debrecen	20	1108
431	Orsolya Valkó, University of Debrecen	20	1104
432	Zsófia Nemoda, Semmelweis University	20	1021
433	Peter Antal Szalmas, University of Debrecen	20	1008
434	Szilvia Veszelka, Biological Research Centre, Szeged, Hungary	20	984
435	György Vámosi, University of Debrecen	20	920
436	Attila Varga, University of Pécs	19	3381
437	Jozsef Fiser, Central European University	19	2501
438	Árpád Molnár, University of Szeged	19	2441
439	Attila Felinger, University of Pécs	19	2044
440	Katalin Szlavecz, <i>Johns Hopkins University</i>	19	1752
441	Tibor Gyimothy, University of Szeged, Hungary	19	1717
442	Brodzsky Valentin, Corvinus University	19	1677
443	Imre Fertő, Hungarian Academy of Sciences	19	1668
444	Zsuzsanna Bata-Csorgo, University of Szeged	19	1663
445	Rudolf Ferenc, University of Szeged	19	1631
446	József Sándor, <i>Babeş-Bolyai University</i> , Romania	19	1610
447	Sándor Damjanovich, University of Debrecen	19	1542
448	Varga Lajos Károly, Wigner Research Centre for Physics	19	1513
449	Balazs Dora, Budapest University of Technology and Economics	19	1488
450	István Groma, Eötvös Loránd University	19	1418
451	Attila Csikasz-Nagy, <i>King's College London</i> , UK	19	1414
452	Laszlo Tretter, Semmelweis University	19	1412
453	Endre Kiss-Toth, <i>University of sheffield</i>	19	1404
454	Katalin Hangos, Computer and Automation Research Institute	19	1384
455	Dán Ádám, missing	19	1367
456	Dénes Schmera, Hungarian Academy of Sciences	19	1357
457	Attila Tóth, University of Debrecen	19	1346
458	Attila Köfalvi, Center for Neuroscience and Cell Biology	19	1332
459	Istvan Ando Istvan, Hungarian Academy of Science	19	1312
460	Peter Igaz, Semmelweis University	19	1286
461	Gombos Zoltan, Hungarian Academy of Sciences	19	1284
462	Peter Igaz, Semmelweis University	19	1274
463	Janos Tapolcai, Budapest University of Technology and Economics	19	1270
464	László Biczók, Hungarian Academy of Sciences	19	1268
465	Antal Koos, MTA EK MFA	19	1252
466	Bódizs Róbert, Semmelweis University	19	1250
467	Peter Balazs, <i>Austrian Academy of Sciences</i>	19	1177

468	Zvara Ágnes, missing	19	1118
469	János Magyar, University of Debrecen	19	1105
470	András Szabó, Semmelweis University	19	1088
471	Imre Miklos Szilagyi, Budapest University of Technology and Economics	19	1080
472	György Csóka, Erdészeti Tudományos Intézet	19	1052
473	Gábor Gyula Kiss, ATOMKI	19	1019
474	József Pálffy, Eötvös Loránd University	19	1012
475	Tamás Sréter, National Food Chain Safety Office	19	1002
476	Sandor Bartha, Hungarian Academy of Sciences	19	971
477	Levente Balogh, <i>Queen's University</i>	19	967
478	Vilmos Simon, Budapest University of Technology and Economics, Hungary, Orcid: 0000-0002-8227-4464.	19	786
479	Illés Farkas, Eotvos University	18	7499
480	eva pallinger, Semmelweis University	18	3269
481	András Arató, Semmelweis University	18	2573
482	Árpád Molnár, University of Szeged	18	2404
483	Maria Barna, <i>Stanford University</i>	18	2216
484	Attila Feher, Hungarian Academy of Sciences	18	2057
485	Mihály Bartók, University of Szeged	18	1952
486	Gyorgy Posfai, Biol Res Centre Hung Acad Sci, Szeged	18	1899
487	József K. Tar, Óbuda University	18	1820
488	Erika Koltai, University of Physical Education	18	1786
489	Peter Gaspar, Computer and Automation Research Institute	18	1568
490	Lajos Rozsa, Hungarian Academy of Sciences	18	1521
491	Gábor Varga, Semmelweis University	18	1477
492	Gábor B Makara, Magyar Tudományos Akadémia	18	1343
493	Laszlo Kozma-Bognar, missing	18	1324
494	Csaba Szekely, Hungarian Academy of Sciences	18	1307
495	Attila Nemes, <i>Norwegian Institute of Bioeconomy Research</i>	18	1304
496	Peter Erdi, <i>Kalamazoo College</i>	18	1301
497	Gyula Tircso, University of Debrecen	18	1274
498	Miklos Kellermayer, Semmelweis University	18	1258
499	Zoltan Kiraly, Plant Protection Institute	18	1249
500	Livija Cveticanin, Óbuda University, Hungary, Orcid: 0000-0002-1061-4685	18	1258

3 Conclusions

Ranking list of best 500 Hungarian reseaches in natural sciences, techniques and human sciences of is presented, The ranking is made based primary on h5-index and citation number based on the database in Google Scholar. Hungarian

researches ranked first by h5-index in decreasing order and then by the number of citations.

References

- [1] Hirsch, J.E.: An index to quantify an individual's scientific research output. *Proceedings of the National Academy of Sciences of the United States of America* 102(46), pp. 16569-16572, 2005, <http://dx.doi.org/10.1073/pnas.0507655102>
- [2] <https://scholar.google.com>, accessed 20th November, 2018.
- [3] Mester Gyula, Honlap szerkesztése Google Tudós alkalmazásával, *Magyar Tudomány Napja a Délvidéken 2013*, (november 23), Vajdasági Magyar Tudományos társaság, pp. 674-679, ISBN 978-86-88077-06-4, Újvidék, Szerbia, 2014.
- [4] Gyula Mester, Rankings Scientists, Journals and Countries Using h-index, *Interdisciplinary Description of Complex Systems, Croatian Interdisciplinary Society*, Vol. 14, No. 1, ISSN 1334-4684, DOI: 10.7906/indecs.14.1.1, pp. 1-9, 2016.
- [5] Gyula Mester, Merenje rezultata naučnog rada, pp. 445-453, *Tehnika-Mašinstvo* 64, 3, ISSN 0040-2176, Beograd, Srbija, 2015.
- [6] Gyula Mester, Academic Ranking of World Universities 2009/2010, Vol. 7, No. 1, pp. 44-47, *Ipsi Journal, Transactions on Internet Research, TIR*, ISSN 1820 - 4503, New York, Frankfurt, Tokyo, Belgrade, 2011.
- [7] Gyula Mester, Aleksandar Rodic, Sensor-Based Intelligent Mobile Robot Navigation in Unknown Environments, *International Journal of Electrical and Computer Engineering Systems*, Vol. 1, No. 2, pp. 1-8, ISSN: 1847-6996, 2010.
- [8] Gyula Mester, New Trends in Scientometrics, *Proceedings of the SIP 2015, 33rd International Conference Science in Practice*, pp. 22-27, Schweinfurt, Germany, 07-08.05.2015.
- [9] Gyula Mester, Rangiranje svetskih univerziteta na bazi citata iz Google Scholar, *TREND 2017, XXIII Skup Trendovi Razvoja, Položaj visokog Obrazovanja i Nauke u Srbiji, Zbornik radova*, Ed. Vladimir Katic, paper No. T2.2-2, pp. 265-268, ISBN 978-86-7892-904-5, Zlatibor, Serbia, 22. - 24.02. 2017.
- [10] Gyula Mester, Naučnometrijski indeksi - primena u robotici, *Zbornik radova ETRAN 2015, 59. konferencija za elektroniku, telekomunikacije, računarstvo, automatiku i nuklearnu tehniku, EDU 1.1*, pp. 1-6, ISBN 978-86-80509-71-6, Srebrno Jezero, Serbia, 08 - 11. 06. 2015.
- [11] Gyula Mester, Novi trendovi naučne metrike, *Proceedings of the XXI Skup Trendovi Razvoja, Univerzitet u Promenama...*, paper No. UP 1-3, pp. 23-30, ISBN 978-86-7892-680-8 DOI: 10.13140/RG.2.1.1754.2486, Zlatibor, Serbia, 23. - 26. 02. 2015.
- [12] Mester Gyula, Új tudományos eredmények mérése, *Konferencia kiadvány XXX. Kandó konferencia*, pp.1-10, ISBN 978-615-5460-24-1, Budapest, november 20, 2014.

The Evaluation of the Impact Factor of the Journal Interdisciplinary Description of Complex Systems

Gyula Mester

Óbuda University, Doctoral School of Safety and Security Sciences, Népszínház utca 8, 1081, Budapest, Hungary, drmestergyula@gmail.

Abstract: The Science Citation Index (SCI®) was first presented in Science in 1955. The Science Citation Index was launched in 1964 and the Annual SCI Journal Citation Reports were officially launched in 1975. The SCI's multidisciplinary database has two purposes: first, to identify what each scientist has published, and second, where and how often the papers by that scientist are cited. Hence, the SCI has always been divided into two author-based parts: the Source Author Index and the Citation Index. The Web of Science® (WoS)—the SCI's electronic version—links these two functions: an author's publication can be listed by chronology, by journal, or by citation frequency. The impact factor was devised by Eugene Garfield: in any given year, the impact factor of a journal is the number of citations, received in that year, of articles published in that journal during the two preceding years, divided by the total number of articles published in that journal during the two preceding years.

In this paper the definition of the impact factor has been implemented on the evaluation of the impact factor of the journal Interdisciplinary Description of Complex Systems. Finally, the value of the impact factor for the journal is presented.

Keywords: Science Citation Index, Journal Citation Reports, Source Author Index, Web of Science, impact factor, Interdisciplinary Description of Complex Systems

1 Introduction

The Science Citation Index (SCI®) was first presented in Science in 1955 [1]. The SCI's multidisciplinary database has two purposes: first, to identify what each scientist has published, and second, where and how often the papers by that scientist are cited.

Hence, the SCI has always been divided into two author-based parts: the Source Author Index and the Citation Index. By extension, one can also determine what each institution and country has published and how often their papers are cited. The Web of Science® (WoS)—the SCI's electronic version—links these two functions: an author's publication can be listed by chronology, by journal, or by citation frequency.

The Science Citation Index was launched in 1964 and the Annual SCI Journal Citation Reports were officially launched in 1975.

The impact factor was devised by Eugene Garfield [1]: in any given year, the impact factor of a journal is the number of citations, received in that year, of articles published in that journal during the two preceding years, divided by the total number of articles published in that journal during the two preceding years [2], [3], [4].

In this paper the definition of the impact factor has been implemented on the evaluation of the impact factor of the journal: Interdisciplinary Description of Complex Systems. Finally, the value of the impact factor for the journal in 2017 is presented.

The paper is organized as follows:

Section 1: Introduction.

In Section 2 Definition of the Clarivate Analytics Impact Factor is illustrated.

In Section 3 the Impact Factor calculation for journal Interdisciplinary Description of Complex Systems is presented.

Conclusions are given in Section 4.

2 Definition of the Clarivate Analytics Impact Factor

The impact factor of a journal is calculated by dividing the number of current year citations to the source items published in that journal during the previous two years [5].

The essential information about the Impact Factor on Clarivate Analytic's website [4]: <https://clarivate.com/essays/impact-factor/>.

The impact factor is useful in clarifying the significance of absolute (or total) citation frequencies. It eliminates some of the bias of such counts which favor large journals over small ones, or frequently issued journals over less frequently issued ones, and of older journals over newer ones. Particularly in the latter case such journals have a larger citable body of literature than smaller or younger journals. All things being equal, the larger the number of previously published articles, the more often a journal will be cited [6-14].

3 The Impact Factor Calculation of the Journal Interdisciplinary Description of Complex Systems 2017

The Impact Factor calculation of the journal Interdisciplinary Description of Complex Systems 2017 is based on the »Definition of the Clarivate Analytics Impact Factor« and on the essential information about the Clarivate Analytic's website:

<https://clarivate.com/products/web-of-science/>

Starting with the Web of Science page for the journal Interdisciplinary Description of Complex Systems (Figure 1, 2):

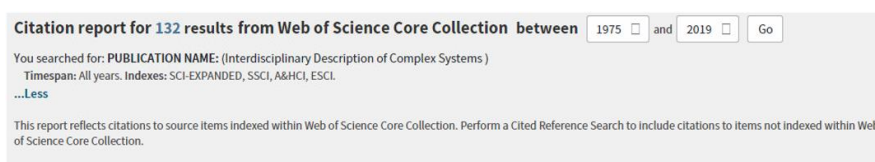


Figure 1

Web of Science page for the journal Interdisciplinary Description of Complex Systems

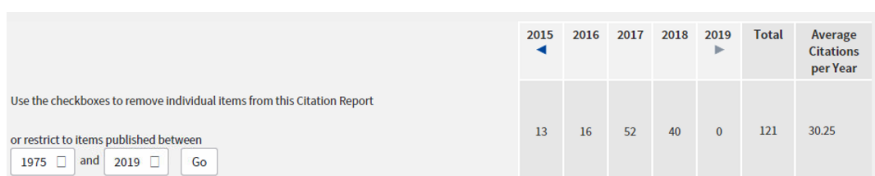


Figure 2

Web of Science presentation of total citations of the journal Interdisciplinary Description of Complex Systems

Interdisciplinary Description of Complex Systems impact factor IDECS 2017 calculation:

The 2017 impact factor of a journal is calculated by dividing the number of current year – 2017 - citations to the source items published in that journal during the previous two years: 2015 and 2016.

Total citations in 2017:

$$A_{\text{Indexs Total Citations 2017}} = 52$$

2017 citations to papers published in 2015+2016:

$$B_{\text{Indexs Citations 2017/2015+2106}} = 49$$

The number of papers published in 2015+2016:

$$C_{\text{Indecs articles 2015+2106}} = 83$$

Finally, the 2017 Impact Factor of the journal Interdisciplinary Description of Complex Systems (Indecs) is the following:

$$IF_{\text{Indecs 2017}} = (B_{\text{Indecs Citations 2017/2015+2106}}) / C_{\text{Indecs articles 2015+2106}} = 49/83$$

$$IF_{\text{Indecs 2017}} = \mathbf{0.590}$$

The Legend of the journal Interdisciplinary Description of Complex Systems (Indecs) is the following:

$A_{\text{Indecs Total Citations 2017}}$:	total citations in 2017
$B_{\text{Indecs Citations 2017/2015+2106}}$:	2017 citations to papers published in 2015+2016 (this is a subset of A)
$C_{\text{Indecs Papers 2015+2106}}$:	number of articles published in 2015+2016
$IF_{\text{Indecs 2017}}$:	2017 Interdisciplinary Description of Complex Systems Impact Factor.

Since the journal Interdisciplinary Description of Complex Systems is not in the 2017 impact factor journal list, it follows that this is the Clarivate Analytics error!

4 Conclusions

This paper presents the evaluation of the impact factor of the journal Interdisciplinary Description of Complex Systems.

The impact factor is a very useful tool for evaluation of journals, but it must be used discreetly. Definition of the Clarivate Analytics impact factor and the calculation for journal Interdisciplinary Description of Complex Systems impact factor is illustrated.

The definition of the impact factor has been implemented on the evaluation of the impact factor of the journal Interdisciplinary Description of Complex Systems. Finally, the value of the 2017 impact factor of the journal Interdisciplinary Description of Complex Systems is presented

References

- [1] Eugene Garfield, Citation indexes for science: a new dimension in documentation through association of ideas, *Science*, 122, 1955, pp.108-111.
- [2] Eugene Garfield, Citation indexing for studying science. *Nature* 227, 1970, pp. 669-71.

- [3] Eugene Garfield, Citation analysis as a tool in journal evaluation. *Science* 178, 1972, pp. 471-479.
- [4] <https://clarivate.com/essays/impact-factor/>
- [5] Gyula Mester, The valuation of the Impact Factor of the Journal *Acta Polytechnica Hungarica*, Proceedings of the TREND 2011, ISBN 978-86-7892-323-4, Kopaonik, Serbia, 07-10.03.2011, pp. 70-73.
- [4] Gyula Mester, Rankings Scientists, Journals and Countries Using h-index, *Interdisciplinary Description of Complex Systems*, Croatian Interdisciplinary Society, Vol. 14, No. 1, ISSN 1334-4684, DOI: 10.7906/indec.14.1.1, pp. 1-9, 2016.
- [5] Gyula Mester, Merenje rezultata naučnog rada, pp. 445-453, *Tehnika-Mašinstvo* 64, 3, ISSN 0040-2176, Beograd, Srbija, 2015.
- [6] Gyula Mester, Academic Ranking of World Universities 2009/2010, Vol. 7, No. 1, pp. 44-47, *Ipsi Journal*, Transactions on Internet Research, TIR, ISSN 1820 - 4503, New York, Frankfurt, Tokyo, Belgrade, 2011.
- [7] Gyula Mester, Aleksandar Rodic, Sensor-Based Intelligent Mobile Robot Navigation in Unknown Environments, *International Journal of Electrical and Computer Engineering Systems*, Vol. 1, No. 2, pp. 1-8, ISSN: 1847-6996, 2010.
- [8] Gyula Mester, New Trends in Scientometrics, Proceedings of the SIP 2015, 33rd International Conference Science in Practice, pp. 22-27, Schweinfurt, Germany, 07-08.05.2015.
- [9] Gyula Mester, Rangiranje svetskih univerziteta na bazi citata iz Google Scholar, TREND 2017, XXIII Skup Trendovi Razvoja, Položaj visokog Obrazovanja i Nauke u Srbiji, Zbornik radova, Ed. Vladimir Katic, paper No. T2.2-2, pp. 265-268, ISBN 978-86-7892-904-5, Zlatibor, Serbia, 22. - 24.02. 2017.
- [10] Gyula Mester, Naučometrijski indeksi - primena u robotici, Zbornik radova ETRAN 2015, 59. konferencija za elektroniku, telekomunikacije, računarstvo, automatiku i nuklearnu tehniku, EDU 1.1, pp. 1-6, ISBN 978-86-80509-71-6, Srebrno Jezero, Serbia, 08 - 11. 06. 2015.
- [11] Gyula Mester, Novi trendovi naučne metrike, Proceedings of the XXI Skup Trendovi Razvoja, Univerzitet u Promenama..., paper No. UP 1-3, pp. 23-30, ISBN 978-86-7892-680-8 DOI: 10.13140/RG.2.1.1754.2486, Zlatibor, Serbia, 23. - 26. 02. 2015.
- [12] Mester Gyula, Új tudományos eredmények mérése, Konferencia kiadvány XXX. Kandó konferencia, pp.1-10, ISBN 978-615-5460-24-1, Budapest, november 20, 2014.
- [13] Gyula Mester, Metode naučne metrike i rangiranja naučnih rezultata, Proceedings of 57th ETRAN Conference, pp. RO3.5.1-3, Zlatibor, 3-6. juna 2013.
- [14] Gyula Mester, Massive Open Online Courses in Education of Robotics, *Interdisciplinary Description of Complex Systems*, pp. 182-187, Vol. 14, No. 2, ISSN 1334-4684, e-ISSN 1334-4676, DOI: 10.7906/indec.14.2.7, 2016.

Experimental investigation of the temperature dependence of the air-gap flux density in a permanent magnet synchronous machine

János Füzési

Óbuda University, Kálmán Kandó Faculty of Electrical Engineering, Bécsi út 94-96., 1034 Budapest, Hungary, fuzesi.janos@gmail.com

István Vajda, DSc

Óbuda University, Institute of Automation, Bécsi út 94-96., 1034 Budapest, Hungary, vajda@uni-obuda.hu

István Laczkó

A.O. Smith Hungary Kft. (former EVIG), Gyömrői út 150., 1103 Budapest, Hungary, istvan.laczko@gmail.com

The condition of the machine can be determined by diagnostic investigation of air-gap flux density in electric motors. The most practical tool for investigating magnetic fields in electric motors seems to be the Hall-cell. However, due to its size and its problematic positioning, it cannot be applied in electric machines of medium size with radial air-gap smaller than ~ 1 mm. The aim of the current research is the experimental investigation of the induction distribution that occurs in the air-gap, using a permanent magnet synchronous motor with increased air-gap. The prior determination of the expected parameter values took place prior to the measurement by means of finite element simulations. Based on these results, we assume that the temperature values can be calculated on the basis of the change in the air-gap induction, which is investigated by means of the currently elaborated procedure. In the experiment, a Hall-cell was positioned at a fix point of the air-gap. The measurement was carried out during rotation. The curve of points measured this way does not indicate the spatial distribution of the static air-gap induction, rather it shows the temporal change of the induction at the given measurement point. However several points of this measurements can represent the spatial distribution of the air gap magnetic field. In the series of measurements, the investigated machine was homogeneously heated in a laboratory furnace until it reached 90 Celsius degrees, while the temporal change of the induction was recorded at several measurement points. The air-gap induction decreased with the increment of the temperature. The correction of the measurement points was carried out in accordance with the temperature coefficient of the Hall voltage. The extent of changes due to the increasing temperature slightly differ from the simulation results. A possible reason for this might be the wide tolerance range of the B-H curve of the applied magnets. The aim of the research, i.e. determining the

temperature of active parts of the electric machine based on the direct measurement of the air-gap, is feasible. The future aim of the research is to improve the measurement setup by eliminating problems that negatively influence accuracy.

Keywords: air-gap, magnetic flux density, electromagnetic field analysis, temperature rise, synchronous machines, permanent magnets, Hall sensor, finite-element computations

1. Introduction

Direct measurement of magnetic flux in the air gap is a relatively new method, by means of which the rotating magnetic field can be measured in the air gap in a coordinate system fixed to the stator. Most of the papers focused on the standard industrial 3 phase asynchronous motors [1][2].

Using Hall-sensors for measurement is the best solution for economical and usability reasons. A wide range of measuring devices exists [3], but due to the relatively high measuring range (0...1 Tesla) and the required small size, the Hall-sensor is considered the best suitable tool.

The application of Hall-sensors was made possible by the fact that the size of the sensors is comparable to the radial air-gap of larger induction motors, and their price is also acceptable. Nonetheless, the size of the radial air gap of motors widely used in industry is below 0.5 mm, which is too small for direct air gap flux measurements by means of Hall-sensors available on the market.

In the experimental setup, the synchronous machine originally was a standard 3 phase industrial induction machine with aluminium squirrel cage rotor. In order to obtain more advantageous conditions for the measurements, it was modified to a permanent magnet synchronous machine. In this paper, we are introducing our first investigation, the effect of temperature rising to the permanent magnets. The question is whether we are able to determine the permanent magnets temperature parameters.

2. Methods

2.1. Introduction of the studied machine

The nominal parameters of the original induction motor prior to the modifications are shown in Table 1. This machine had a single-layer concentric winding, all the coppers has been removed.

Table 1.
Parameters of original induction machine

Induction motor: 4AM 63B 4			
Parameter		Values	Units
P_n	Rated power	0,37	kW
U_n	Nominal voltage	Δ/Y 380/220	V
I_n	Nominal current	2,08/1,20	A
n_n	Rated speed	1320	min^{-1}
$\cos\phi_n$	Rated power factor	0,69	-
η_n	Rated efficiency	68	%
Z_1	Number of stator slots	24	-
D	Stator hole diameter	61,45	mm
l	Active length of iron core	73	mm
δ	Original radial air-gap	0,3	mm

The squirrel cage rotor had also been removed and replaced with a newly made permanent magnet rotor which is shown in Figure 1.

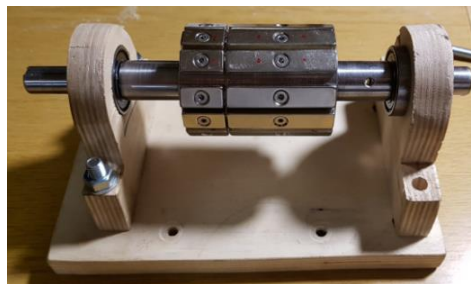


Figure 1.
New rotor with magnets

Due to some practical reasons, the motor bearing shields have been replaced to a bracket type bearing house. All physical parameters of the active parts of the motor have been measured. The new machine parameters were calculated on the basis of the article of J. Varga *et al.* [4]. In order to operate a permanent magnet

synchronous machine, it is required to use an electronic driver circuit. The driver has 24V output voltage, so the new stator parameters was determined in accordance with this requirement. Figure 2. shows the new 2 dimensional drawing of the re-designed machine.

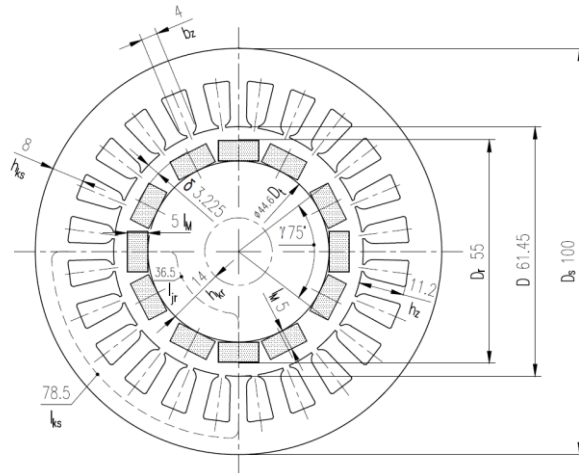


Figure 2.
Dimensional drawing of the magnetic circuit

Similarly to the original version, the synchronous machine also has a single layer concentric winding, schematically shown in Figure 3.

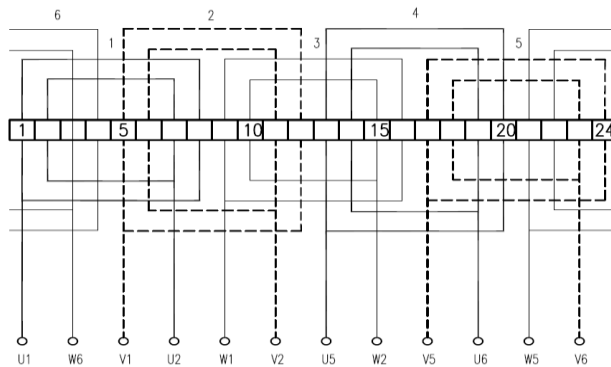


Figure 3.
Stator winding schematics

Moreover, the field in the machine has been computed by using a finite element representation in FEMM 4.2 software, shown in Figure 4.

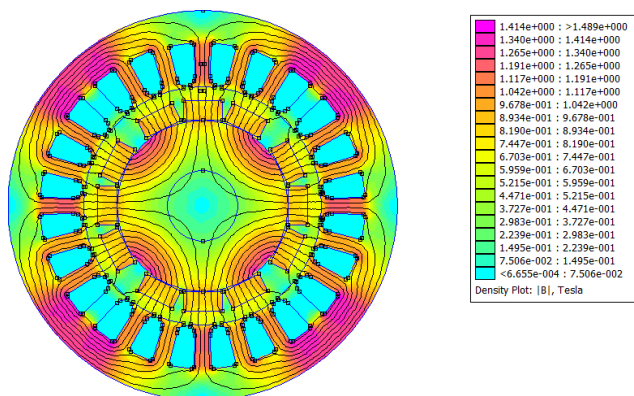


Figure 4.
Finite element simulation of the magnetic circuit

2.2. Temperature dependence of the NdFeB magnet

The temperature-dependent B-H curves of the used N48 type NdFeB magnet are illustrated in Figure 5.[5]. It can be observed that the remanence flux density decreases while the temperature is increasing. The decrementation effect is reversible until the operating point does not go beyond the knee-point of the curve which was taken into account during the calculation.

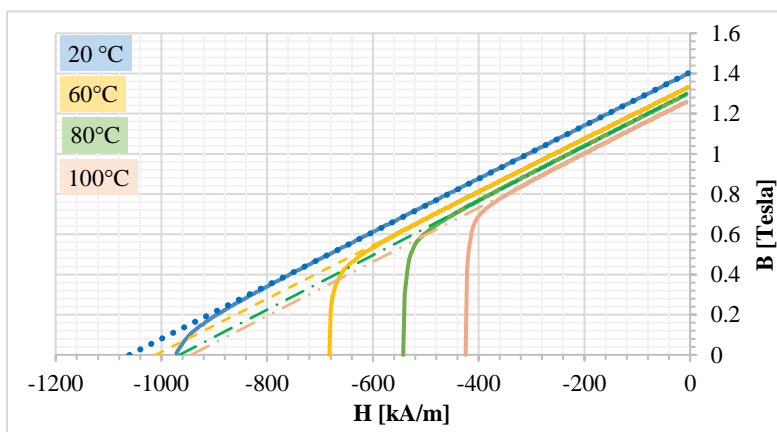


Figure 5.
Demagnetization curves of N48 type NdFeB magnet [5]

2.3. Applied Hall-sensors

In order to carry out the measurements, we used one piece of CYSJ362A GaAs Hall effect element [6] placed beneath the centre of one stator slot. This sensor has a linear $U_{\text{HALL}}\text{-}B$ characteristic. Because of the lower thermal dependence (Figure 6.), we used 5mA constant current source for the sensor supplement. The physical sizes (2,7x2,4x0,95 mm) of the sensor are optimally small for the direct placement in the air-gap.

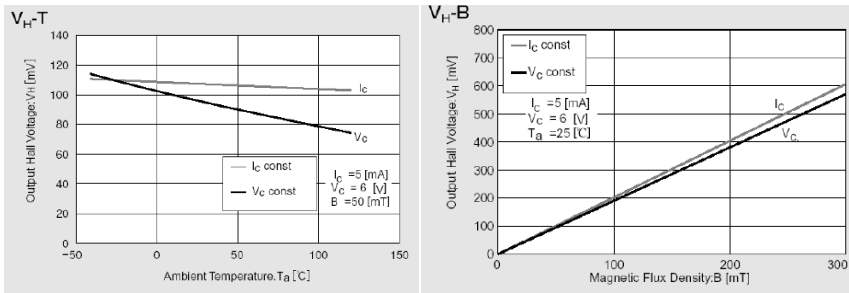


Figure 6.
Main characteristic of CYSJ362A GaAs Hall sensor [6]

2.4. Predictions of the FEMM simulation

In the FEMM model we also represented the Hall cell by a 1mm line marked with the red rectangle in Figure 7. The average flux density along this line can be obtained from FEMM.

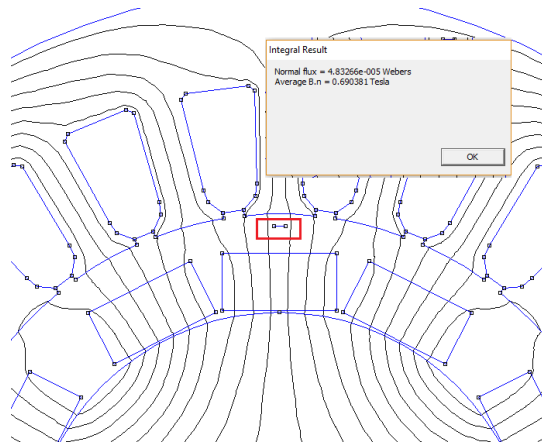


Figure 7.
Sensor placement and modelling in FEMM

In FEMM software environment, the LUA script language allows the rotation to be simulated. One hundred steps have been added to a text file in 1-degree increments. To take the temperature rise into consideration, the permanent magnet's different B-H curves can be adjusted in FEMM according to Figure 5. The simulation result for 100 steps in 20 and 80° Celsius degree is shown in Figure 8. According to the thermal dependent B-H curves, a smaller flux density belongs to the same coercive force at higher temperature. The difference between the two peak value is 7,68 percent.

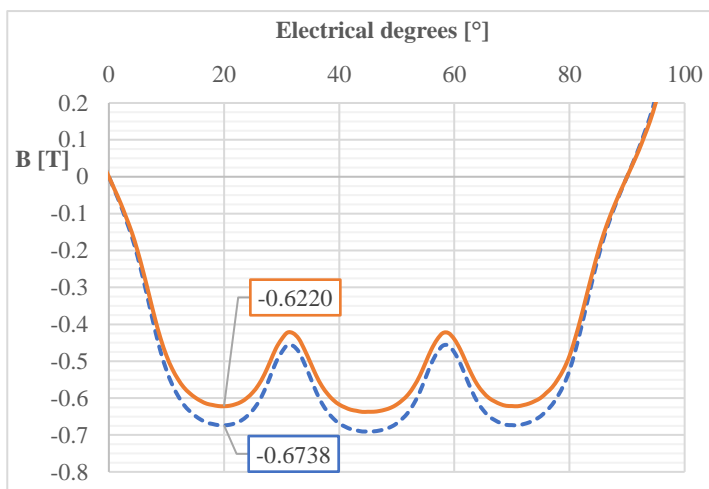


Figure 8.
Temporal change of the induction at the given measurement point

2.5. Experimental setup

To reach the requested temperature of the motor, a laboratory furnace was used. The furnace was sufficiently large so that the entire experimental setup could be placed in it, Figure 9. One Pt100 platinum resistance thermometer was placed inside the motor. Our starting point was our assumption that if the temperature rising of the overall motor reaches the maximum point then the temperature of all parts will be equal, including the magnets.



Figure 9.
Experimental set with sensors inside of the furnace

After 2 hours, the temperature stabilised at 90° Celsius degree. During the heating procedure, the motor was rotated, and the parameters were monitored.

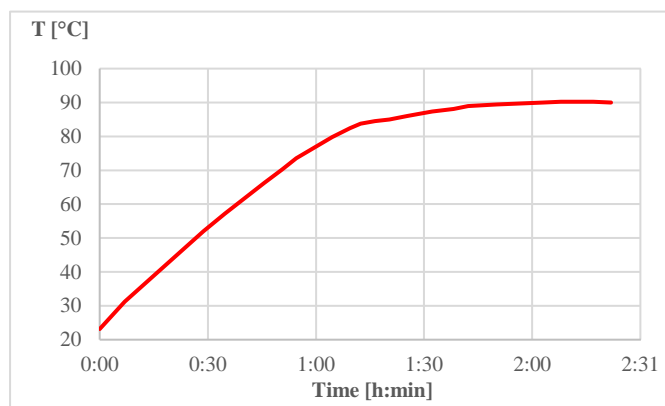


Figure 10.
Temperature rising curve, measured by Pt100

3. Results and discussion

The first measuring point was at 23,14°C ambient room temperature. At this point, a screenshot was taken from the oscilloscope (shown in Figure 11.) The Y-axis represents the directly the sensor Hall-voltage.

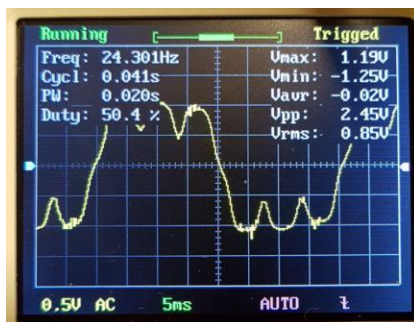


Figure 11.

Oscilloscope screenshot at starting temperature point

The rotating speed was 729 min^{-1} . The rotating speed can be calculated from the measured frequency (1).

$$f = \frac{n \cdot p}{60} \rightarrow n = \frac{f \cdot 60}{p} = \frac{24,301 \cdot 60}{2} = 729,03 \text{ min}^{-1} \quad (1)$$

where f , frequency in Hz, n , rotating speed in min^{-1} , p the number of poles.

The signal shown in Figure 11. has several needle pulses. These pikes are not due to the magnetic field in the air-gap rather these are caused by EMC effects of driver circuit.

The final measuring point, at thermal equilibrium, was measured after 2 hours at $89,96^\circ\text{C}$ degree. According to the oscilloscope screenshot in Figure 12, the magnetic flux density in the air-gap decreased in accordance with the prediction of the theory.

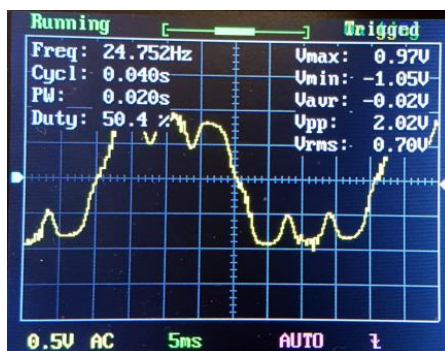


Figure 12.

Oscilloscope screenshot at thermal equilibrium point

The summary of results of hot and cold state measurements are shown in Figure 15. The measured Hall voltages were converted into magnetic flux values.

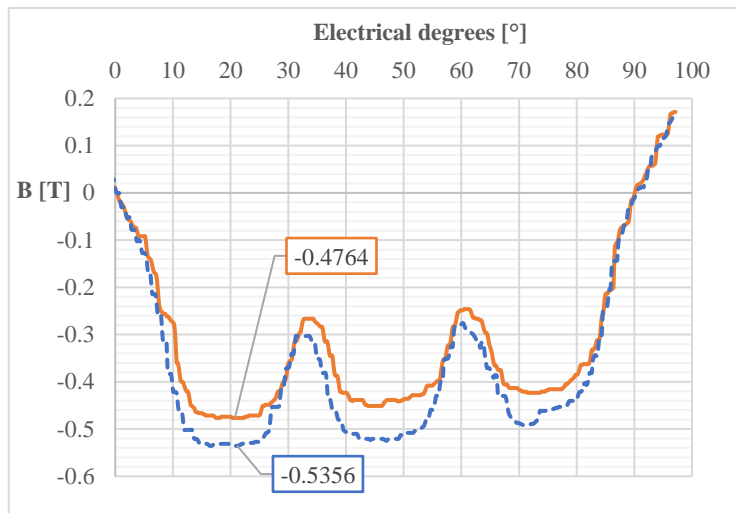


Figure 13.
Summary of results

Between the cold and the hot state, the temperature difference is $\Delta T=66,82\text{K}$. The reduction was found to be $\sim 12,7\%$.

Conclusions

It is obvious that the temperature rise caused significant drop of the air-gap flux density, however, by means of appropriate measurements and calibration, the temperature of the magnets can be obtained without physical contact of the magnet surface.

Experimental results are in accordance with the FEMM simulation. Minor differences between FEMM simulation and test results are caused by the uncertainty of the magnet characteristics.

Obviously, more than just one sensor is needed for accurate investigation of the spatial distribution of air gap flux density. Future work should be carried out in this direction.

Acknowledgement

This research has been partly supported by “GINOP-2.3.4-15-2016-00003” for Higher Education and Industrial Cooperation Centre in Győr.

References

- [1] K. Saad and G. Mirzaeva, "Fault diagnosis of induction motors by space harmonics analysis of the main air gap flux," *Proc. - 2014 Int. Conf. Electr. Mach. ICEM 2014*, no. September 2014, pp. 1608–1613, 2014.
- [2] V. Kindl, K. Hruska, J. Sobra, and M. Byrtus, "Effect of induction machine's load and rotor eccentricity on space harmonics in the air gap magnetic flux density," in *Proceedings of the 16th International Conference on Mechatronics, Mechatronika 2014*, 2014, no. December, pp. 463–468.
- [3] J. E. Lenz, "A Review of Magnetic Sensors," *Proc. IEEE*, vol. 78, no. 6, pp. 973–989, 1990.
- [4] D. Basic and J. Varga, "Permanens felületmágneses forgórészű szinkron szervomotorok tervezésének irányelvei," *Villamosság*, vol. 39. évf., no. 9. szám, pp. 257–288, 1991.
- [5] Arnold Magnetics, "Neodymium Magnets (NdFeB) | Arnold Magnetic Technologies." [Online]. Available: <http://www.arnoldmagnetics.com/products/neodymium-iron-boron-magnets/>. [Accessed: 12-May-2018].
- [6] ChenYang Gmbh, "Hall effect sensor CYSJ362A Datasheet," vol. 49, no. 0, pp. 0–3, 2016.

Application of IoT Based Intelligent Automated Technologies in Smart Homes

János Simon, Igor Fürstner, Zlatko Čović, László Gogolák

Subotica Tech – College of Applied Sciences, Marka Oreskovica 16, 24000
Subotica, Serbia

simon@vts.su.ac.rs, ifurst@vts.su.ac.rs, chole@vts.su.ac.rs, gogolak@vts.su.ac.rs

Abstract: A smart home gives users comfort and control, because it adapts to their activities, mood, habits and lifestyle, thanks to applications that use the Internet as communication standard with other devices. The goal of automation is to make it easier for the user to access and control the home accessories in daily life. Control of lighting, multimedia devices, air conditioning, heating, video surveillance, alarm systems, even control of beds, wardrobes, stoves, bathrooms etc. are some of the features that are easily managed via the remote control. All this does not require a technical pre-knowledge. Houses that function in an intelligent way, communicating with other houses, are distinguished for the purpose of gathering information and anticipating the needs of users, houses that allow remote access to information and control. Intelligent devices in a smart home communicate through different protocols, the selection often depends on the manufacturer's choice. In the integration of different intelligent devices, frequent incompatibility of protocols is generally different to the extent of the data they exchange and the speed of their processing. This paper describes a numerous advantages of using these advanced technologies, such as automating various processes, facilitating everyday tasks, increasing comfort and energy savings, helping older and sick people, for example, to people with visual impairments who do not use a touch screen or hearing impaired people to receive sound information. The biggest limitation for wider application is the high cost of implementation, but it is expected that the construction of smart homes and apartments will be encouraged in the future.

Keywords: Smart home, Internet of Things, Raspberry Pi, Python

1 INTRODUCTION

Within this work, a documented remote control of heating via the http protocol has been made and a brief description of the Internet of Things paradigm and the smart home. The platform on which the work was made is the popular PC Raspberry Pi, with the Raspbian version of Linux. Software has been written to run on Raspberry Pi (Python and bash shell) and a simple user interface in

JavaScript and HTML. Raspberry Pi also spins the apache server on itself. There is also a simple demonstration with servos. PWM modulation was used to adjust the position of the valves. The introduction introduces a brief description of the fields to be processed, and IoT is described further. It is based on the technical performance itself and the description of the hardware part (Raspberry) and the software part with the code snippets. In conclusion, the proposed system improvements were suggested.

Home Automation is the use and control of home appliances via remote control or automatically. For this purpose, the Internet of Things has recently started to be mentioned, ie, a network of sensors and actuators inside a home controlled by a central system that automates the home. It is estimated that by 2019, 68 million homes in America and Europe will be "smart homes". Also, it is assumed that up to 2020, 50 billion devices will be networked within the Internet of Things paradigm. Within this paradigm there is also the "smart lighting" discussed in this final work. 19% of the world's electricity consumption is used for lighting and 6% of greenhouse emissions comes from that energy. Smart lighting is a good way to minimize and save on lighting, with remote on and off lights. It also provides a greater level of comfort within the home itself.

This theme was selected because of the ease of availability of the Raspberry Pi platform, due to the many open source codes and the interest of the same theme. The aim is to approach Raspberry Pi platform students, learn something about the Internet of Things paradigm and study smart homes as the coming new technology.

2 THE INTERNET OF THINGS PARADIGM

In general, the term Internet of Things (internet stuff) was coined by British entrepreneur Kevin Asthon 1999. It is a network of facilities (electronics, software, sensors) that allows data collection and processing. This allows objects to be controlled over the existing network infrastructure. Objects can be, for example, cardiac implants, car-built sensors, smart home appliances, etc.

3 SMART HOUSE

An intelligent or smart house is a house that has a built-in central control system. Such a system is able to integrate multiple systems (heating, hot water consumption, cooling, lighting, safety).

The market for smart homes in 2015 is worth \$ 5.77 billion, while the forecast for 2020 is \$ 10 billion. Early home automation has started with energy-saving machines.

Independent household appliances with electricity or gas became viable during the 1900s with the introduction of electricity distribution and led to the introduction of washing machines (1904), water heater (1889), refrigerators, sewing machines, dishwashers and dryers for clothing. In 1975, the first home automation technology for general purpose X10 was developed. It is a communication protocol for electronic devices. Primarily uses wiring harness for signaling and control. By 2012, in the United States, according to ABI Research, 1.5 million households installed.

According to [7], there are 3 generations of smart homes:

- First Generation: wireless technology with a proxy server, eg Zigbee, Z-Wave
- Second Generation: Artificial Intelligence that manages electrical appliances, eg Amazon Echo
- Third Generation: a robotic friend who communicates with people, eg Robot Rovio, Roomba.
- The apps and technology that the Smart House is having are:
- heating, ventilation and air conditioning (HVAC): remote control of all home energy monitors over the internet with a simple and friendly user interface
- Lighting control system
- In-house control system: it is possible to know the current number of people using smart meters and environmental sensors such as CO2 sensors that can be integrated into the building automation system to increase energy efficiency
- device control and smart grid integration with a smart gauge, by exploiting, for example, high solar panel output in the middle of the day to start washing machines
- security: home security system integrated with the home automation system can provide additional services such as remote surveillance of security camera over the internet or central locking of all external doors and windows
- Flood detectors, smoke detectors and CO detectors.

Smart homes could bump into two types:

- Complete house automation - houses / apartments designed before construction to be smart. These are expensive and advanced solutions, which can be wireless (Wi-Fi, Zigbee, Z-Wave) or wired (PLC - Power Line Communication). Such systems work big companies, systems are closed and incompatible with others in the market. Examples of such systems are Creston, Control4, AMX, Elan Home Systems, HomeSeer.

- Non-invasive / consumer friendly home automation - inexpensive and user friendly solutions. The user usually obtains a central unit that collects data from the device and various plug and play devices that can be installed by themselves. Examples of such systems are Insteon, NEST, WeMo, Archos, Qivicon, Philips Hue, Iskon Smart Home.

The current biggest problem for smart home users is the unsafe systems (Wi-Fi and its vulnerability), and the fact that technology is still in peril, so users may buy devices, and after some time the manufacturer decides to abandon that service, shuts down servers and devices become useless.

Also, the problem is lacking the right standards. There are many different and incompatible technologies where real IoT can not be achieved if all devices do not work together.

4 MQTT

MQTT is a communication protocol designed for use at the top of the TCP-IP protocol. It uses very little network traffic and is suitable for sensors that send their data to the "cloud". It requires connection to a type of dispatcher (Broker), who receives a subscriber of a particular sensor / device on a topic.

The Message Queue Telemetry Transport Protocol (MQTT) was developed by Andy StanfordClark (IBM) and Arlen Nipper (Eurotech) in 1999 to track the pipeline in the middle of the desert. They needed a protocol that would enable efficient data transfer rates with low battery consumption and a cheaper overall system. Developed MQTT protocol with subscription - subscription to architecture has proven to be easier and more economical than HyperText Transfer Protocol (HTTP) protocol with request and response model. The Reveal Model - Subscription is triggered for events and allows customers to post messages without worrying about their final destination. The final destination of the posted message is determined by the MQTT broker who passes messages on the basis of client subscriptions and thus frees clients from sending requests for messages of interest, as opposed to the HTTP protocol where clients have to look for the information they need from the server. The MQTT protocol also features a small 2-byte fixed header size that further reduces network load

5 RASPBERRY PI

Raspberry Pi is a small-print computer that incorporates all the elements needed to work, created as a product of Raspberry Pi Foundation with the desire to

encourage the development of computer literacy with emphasis on programming. The original model has become much more popular than it was expected to be sold out of a targeted market (eg in a robotics). By 2016, 11 million devices were sold, which is the best-selling British computer of all time.

The base of Raspberry Pi computers consists of Broadcom chips that are responsible for the central ARM processor (700 MHz ARM1176JZF-S core ARM11 family) and a graphical processor (Broadcom VideoCore IV, OpenGL ES 2.0, MPEG-2 and VC-1, 1080p30 h.264 / MPEG -4 AVC high-profile decoder and encoder). The operating memory is 256 MB (A model), ie 512 MB (B model).

The base also consists of 21 GPIO 3.3V data lines and 10/100 Ethernet module for wired network and USB hub with 2 external ports.



Figure 1
Raspberry Pi B

The connectors available on the board are:

- video - HDMI 1.3 and 1.4, RCA
- Audio - HDMI, 3.5 mm stereo
- External memory a - SD card
- USB - 2 USB 2.0 ports
- AC adapter - standard RJ45 connector
- power supply - micro USB adapter

The recommended selling price (excluding other costs) is \$ 25 for model A and \$ 34 for model B. To make Raspberry Pi a usable little personal computer, you should at least add the following components:

- SD Memory Card with a capacity of 4 GB or greater
- External power supply of 5 V / 1-2 A.

At Raspberry Pi it is possible to install a variety of operating systems that are mostly based on Linux basics or Linux distribution itself. Some of the most famous are:

- Raspbian - Linux Debian distribution with basic OS elements, oriented to programming learning
- Android 4.0 - standard distribution
- OpenELEC - a home multimedia platform
- Instant WebKiosk - an operating system based on a web browser.

This paper uses Raspberry Pi B version and Raspbian OS. For Raspberry Pi it is possible to buy a variety of additional peripherals connected to it, such as a camera, a Gertboard (sensor board), an infrared camera and various other expansion tiles.

Conclusions

This work has shown that Raspberry Pi as a widespread platform for IoT projects is very good for such projects. It has also been shown that MQTT as a system for connecting IoT devices is very flexible and easy to use. For the entire programming, Python programming language is used, which is convenient for such projects because it is very simple and easy to use. It has been shown to be well-used by a widespread platform such as Raspberry Pi because of its readability and a very large online community that allows sharing of ideas and programming code.

Testing was done so that Raspberry Pi was included in the home router. The power is supplied via a micro USB cable and a mobile charger. After booting, Raspberry sends its IP address to the selected e-mail. If this IP address is entered in a web browser, and if the computer / mobile phone is in the same local network as Raspberry, then the data management and visualization page is accessed. If your computer or cell phone is not in the local network, you must manually launch the file `index.html`. In this paper, it has been shown that easy-to-access platforms and open code can easily make visible results in the Internet of Things paradigms. Using easily accessible materials, it is possible to achieve results that are easy to apply in practice, industry and science.

References

- [1] A. Papp, L. Szilassy, J. Sárosi: (2016) "Navigation of Differential Drive Mobile Robot on Predefined, Software Designed Path", *Recent Innovations in Mechatronics (RIIM)*, Vol. 3, No. 1-2, ISSN 2064-9622, 1-5.
- [2] Chirila S, Lemnaru C, and Dinsoreanu M. (2016) Semantic-based IoT device discovery and recommendation mechanism. In *Proceedings of the 2016 IEEE 12th International Conference on Intelligent Computer Communication and Processing (ICCP'16)*, 111-116.
- [3] Gyorgy Terdik, Zoltan Gal (2013): *Advances and practice in Internet of Things: A case study*, *Proceedings of IEEE 4th International Conference on Cognitive Infocommunications (CogInfoCom 2013)*, Budapest, Hungary, December 2-5, 2013, ISBN: 978-1-4799-1544-6, 435-440.

- [4] Gyula Mester, Szilveszter Pletl, Gizella Pajor, Zoltan Jeges, (1992) Flexible Planetary Gear Drives in Robotics, Proceedings of the 1992 International Conference on Industrial Electronics, Control, Instrumentation and Automation - Robotics, CIM and Automation, Emerging Technologies, IEEE IECON '92, Vol. 2, 646-649, ISBN 0-7803-0582-5, DOI: 10.1109/IECON.1992.254556.
- [5] Habibi, Robet. (2017) "Perencanaan sistem smart academic dengan smart classroom dan teknologi internet of things pada stmik bina patria." jurnal transformasi 13.1.
- [6] <http://www.ibm.com/bluemix/>.
- [7] Imre Petkovics, János Simon, Ármin Petkovics, Zlatko Čović, (2017) "Selection of Unmanned Aerial Vehicle for Precision Agriculture with Multi-criteria Decision Making Algorithm", Proceedings of the Conference SISY 2017, pp. 1-5, Subotica, Serbia.
- [8] J. Sárosi (2014): Measurement and Data Acquisition, University of Szeged, Faculty of Engineering, Szeged, ISBN 978-963-306-284-5, 100 p.
- [9] János Simon, Monika Trojanova, Jozef Zbihlej, József Sarosi, (2018) "Mass Customization Model in Food Industry Using Industry 4.0 Standard with Fuzzy Based Multi-criteria Decision Making Methodology", Advances in Mechanical Engineering Vol.10, No.3, 1-18.
- [10] János Simon, Zlatko Čović, Dalibor Dobrilović, (2016) "The Web of Things and Database Management Systems", Analecta Technica Szegedinensia, Vol 10, No 2, 61-68.
- [11] Khan, Rafiullah, et al. (2012) "Future internet: the internet of things architecture, possible applications and key challenges." Frontiers of Information Technology (FIT), 2012 10th International Conference on. IEEE.
- [12] Khari, Manju, et al. (2016) "Internet of Things: Proposed security aspects for digitizing the world." Computing for Sustainable Global Development (INDIACom), 2016 3rd International Conference on. IEEE.
- [13] Mehta, Vishal. (2018) "A Novel Approach to Realize Internet of Intelligent Things." Big Data Analytics. Springer, Singapore, 413-419.
- [14] Mohammad Abdullah Al Faruque and Korosh Vatanparvar. (2016) Energy management-as-a-service over fog computing platform. IEEE Int. Things J. 3, 2, 161-169.
- [15] Nukala R, et al. (2015) An IoT based approach towards Global Food Safety and Security. In: The 14th IT&T Conference, 10-17.
- [16] Nyikes, Z., Rajnai, Z. (2015) "The Big Data and the relationship of the Hungarian National Digital Infrastructure", International Conference on Applied Internet and Information Technologies, ICAIT 2015, 6-12.
- [17] Odry, Á., J. Fodor, and P. Odry. (2016) "Stabilization of a two-wheeled mobile pendulum system using LQG and fuzzy control techniques." International Journal On Advances in Intelligent Systems 9.1.
- [18] Simon János, (2015) "Concepts of the Internet of Things from the Aspect of the Autonomous Mobile Robots", Interdisciplinary Description of Complex Systems Vol.13 No.1, 34-40.
- [19] Simon János, (2016) "Industrial Data Acquisition Applications Using Relational Databases, IIoT Environment and Multi Criteria Decision Making Systems", International Journal of Current Research in Engineering, Science and Technology, Vol 1, No 1, 11-18.
- [20] Simon János, Zlatko Covic, (2015) "Data Management of the Automomous Mobile Devices and Internet of Things", ANNALS of Faculty Engineering Hunedoara – International Journal of Engineering Vol. XIII, No. 3, 265-268.
- [21] Simon János, Zlatko Čović, Igor Fürstner, Laslo Gogolak, Dalibor Dobrilović, (2015) "The Web of Things and Database Services", Proceedings of the International conference on Applied Internet and Information Technologies AIIT 2015, 235-238.
- [22] Simon János, Zlatko Covic, Imre Petkovic, (2017) "Industrie 4.0 Based Customized Mass Production Overview", Proceedings of the Conference MECHEDU 2017, 1-5.
- [23] U. Alvarado, A. Juanicorena, I. Adin, B. Sedano, I. Gutierrez, and J. de N6. (2012) Energy harvesting technologies for low-power electronics. Trans. Emerg. Telecommun. Technol. 23(8), 728-741.

- [24] Xiaorong Z, et al. (2015) The design of the internet of things solution for food supply chain. In: 5th International Conference on Education, Management, Information and Medicine, Shenyang, China, 314-318,
- [25] Židek K, et al. (2016) Embedded vision equipment of industrial robot for inline detection of product errors by clustering-classification algorithms. *Int. J. Adv. Robot. Syst.*, 13(5): 1-10.

SOLUTIONS IN PROPERTY PROTECTION BASED ON PHANTOM 4PRO+ UAV, IN FAVOR OF LOWERING OF THE TERRORIST THREAT

Krisztián Bálint

Óbuda University, Doctoral School on Safety and Security Sciences, Népszínház street 8, 1081, Budapest, Hungary, balint.krisztian@phd.uni-obuda.hu

Abstract: Property protection represents an outstandingly important aspect these days. Terrorist attacks are occurring ever more frequently in the European Union and abroad, so the preservation of human lives is a question of key importance. It is impossible to have an efficient property protection without solutions based on computer science. By means of the appearance of UAVs, the human forces can monitor given buildings or building complexes more efficiently. These remotely controlled miniature airplanes are fitted with a camera enable the possibility of reconnoitering a large land surface in a short time period. However, it is important to note that the adequate choice of UAVs is an imperative, as these vehicles possess a number of specific characteristics, which may influence the defense. These features may be the length of flying time, the resolution of the onboard camera system, the obstacle sensor, or the resistance against various weather conditions. The deployment of the Phantom 4Pro+ UAV in property protection is formulated as a proposal, as it possesses a number of technical characteristics, which are enabling it for the execution of various tasks of defense and reconnaissance. This vehicle facilitates and simplifies the flight engagement by means of its intelligent flight characteristics, while the onboard infra-red sensor identifies the obstacles and corrects the flight in order to avoid them. The vehicle uses 7 various cameras during the flight, with an infra-red sensor system, along with a double satellite positioning system (GPS & GLONASS), respectively two ultrasound employing distance measuring units, facing downwards. These all are specific traits, which may greatly enhance the effectiveness of the property protection.

Keywords: keyword1; terrorism; property protection; UAVs

1 Preface

In the second part of the 20th century, the measure of urbanization has sped up. Utilizing the dynamically developing urbanization, the terrorists attack various complexes and properties more frequently.

The urban space and lifestyle subserve the terrorists. This is facilitated by the factors (besides the density of built-in areas and populousness) like the fact that in the large cities, political, administrative, economic, cultural, touristic and entertaining institutions and their serving infrastructure are densely present. All these factors are "offering" a multitude of possible targets, for the terrorist organizations. From the aspect of statistical data and the experienced terrorist attacks:

- religious sanctuaries (places of worship, temples, mosques, and synagogues);
- various facilities (vehicles of public transport, railway and underground carriages, airplanes, railway- and public transport terminals, stations, tunnels),
- services (post offices, mail-order networks);
- offices of political organizations and parties;
- premises of multinational enterprises (banks, offices, branch offices);
- buildings of jurisdiction (courts and prosecutor's offices);
- buildings of the government, the administration and of law enforcement,
- diplomatic organizations (embassies, residencies, consulates).

The choice of possible targets depends on more factors. From one side, the characteristics of the urban architecture are influential, the number, location, and accessibility of more vulnerable complexes, which are relatively easier to attack [1].

In order to lower the terrorist threat, the estates and premises should be defended by efficient methods. This can be greatly facilitated the reconnaissance based on UAVs, which elevates the operation of security services, as it is able to oversee the greater area of defense in the same timeframe. The characteristics of the Phantom Pro4+ UAV enable the vehicle to perform the tasks of property protection.

2 Terrorist threat

Acknowledging that no one definition of terrorism has gained universal acceptance, the U.S. Office of the Coordinator for Counterterrorism has endorsed the following definition, found in the United States Code (Title 22, Section 2656f[d]) and adopted by the Department of State, Department of Defense, and Central Intelligence Agency:

The term ‘terrorism’ means premeditated, politically motivated violence perpetrated against noncombatant targets by sub-national groups or clandestine agents, usually intended to influence an audience. The term ‘international terrorism’ means terrorism involving citizens or territory of more than one country. The term ‘terrorist’ group means any group practicing, or that has any significant subgroups that practice, international terrorism [2].

As a result of recent events, governments have shown growing interest in the protection of strategic infrastructures against sabotage and terrorist attacks in particular, are vulnerable because they cover large geographical areas and are difficult to protect [3]. The UAVs may lend an efficient aid in the reconnaissance of large land areas in a short time period. In favor of the prevention and a successful defense against terrorist attacks, property protection based on UAVs may be of outstanding importance.

The terrorist threat concerns mainly cities, amongst which the more significant threat looms over large cities. The experiences of terrorist attacks happened in the world until now unanimously prove this. The characteristics of urban space and way of life more likely subserve the operation of terrorist organizations. Due to their traits and possibilities, large cities count as a real “paradise” and a series of easy targets from the aspect of these terrorist groups. The explanation of this phenomenon is not very complicated, as due to the processes of urbanization, the metropolises of our time concentrate systems of political, administrative, economic, touristic and entertaining institutions, and their serving infrastructures. Terrorists may choose infinite number of possible targets based on the density of the built-up areas, the buildings, other facilities, premises, and the high number of people living in cities. Large cities possess developed infrastructural, traffic and telecommunication networks, in order to accommodate and supply the population and to attend and secure the functional conditions of the infrastructural facilities and elements of institutions and their systems. These networks form a complex system, and they are vulnerable, so their defense against a terrorist attack is very expensive and presents a nearly impossible task. Besides the high concentration of population, the relatively high vulnerability of infrastructural facilities and networks increases the defenselessness and sensibility of large cities against the terrorist attacks. Upon a successful terrorist attack, depending on the characteristics of the facilities or systems harmed or destroyed, or on the modality of the destruction, the extemporal lack of services, paralysis of the communication network and/or considerable traffic jams may be expected. Based on the high populousness, the specificities of urban structure and the vulnerability of infrastructural systems, it is not an exaggeration to state that it is easy to execute terrorist attacks in large cities, with a relatively small effort, claiming even mass casualties [4].

3 Property protection

A property is an accurately confinable area, on which buildings of various function may be located. The level of endangerment is defined by the building's operation, the security level of the upkeep, the materials used in its construction, the technical devices present, the demand for information, also their value and marketability, the presence of (contamination with) crime, the business hours, the time of day, the dependability of the property defense system deployed, the objective and subjective rapidity of countermeasures and a reaction force, the character (criminality) of unwanted actions, and their influence in the area [5].

Property protection represents a field of safeguarding, which is accomplished by the combined deployment of up-to-date mechanical and electronic devices, besides manpower. Various objects, implements, material goods, and so the properties must be defended against all the outer and inner influences and factors, which by any way endanger their proper usage or the performing of their designated functions. Their status and value producing processes within them need to be supported by a continuous defense, upholding their safe environment [6].

Possible solutions in property protection:

- Manpower (by a security service);
- Mechanical solutions of defense (locks, doors, fences, portals);
- Electronic solutions of defense (UAVs, alerting and camera system, admission system).

As it can be seen, the defense based on the UAVs is categorized in the class of electronic defense solutions, and their operation demands an adequate training, presumably possessed by the security service.

4 UAVs

UAVs (unmanned aerial vehicles) are of a great interest in military and civilian applications, including mapping, patrolling, and search and rescue [7]. UAV quadrotors are designed to easily move in different environments while following specific tasks and providing a good performance as well as a great autonomy [8]. The possibilities offered by UAVs may be efficiently utilized in property protection. These miniature airplanes can scan the whole defended object, as they soar at high enough altitudes. They are capable of tracking humans, or rather of performing various tasks of reconnaissance. In these cases, UAVs are performing tasks of prevention and defense. The first priority of defense timeframe is the protection of human lives, only then the protection of material goods may follow [9]. UAVs may uncover potential threats and unauthorized intruders more easily.

The given property may well be supervised through continuous or periodical overwatch. If the solutions of property defense involving UAVs are utilized on a daily basis, the manpower in defense is tasked with yet another group of assignments:

- The upkeep of UAVs;
- Monitoring tasks (the analyzing of the UAVs' recordings);
- Adequate level of training in relation to the UAVs' operation;
- Continuous state of alertness (through 24 hours) - (keeping up battery charge, monitoring the state of charge);
- Providing an area for the UAVs, so it may be deployed at any time.

Three categories of UAVs may be distinguished:

- Fixed-wing UAVs;
- Rotary-wing UAVs;
- UAVs operated by upward propulsion.

The rotary wing, pilotless flying vehicles appeared in common knowledge about 11 years ago, hence their quantity is continuously growing. Determined by the tasks beforehand, these devices may appear in various sizes, ranging from extra light (16 grams) to heavy (22 kg). In case of a deployment involving UAVs, numerous characteristics must be taken into account:

- the size of the monitored area;
- the type of recording of field data,
- the weight of the camera and;
- the anticipated in-flight time.

These parameters basically determine what type of UAV will be needed during the operations. During the repetitive straight-lined or circular path flights, records are often made. In order to successful recording or photographing, intelligent methods, provided by the manufacturers may be implemented. During time sliced photographing, or by the use of more cameras at a time above a given area, the flight mode called "Waypoints" is useful. The subject is, that the UAV must fly between two grid-points, at a precisely determined altitude with a constant set airspeed.

UAVs have not only positive qualities. The flight time is a critical point. While the smaller UAVs are capable of 18 to 20 minutes of flight time, greater machines or ones equipped with heavier cameras can fly only for 6 to 12 minutes. Accordingly, the mapping of vast areas is not possible. Another important factor is the weather conditions. In high winds, above 20 to 40 km/h of wind speed,

depending from the UAVs' size, precise navigation is not possible anymore. In the case of smaller machines, the wind may prevent them from a safe return or landing [10].

4.1 Two-way communication with UAVs

The guidance of RC aerial vehicles and UAVs has undergone a huge transformation during the recent years. The remote controlling utilizing a single signal direction has been changed to two-way communication, where the pilot gets feedback information from the UAV. The two-way communication has enabled the operator to see and handle all the telemetry data of the UAV and all of the attached supplemental sensors in real time. By the frequency jumping communication (FSHH), utilizing the digital ISM-band at 2,4 GHz, not only the pilot is capable of giving navigational orders to the UAV, but the vehicle can send back telemetry data, and the sight picture of the on-board camera towards the user. Thus, the actual GPS coordinates, the charge level of the batteries, or data sent by other sensors may be followed. The duplex-digital signal transfer uses the ISM-band, thus the maximal distance between the UAV and the user is greatly influenced by the saturation of the frequency band, and it is further determined by other factors, like the geographic position, ratio of built-up areas or time of the day. By means of the digital signal transfer, the system is less prone to disturbance, in comparison with the vehicles of earlier generations (thus, their sabotage is harder to accomplish). A great problem is, however, the saturation of the ISM-band at 2,4 GHz, which is used by most of the vehicles [11].

5 Phantom 4Pro+ UAV

The Phantom 4Pro+ UAV has specific characteristics, which are perfectly enabling it to perform tasks of property protection.



Figure 1
Phantom 4Pro+ UAV

5.1 Navigation system

Three sets of double visual sensors form a navigation system of six-cameras, which is in constant operation; it calculates the air-speed and distance between the drone and the obstacle. Using this front, back and downward facing visual sensor grid, the Phantom 4 Pro is capable of a precise hovering in places without GPS signal, during indoor missions, or even when flying through a window, with a minimal input from the pilot. The Phantom 4 Pro is capable of flight in a complex environment, even with an air-speed of 50km/h, while dodging or evading the obstacles in its way. It automatically adjusts the obstacle sensing system to the air-speed, enabling the evasion at lower or higher speeds.

5.2 Obstacle sensor

The Phantom 4 Pro+ has been expanded with a high definition stereo-visual sensor at its back side, also a pair of these at its front, plus further infrared sensors can be found on the left and right side of the hull. This grid is sensing obstacles in five directions, and the vehicle is able to evade in four directions, thus it defends the integrity of the Phantom 4 Pro.

5.3 Flight Autonomy

Flight Autonomy is an automatization platform with a developed intelligence. It consists of a complex network of ten components, including two cameras (front and back, plus dual visual sensors at the bottom, and the main camera), an infrared

sensor system, double satellite positioning (using GPS & GLONASS), two ultrasound rangefinders facing downward, IMU and a compass, and a group of powerful, specialized processor cores. The Phantom 4 Pro acquires data in real time from the environment, and it gathers information considering the altitude, and the position of the obstacles in the vicinity, thus devising a 3D map, on which it places itself. The basic flight data is gathered by the IMU and the compasses, like the air-speed and the flight direction, while the secondary IMU and compass are responsible for the critical data and are designated to filter out possible mistakes, ensuring a more secure flight.

5.4 Active Track

Automatically recognizes (even moving) objects, follows and records them. The fast-moving objects are hard to track, but by means of an advanced image-identification technology, the system easily identifies objects and focuses on them while the tracking. This new algorithm is able to identify more images and objects, ranging from vehicles to animals, and it adjusts the in-flight dynamics accordingly.

5.4.1 The pilot may choose

- Trace – the object to be followed is pursued from the front or back while evading the obstacles automatically;
- Profile – flies beside the object, nearing it at various angles;
- Spotlight – the object is kept in the center, while the flight path may be anywhere [12].

5.4.2 The infrared tracking system

The UAV uses infrared sensors. Those are located on the left and right side of the hull, and tasked with the measuring of the distance between the vehicle and all types of obstacles, utilizing a 3D infrared scanner. These sensors possess a viewing angle of 70° horizontally, and 20° vertically, both in default or tripod mode, ensuring the wide viewing angle on the hull sides of the Phantom, up to 7 meters. The traditional ultrasound sensors were efficient only up to 3-5 meters, and they could be easily disturbed, due to the vibrations from the propeller or upon sensing an uneven surface. The infrared sensor system is capable of mapping a great surface, while measuring the distance, determining the nearest object, dodging the interference and providing a reliable defense.

The Obsidian remote control unit of the Phantom 4 Pro has been provided with a Lightbridge HD video signal transmitter, so it supports data transfers at 5.8GHz. A possibility is left for the choice of the 2.4 GHz and the 5.8 GHz bands, which enables the pilots to minimize the interference noise, or in case of an overload of a frequency, the latency may be eliminated by switching over to the other band. The Wi-Fi video signal transfer system usually uses the 2.4 GHz band, while the remote control functions at 5.8 GHz, avoiding the disturbance from the interference, stemming from the use of the same channel. The use of two dissimilar frequencies influences negatively the flight performance.

The Lightbridge HD video signal transmitting system, used in the Phantom 4 Pro remote control unit called Obsidian, utilizes TDM (Time Division Multiplexing) for the signal transmission, provided with sending and receiving the information on the very same frequency. The frequency of 2.4GHz is often disturbed because of the Wi-Fi signal, while the 5.8GHz band increases the efficiency of signal transfer. Upon being switched on, the Phantom 4 Pro measures the level of saturation of the local frequencies and chooses automatically the band least disturbed by the interference. Thus, it enables the maximal effectiveness of video signal transfer, which could even peak at 3.5km.

5.5 Intelligent flight

As the time passes, UAVs are increasingly easier to fly, although practice and experience are unavoidable for the mid-air photographing of acceptable quality. As the UAV uses seeing and depth-perception technology, the Phantom 4 Pro Obsidian is capable of complex movements, while the commands themselves are simple. Contrary to the intelligent flight based on satellite positioning, the Intelligent Vision provides precise camera view and control.

5.6 Draw

A flight path may be drawn on the display of the remote control unit, thus, the UAV will move to the desired direction, while it would keep the flight altitude. By these means, the pilot is able to concentrate on camera control. There are two modes of operation in the Draw function, which may be used in various cases, as the actual situation requires.

- **Standard:** The vehicle flies at a constant speed through the determined flight path, while the camera faces forward;
- **Free:** The UAV follows the determined path only when it receives a command for that, while the camera may be turned to whichever direction in this mode [13].

The vehicle's technical specifications are described in the table below:

Table 1
Technical specification of Phantom 4Pro+ drone

Weight (Battery & Propellers Included)	1388g
Diagonal Size (Propellers Excluded)	350mm
Max Ascent Speed	S-mode: 6 m/s; P-mode: 5 m/s
Max Descent Speed	S-mode: 4 m/s; P-mode: 3 m/s
Max speed	S-mode: 72 kp/h; P-mode: 58 kp/h;
Max Tilt Angle	42° (S-mode); 35° (A-mode); 25° (P-mode)
Max Angular Speed	250°/s (S-mode); 150°/s (A-mode)
Max Flight Time	6000m
Max Service Ceiling Above Sea Level	32° to 104° F (0° to 40° C)
Satellite Positioning Systems	GPS/Glonass

The UAV's battery determines the in-flight time. The more potent the battery is, the longer time the vehicle may spend in the air. The capacity of the vehicle's battery is described in the table below:

In order for the UAV to be deployed successfully in various tasks involving property protection, the camera system is greatly involved, since in flight, the user may rely only on the remote control and the camera system mounted on the vehicle itself.

Table 2
Battery specification of Phantom 4Pro+ drone

Capacity:	5870 mAh
Voltage:	15,2 V
Energy:	89,2Wh
Net weight:	468 gr
Max charging power:	100W

Conclusions

The property protection based on UAVs is considered a novelty these days. Numerous sources of endangerment may arise on a daily basis, which has to be mapped and reacted to timely, in order to avoid the undesired events.

The solution for property protection supported by the Phantom 4 Pro+ UAV greatly contributes to the successful defense of the building designated for protection. The vehicle can be easily controlled by means of its advanced navigational system. The obstacle sensors prevent the accidental collision with a potentially harmful object. The vehicle is able to map its surroundings efficiently, through the data gathered in real time. By the ActiveTrack solution, the UAV is capable of tracking even moving persons. Finally, the Draw function must be mentioned, which is essential in property defense, since a flight path may be drawn on the display of the remote control unit, which the vehicle is able to follow. Thus, the borderline of the defended perimeter may be set, in which area the UAV may perform reconnaissance flights.

References

- [1] Horváth, Attila: Characteristics of the terrorist threat of European cities during the period before the Islamic State came. (Az európai nagyvárosok terrorfenyegetettségének jellemzői az Iszlám Állam megjelenése előtti időszakban) *Hadtudomány: A magyar hadtudományi társaság folyóirata* 28.E-szám (2018): 19-32.
- [2] Stevens, Michael J.: What is terrorism and can psychology do anything to prevent it?. *Behavioral sciences & the law* 23.4 (2005): 507-526.
- [3] Arroyo, José M., and Francisco D. Galiana: On the solution of the bilevel programming formulation of the terrorist threat problem. *IEEE transactions on Power Systems* 20.2 (2005): 789-797.
- [4] Horváth, Attila.: Terror threat: targets, big cities traffic. (Terrorfenyegetettség: célpontok, nagyvárosok közlekedés), *Nemzetvédelmi Egyetemi Közlemények* 10.3 (2006): 136-152.
- [5] Tamás, Berek, and Bodrácska Gyula.: Live guarding in the building industry of object protection. (Az élőerős őrzés az objektumvédelem építőipari ágazatában), *Hadmérnök* 5:(4) pp. 38-49.(2010) (2010).
- [6] Kasza, Zoltán: Evaluation of external structures and architectural solutions that compromise the security of buildings as objects. (Épületek, mint objektumok vagyonszükségét veszélyeztető külső szerkezetek és építészeti megoldások értékelése), *Bánki Reports* 1.2 (2018): 12-19.
- [7] Ryan, Allison, et al.: An overview of emerging results in cooperative UAV control. *Decision and Control, 2004. CDC. 43rd IEEE*.
- [8] Benallegue, Abdelaziz, Abdellah Mokhtari, and Leonid Fridman: High-order sliding-mode observer for a quadrotor UAV. *International Journal of Robust and Nonlinear Control: IFAC-Affiliated Journal* 18.4-5 (2008): 427-440.
- [9] Nagy, Sándor.: The relationship between natural and civilization hazards with the protection of the population, the role of drones in effective event management. (A természeti és civilizációs veszélyforrások kapcsolata a

lakosságvédelemmel, a drónok szerepe a hatékony eseménykezelésben), Repüléstudományi Közlemények (1997-től) 29.3. (2017): 85-94.

- [10] Krisztina, Major, et al: Use of visual research data for remote control drons in education. (Távirányítású drónok kutatási célú vizuális adatainak alkalmazása az oktatásban), ResearchGate, 2016.
- [11] Hell, Péter: Safe communication of Drón systems. (Drón-rendszerek biztonságos kommunikációja), Köztes-Európa 8.1-2 (2016): 169-175.
- [12] Extreme Digital: DJI Phantom Pro4+ drone. <https://goo.gl/5qLVNM> (Download time: 2018-08-09), 2018.
- [13] Myactioncam: DJI Phantom Pro4+ drone. <https://goo.gl/7FDBdG> (Download time: 2018-08-09), 2018
- [14] DrónExpert: DJI Phantom Pro4+ drone. <https://goo.gl/Mxwbpx> (Download time: 2018-08-09), 2018.
- [15] Hobbycity: DJI Phantom Pro4+ drone. <https://goo.gl/k3achS> (Download time: 2018-08-09), 2018.

System Tests and Simulations for a Power Efficient Portable Solar Panel

Laura-Mihaela Leluțiu, Istók Róbert

Electrical Engineering and Computer Science, Transilvania University of Brasov,
B-dul Eroilor nr. 29 Brașov România

Power System Department, Óbuda University, Bécsi út 94-96/a 1034 Budapest,
Hungary

laura.lelutiu@unitbv.ro, istok.robert@kvk.uni-obuda.hu

Abstract: This paper is concerned with a portable automatic solar panel, mounted on a mobile trailer. Our work approaches the efficiency of the solar panel with respect to the incident angle of the sunshine on the panel. The work pointed out the benefits of higher output power generated by a mobile solar tracking device used for solar panels, compared to fixed PV systems.

Keywords: solar panel, test, simulations, portable system

1 Introduction

This paper is concerned with a portable automatic solar panel, mounted on a mobile trailer. The benefits of a mobile solar panel versus one mounted in a fixed position are highlighted. The paper focuses mostly on the efficiency of the solar panel, in relation to the sunlight angle with respect to the panel surface [9, 10]. The results of the analysis performed demonstrate the higher efficiency of the panel mounted on a sun tracking device with quantifiable differences reported in the paper. This automatic solar panel on a trailer, it's mobile, so one can take it everywhere he needs and after stopping the solar panel turns itself after the sun for best efficiency. Being mobile, the position of the solar panel differs a lot, so it is important that the panel rotates after the sun in order to get a satisfying power output.

This paper approaches the efficiency of the solar panel with respect to the incident angle of the sunshine on the panel.

The analysis performed quantifies the performance difference between a fixed position PV panel and one linked to a sun tracking device, thus demonstrating that they are noticeable. The research work led to the design of a highly efficient, portable and cheap automated solar panel power supply system, capable of

providing the energy needed to sustain the automatic system and some small power consumers [1, 2].

Several software packages have been used in this project. LabView and Solidworks were used for the simulation, while Arduino IDE and Fritzing (used for sketching the circuit diagram) were used for designing the schematic and programming the Arduino microcontroller board; Lab View software is useful for any measurement or control system development [7, 8]. This visual programming language is easy to use and can program an Arduino board or even motions in Solidworks.

The current work has confirmed that a fixed solar panel is characterized by big variations of the power output delivered during a day and also during different seasons of a year. It was also confirmed that a solar tracking device increases the average output power delivered during a day. A solar tracking device is normally cost-effective only for larger installations, due to the added cost of the tracking systems. For this reason, a cheaper solar tracking device was proposed as prototype [3, 4].

2 Pretest using a mobile Panel

It is known that the angle of incidence of sunlight impacts the efficiency of a solar panel a lot. That's why, the first pre-test we made, was to find out how different incidence angle of sunlight on a solar panel impacts the efficiency of it.

The independent variable is the angle of the solar panel while the dependent variable is the power output.

We chose 7 angles for this test: 90° to sunlight, 75° to sunlight, 60° to sunlight, 45° to sunlight, 30° to sunlight, 15° to sunlight, 0° to sunlight. First, the pretest is made outdoors at noon when the sun is up on a clear day. For measuring the current and voltage we used a Digital Multimeter, DT-838.

The measurements it is made by adjusting the inclination angle until it reaches the position corresponding to the highest generated voltage (while measuring the voltage generated by the panel). The maximum power is calculated with the equation 1. As soon as a load is connected to the solar panel, the power P_{out} will decrease.

$$P_{out} = I_{sc} \cdot V_{oc}, \quad (1)$$

where P_{out} is the maximum output power, I_{sc} is the short-circuit current, V_{oc} is the open-circuit voltage.

As we can see in Table I and Table II, we made two measurements at 13:00 PM and 13:10 PM, for better results.

TABLE I. THE MEASUREMENT 1

Measurement 1				
Angle[°]	U[V]	R[Ω]	I[A]	P[W]
0	12.460	500000	0.249	3.105
15	18.400	500000	0.368	6.771
30	18.560	500000	0.371	6.889
45	18.680	500000	0.374	6.979
60	18.750	500000	0.375	7.031
75	18.820	500000	0.376	7.084
90	18.900	500000	0.378	7.144

TABLE II. THE MEASUREMENT 2

Measurement 2				
Angle[°]	U[V]	R[Ω]	I[A]	P[W]
0	16.500	500000	0.330	5.445
15	18.320	500000	0.366	6.712
30	18.550	500000	0.371	6.882
45	18.640	500000	0.373	6.949
60	18.710	500000	0.374	7.001
75	18.790	500000	0.376	7.061
90	18.870	500000	0.377	7.122

The results shown in the tables above and the chart results of Figure 1, confirm the hypothesis that the solar panel has the highest power output when it is perpendicular to the sunlight and declines as the angle decreases.

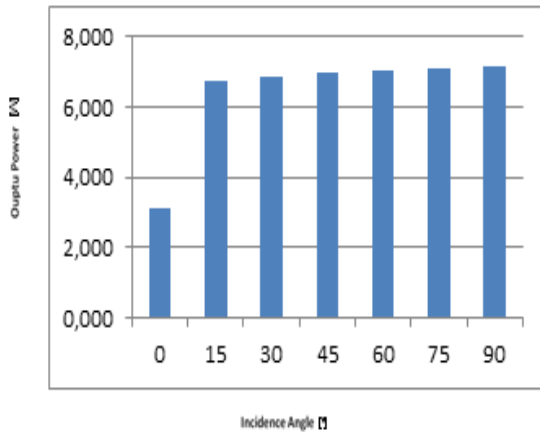


Fig. 1. The Output power using a mobile panel

3 Pretest using a fixed Panel

While the first pretest we made was to find out how different incidence angle of sunlight on a solar panel impacts the efficiency of it, our second pretest we made us a fixed Panel. The pretests consist in measurements of the power output during a day when the solar panel is south oriented and positioned at an angle of 45° .

The measurements are taken from 8 o'clock to 20 o'clock, at 15 minutes interval. Our pretest will show that the power output is small in the morning, reaches a peak at around 2 PM and decreases afterwards. Hypothesis was right, the power increases, reaches a peak and decreases during a day if the solar panel is fixed on a position facing south at a 45° angle (Fig. 2).

It can be noticed that the power output varies significantly during a day; in the morning and evening, because the panel is fixed, the sunlight does not fall perpendicular to the solar panel, thus this is a case of reduced energy output.

The results of the two pretests show that the incident angle is very important and that the panel should always be oriented towards the sun.

A small difference in the incidence angle is already visible in the power output. Later, another test will be performed when the solar panel will track the sun, aiming to quantify the differences between a solar tracking device and a fixed mounted solar panel.

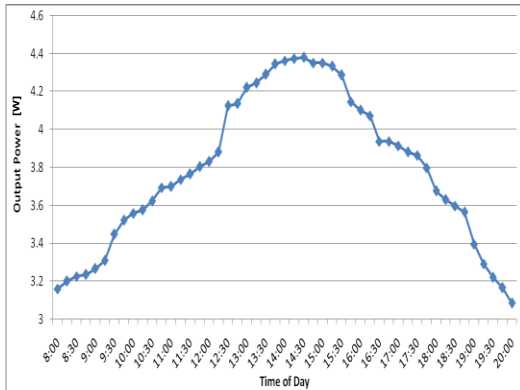


Fig. 2. . The Output power during a day, using a fixed solar panel

4 Simulations

For the simulation we made a simple project where we added the Solidworks assembly and the axis needed for the motion study. Each axis was connected to a "Motion-Motor" attached in Solidworks Simulation.

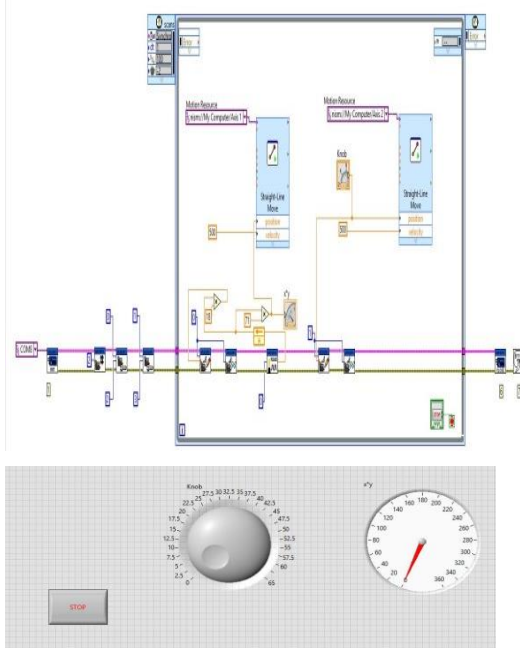


Fig. 3. The LabView back-end and LabView front-end

We used the LabView software for connecting the simulation with Arduino and Solidworks software was used for the 3D model. In order to see the movement of the panel and to determine how to build the trailer for the panel the 3D simulation was made.

As we can see in the following images, in Figure 3 it is shown the front-end and the back-end VI. We used for simulations Solidworks software to create a 3D model of the trailer containing the solar panel that we will build, in order to study the design and the motion of the panel. With help of Solidworks we made the file with all the parameters needed in order to build the physical version of it.

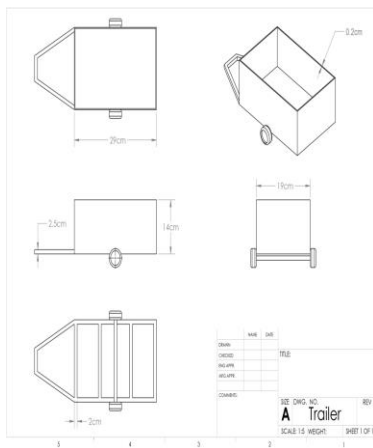


Fig. 4. The model of the Trailer

The Model is a basic one, it could be developed a lot more in Solidworks, but since the simulation was not my main concern, a simple model for the simulation was enough to test it and see if it would work. (Fig. 4). The motion in Solidworks is made through LabView, changing the position of the potentiometer or the position of the knob moves the position of the Servo Motors in the Simulation and also of those connected to the Arduino. With the cosimulation of Arduino, LabView and Solidworks we can easily make a 3D version of a bigger project and simulate it in Labview, controlled directly from Labview or from Arduino (Fig. 4).

The LabView software is useful for many measurement or control system developments [7]. This visual programming language can program an Arduino board or even motions in Solidworks and is also easy to use. So we are using LabView because it's the medium from which we can control the Microcontroller and see the movements live in 3D Solidworks motion analysis (Fig. 5).

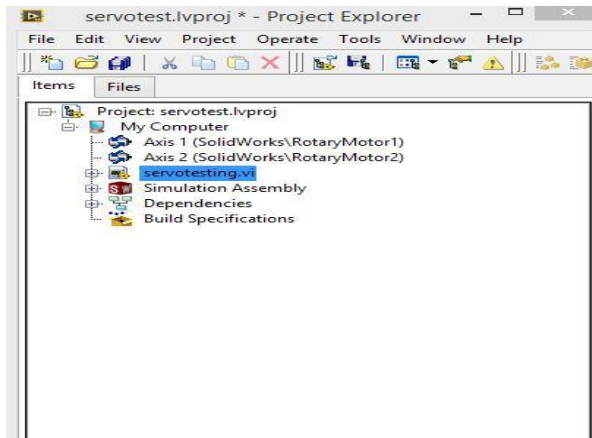


Fig. 5. The LabView Project

The Arduino IDE and Fritzing (used for sketching the circuit diagram) were used for designing the schematic and programming the Arduino microcontroller board. "Arduino is an open-source physical computing platform based on a simple microcontroller board, and a development environment for writing software for the board. Arduino can be used to develop interactive objects, taking inputs from a variety of switches or sensors, and controlling a variety of lights, motors, and other physical outputs. Arduino projects can be stand-alone, or they can communicate with software running on the computer. Arduino is simple to use, cheap and very flexible.

In Figure 6 it is shown the Servo and Photocells connection to Arduino

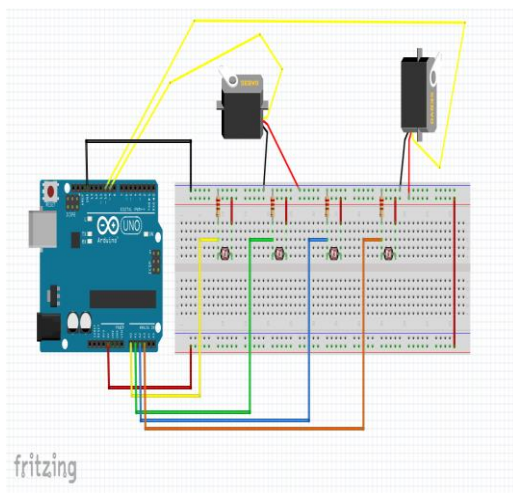


Fig. 6. Photocells and Servo connection to Arduino

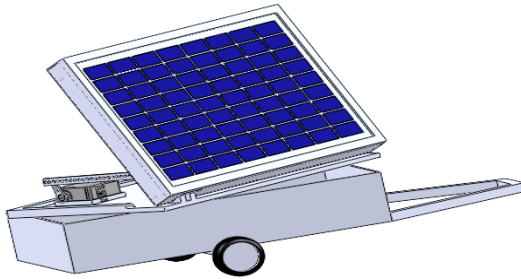


Fig. 7. The Solidworks 3D model of the Trailer

The simulation provided helpful information about the movement of all the elements in the system and about the difference between the angle of the servo and the actual angle in which the solar panel will be positioned (Fig. 7). Because the servo is not exactly at the joint, the angle of the panel is smaller than the angle of the servo. A 90° angle on the servo will be approximately equivalent to a 75° angle on the solar panel.

5 Real System Building

After the simulation, the building of the real model started. First the upper part was done, the Solar Panel, was attached with two hitches on one side of a board having the size of the panel. On the other side it was free so that the tilt of the panel could be possible. Unlike the simulation, the servo motor was mounted near the hitches and not on the far side of the hitches for easier lifting of the panel. The Analog Servo - HD - 1501MG has been used for the tilt movement because it is more powerful than the other Servo used in this project and could tilt the Solar Panel unlike the Analog Servo Power HD Standard 6001HB that has been used for the rotation of the board with the Solar Panel. Another difference between the 2 Servos is that the first one has a slightly different mechanism, which remains in the position it was left, even when the current is turned off. That means that after the panel is inclined to an angle (different than 0), the panel will not return to its initial position, but will stay in the last position it found itself when the power was turned off.

After finishing the tilt movement, the upper part of the model was almost done, another 4 holes were made where the Photo resistors were put for the automation of the panel.

The second part of building the model was the trailer inside. The storage battery was placed inside, as well as the Arduino with all the wirings. The battery had quite a big housing for my model, where it had 1 USB output, two 12V outputs, 1

LED, 1 Push-Button (ON/OFF) and 1 input from the solar panel. In order to fit all this inside, I disassembled the housing, fixed the battery into the front part of the trailer in the middle, and drilled holes in order to have the Push-Button, the LED and the two 12V outputs on the outside.

The USB will be used for the Arduino, so together with the input hole, I mounted them inside. If we analyze the Fig. 8 we see that the differences between the power outputs during

a day with a solar tracker system are not so big and we notice that the average power output during the test day with the solar tracker is 4.390. The solar panel reaches the peak output value early and keeps it constant for a longer period of time before decreasing again.

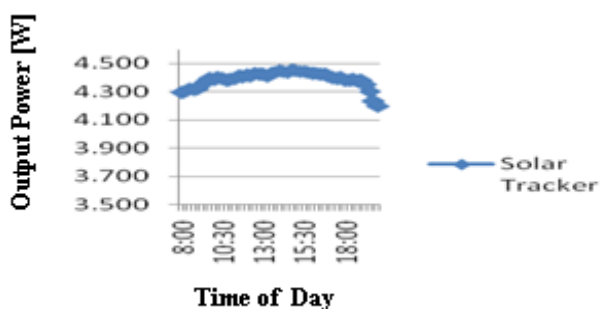


Fig. 8. Power output during a day using a mobile panel

It is seen that the power output is constant during a day with the solar tracker system, while with a fixed panel the power output is low in the morning, increases until midday and drops afterward (Fig. 9).

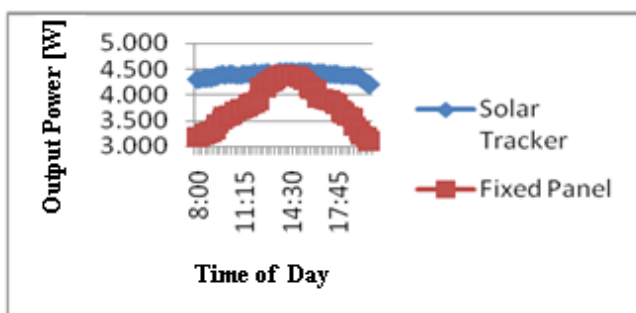


Fig. 9. Power output between a fixed and a portable panel

The tests were carried out in two different days, with the test for the fixed panel being done on a sunnier day. The real gain achieved through the use of the mobile system is expected to be higher in reality, because of the different weather conditions

during the two test days. As it can be seen in Fig. 9, the highest differences in the power generated as part of the two tests are in the morning and afternoon, due to the fact that the angle at which the sunlight aligns with the fixed solar panel is not optimized in the morning, thus losing a significant amount of energy. In the morning, using a solar tracker, the solar panel is turned towards the sun, thus increasing the power output in the early hours of the day. The peak value is reached faster and it is then maintained for a couple of hours, while in the afternoon, the output power decreases slower, increasing the average output power during a day. This difference increases if the fixed panel is set at an average incidence angle between summer and winter. The tests performed and presented in our work were done in June and July.

We will continue our research to have more data to confirm that the portable solar panel is profitable either for low solar productivity (winter) or for high solar productivity. Thus, in order to achieve a more complete research and some will yield results that belong to different seasons in a year.

Conclusions

Our paper approaches the efficiency of the solar panel with respect to the incident angle of the sunshine on the panel [10].The present work has confirmed that a fixed solar panel is characterized by big variations of the power output delivered during different seasons of a year and during a day also. Solar cell efficiency may be broken down into reflectance efficiency, thermodynamic efficiency, charge carrier separation efficiency and conductive efficiency. The overall efficiency is the product of these individual metrics. The power conversion efficiency of a solar cell is a parameter which is defined by the fraction of incident power converted into electricity. A solar cell has a voltage dependent efficiency curve, temperature coefficients, and allowable shadow angles.

References

- [1] R. Pitz-Paal, "Solar Energy - Concentrating Solar Power," in *Future Energy: Improved, Sustainable and Clean Options for our Planet*, London, London Elsevier, p. 738, 2013.
- [2] D. Yogi Goswami, "Principles of Solar Engineering," "Second Edition, Taylor and Francis, p. 694, 2000.
- [3] P. Gevorkian, "Sustainable energy systems engineering: the complete green building design resource," McGraw Hill Professional, ISBN 978-0-07-147359-0, 2007.
- [4] J. Peng and L. Lu, "Review on life cycle assessment of energy payback and greenhouse gas emission of solar photovoltaic systems," *Renewable and Sustainable Energy Reviews*, vol. 19, pp. 255-274, 2013.
- [5] E. Helerea, C. Marinescu, L.M. Rab, "Energy and environmental engineering," ISBN 978-973-508-065-6, Transilvania University of Brasov, 2007.
- [6] M.S. Nicolae, "Optimization design of photovoltaic systems and improving their energy efficiency through a novel technology installation of the support", *Int. Conf. on Applied and Theoretical Electricity*, pp. 1-6, 2014.
- [7] K. Bhise, N. Pragallapati, S. Thale, V. Agarwal, "LabVIEW based emulation of photovoltaic array to study maximum power point tracking algorithms," *38th IEEE Photovoltaic Specialists Conf.*, pp. 002961-002966, 2012.

- [8] Lelutiu L., “Measuring, data acquisition and processing systems,“ Transilvania University of Brasov, ISBN 978-606-19-0304-7, 2013.
- [9] F. H. Aghdam; “Reliability and cost analysis of multistage boost converters connected to PV panels,“ IEEE Journal of Photovoltaics, vol. 6, no. 4, pp. 981-989, 2016.
- [10] H. I. Cristian; M. Raducu, “Energy efficiency analysis of various topologies, control techniques and technologies used for photovoltaic panels Part I: On the PV modeling and problem of extracting the maximum power”, Proceedings of the 6th Int. Conf. on Electronics, Computers and Artificial Intelligence, pp. 23-28, 2014.

Comparison of Digital Image Compression Methods in Spatial and Frequency Domains

Póth Miklós

Subotica Tech, Subotica, Serbia

Abstract – In this paper we compare one spatial domain and one transformed domain image compression methods. In the spatial domain we present the five modulus method (FMM), and in the transformed domain we present the JPEG method. Both methods are compared according to their compression ratio and signal to noise ratio with the original image. The testings were performed on 256x256 grayscale images.

Keywords: digital image compression, five modulus method DCT.

1. INTRODUCTION

Image compression gained much attention during the past decades because it helped storing image data in a more compact way. Efficient storage is very important because it saves memory space. This is especially important since the quantity of data produced increases day-by-day. Researchers and scientists come up with new compression algorithms all the time. The main goal of image compression is to reduce the redundancy that is included in the image. There are 3 types of redundancy:

- Coding redundancy;
- Psychovisual redundancy, and
- Interpixel redundancy

The main goal of image compression is to find the representation of the image that is less correlated than the original. Parts of the image that are not noticeable for the human visual system can be omitted without loss in the subjective quality.

The rest of this paper is organized as follows: Section II explains the spatial domain compression technique, the five modulus method, section III explains the transformed image compression method, the JPEG. In section IV we present the results we obtained after testing our methods, and we conclude in Section V.

2. FIVE-MODULUS METHOD (FMM)

When image processing is done in the spatial domain, the operations are performed directly on image pixels, no transformation is needed. The method we explain here reduces the standard deviation of the image by dividing each pixel value by 5. We will limit our research to grayscale images with 256 shades of gray (8-bit images).

The FMM method divides the digital image into 8x8 image blocks first. After that, each pixel is transformed to be a multiple of 5. This transformation has no effect on the subjective quality of the image, since the maximum change in pixel intensity is 2, and can not be visible for the human visual system, see Table I.

Table I. Pixel values before and after the KMM transformation

Before		After		Before		After
0	→	0		243	→	245
1	→	0		244	→	245
2	→	0		245	→	245
3	→	5		246	→	245
4	→	5		247	→	245
5	→	5		248	→	250
6	→	5	...	249	→	250
7	→	5		250	→	250
8	→	10		251	→	250
9	→	10		252	→	250
10	→	10		253	→	255
11	→	10		254	→	255
12	→	10		255	→	255

After this, all pixel values will be the multiple of 5. An example is shown in Figure 1.

9	11	13	11	11	11	16	106	10	10	15	10	10	10	15	105
12	12	12	11	12	11	69	181	10	10	10	10	10	10	70	180
13	12	12	11	12	82	168	60	15	10	10	10	10	80	170	60
11	10	9	10	69	182	67	14	10	10	10	10	70	180	65	15
10	10	10	71	200	81	15	12	10	10	10	70	200	80	15	10
12	12	58	204	91	17	12	14	10	10	60	205	90	15	10	15
11	46	201	106	18	14	16	15	10	45	200	105	20	15	15	15
34	185	122	23	10	14	17	16	35	185	120	25	10	15	15	15

Figure 1. (a) Original 8x8 image block (b) Image block where all pixel values are divisible by 5.

The FMM method will be completed when we divide each pixel value in the block with 5. This is shown in Figure 2.

Prior to the transformation the standard deviation of the original block was 20.38, while after the transformation the standard deviation dropped to 4.03. From this reduction it can be concluded that the storage space will be considerably less for the transformed block than for the original one. The range of the pixels in the original image was (0-255), but because of the FMM the range was shrunk to interval (0-51).

2	2	3	2	2	2	3	21
2	2	2	2	2	2	14	36
3	2	2	2	2	16	34	12
2	2	2	2	14	36	13	3
2	2	2	14	40	16	3	2
2	2	12	41	18	3	2	3
2	9	40	21	4	3	3	3
7	37	24	5	2	3	3	3

Figure 2. block pixel values after division by 5

After that, the minimal value of the FMM block can be subtracted from the matrix that is shown in Figure 2. In this case that value is 2, and the matrix after this operation is showed in Figure 3.

0	0	1	0	0	0	1	19
0	0	0	0	0	0	12	34
1	0	0	0	0	14	32	10
0	0	0	0	12	34	11	1
0	0	0	12	38	14	1	0
0	0	10	39	16	1	0	1
0	7	38	19	2	1	1	1
5	35	22	3	0	1	1	1

Figure 3. Image block after subtraction of the minimal value.

The resulting block has lot of zero elements that is easy to compress. The impact of subtraction would be even greater if the range of the image block would be smaller, but even in this case more efficient compression is possible.

The original image consisted of 8-bit pixels (range 0-255), so for each pixel we needed 8 bits to store. The whole image required 256x256x8 bits for storage. In total it is 524288 bits, or 64kB. After the FMM manipulation, the range dropped to (0-51), so each pixel could be represented using only 6 bits instead of the original 8.

In this paragraph we'll explain the coding strategy of the transformed block. Since the range varies between 0 and 51, 6 bits are used to represent the minimal value of the block. The coding of the remaining values depends on the maximal value of the block. The smaller the maximal value, the more efficient the coding will be.

The coding gain is greater if the variation of the block is smaller. For example, if the maximum value of the block would be 7 after subtraction, then each block entry could be coded using only 3 bits.

The quality measure used was the power signal-to-noise ratio that is defined through the following formula:

$$PSNR = 20 \log_{10} \left(\frac{MAX_f}{\sqrt{MSE}} \right)$$

$$MSE = \frac{1}{mn} \sum_0^{m-1} \sum_0^{n-1} \|f(i,j) - g(i,j)\|^2 \quad (1)$$

In the above formula, m and n is the size of the image, f and g are the original and resulting images, respectively.

For different images we got different PSNR values, so the quality depends also on the content of the image. For the purpose of this research 10 test images were examined. The test images are shown in Figure 4.



Figure 4. Test images. Baboon, Barbara, Boat, Cameraman, Clock, F16, Lake, Lena, Peppers, Pirate

The results of the FMM compressions are summarized in Table II.

Table II. Power signal to noise ratio and compression percentage for the test images after FMM compression

Image	PSNR	Compression percentage
Baboon	39.90	51.21
Barbara	39.93	43.20
Boat	39.94	43.59
Cameraman	39.82	50.04
Clock	39.39	57.07
F16	40.12	48.47
Lake	39.89	40.66
Lena	39.84	44.37
Peppers	39.88	39.69
Pirate	39.83	41.25

In this paper we presented the 5-MM, but other modulus methods such as 3-MM, 9-MM, 15-MM also exist. For comparison purposes we show a zoomed detail from one test image (Lena) after those transformations. In comparison to the original image, signal to noise ratios are 52.88dB (3-MM), 48.09dB (5-MM), 42.83dB (9-MM) and 38.31dB (15-MM). Artifacts due to the modulus method are visible on the two lower images, the 3-MM and 5-MM produced no visible degradation of the image.

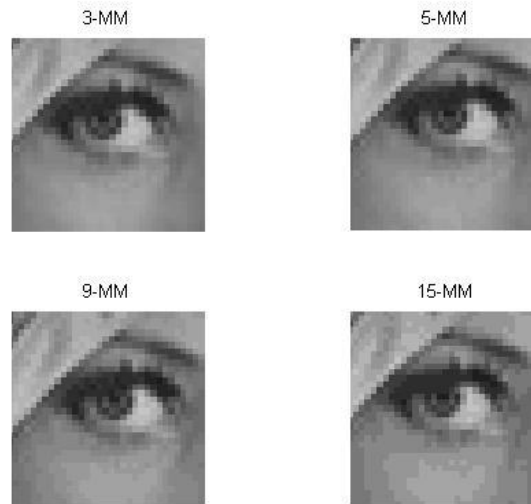


Figure 5. Detail of Lena test image after 3-MM, 5-MM, 9-MM and 15-MM.

3. FREQUENCY DOMAIN IMAGE COMPRESSION

Two main types of image compression are the lossless and lossy compressions. Either lossy or lossless, the main goal is the same: to represent the digital image with fewer bits. Lossless compression can retrieve the original digital image after decompression. Because it is impossible to compress image with high compression factor without errors, the desired type of compression is the lossy one. During the mid-eighties of the last century the International telecommunication Union and the International standardization Union together worked out a standard for compressing still digital images. The standard is known as JPEG (Joint Photographic Expert Group). The JPEG became the international standard in 1992.

The JPEG standard is based on the discrete cosine transform (DCT). DCT is capable of compacting the signal energy with high efficiency. The JPEG process consists of the following steps: dividing the image into 8x8 pixel blocks, subtracting 128 from all pixel values to make the (0-255) image range symmetric around 0, performing DCT on each block, quantization of the DCT coefficients using a predetermined quantization matrix, zig-zag coding to transform the 2-D block to a 1-D stream, run-length encoding and Huffman coding. The image is recovered from the stream using the inverse process.

The loss of information comes from the quantization step. The quantization matrix is not part of the JPEG standard, and the user can control the compression by varying the quantization matrix entries. Higher values in the quantization matrix will result in higher compression ratio and lower signal to noise ratio with the original image. The user has to decide how much quality he will trade for high compression ratio. Usually the desired quality is around 30dB. Below that value artifacts will become visible. The content of the digital image also has to be taken into consideration. Images with high frequencies are more sensitive to low quality quantization matrices. Those analysis hold only for the Y component of the image, the two color components are compressed in a slightly different way. Figure 7 shows the standard luminance quantization matrix (Q50) that was obtained empirically by a huge number of image processing experts. In the upper left corner there are smaller entries what means that the DC component and low frequencies have a bigger ability to survive, while in the lower right corner numbers are bigger. After division and rounding, most of the high frequency components will be equal to zero.

16	11	10	16	24	40	51	61
12	12	14	19	26	58	60	55
14	13	16	24	40	57	69	56
14	17	22	29	51	87	80	62
18	22	37	56	68	109	103	77
24	35	55	64	81	104	113	92
49	64	78	87	103	121	120	101
72	92	95	98	112	100	103	99

Figure 7. Standard luminance quantization matrix

From the Q50 matrix it is possible to derive other quantization matrices. For quality level greater than 50, the standard quantization matrix is multiplied by $(100 - \text{quality_level})/50$. For quality levels less than 50, the standard quantization matrix is multiplied by $(50/\text{quality_level})$.

4. RESULTS

After compressing the test images from Figure 4, we get the results that are presented in Table III. Two numeric parameters are used to evaluate the quality of the compression. Compression ratio (CR) is the quotient of the total number of bits in the original image and the number of bits in the compressed bit stream. For 256x256 pixel 8-bit grayscale images the original image has $256 \times 256 \times 8$ bits = 524288 bits. This number drops significantly after compression and varies between 40943 and 74022. Now it is easy to calculate the compression ratio (CR). CR vary between 7.08 and 12.81. The other parameter we measured was the signal to noise ratio that was defined in equation (1). Depending on the content of the image PSNR was between 29.35 and 34.69 dB. In most cases this is a satisfactory result with no, or very few visual artifacts.

Table III. CR and PSNR for test images compressed with JPEG and standard quantization matrix

Image	Bitstream	PSNR	CR
Baboon	59250	29.35	8.85
Barbara	63303	33.37	8.28
Boat	66067	31.86	7.94
Cameram.	54223	31.50	9.67
Clock	40943	34.69	12.81
F16	58458	32.61	8.97
Lake	74022	31.09	7.08
Lena	52342	33.58	10.02
Peppers	56106	34.14	9.34
Pirate	68075	31.59	7.70

5. CONCLUSION AND FUTURE WORK

In this paper we compared one spatial domain (FMM) and one transformed domain (JPEG) image compression algorithm. Both methods introduced some image quality degradation. The degradation in the FMM came because we limited the pixel values to be multiples of 5, thus the biggest change in pixel values was 2. This degradation is not noticeable for the human visual system. This method achieved very high signal to noise ratio, and a somewhat modest compression ratio of around 50%. On the other hand, the JPEG compressed the original image around 10 times, what resulted in only 10% of the original size, but the price had to be paid for it. The other parameter measured (PSNR) was one order of magnitude lower than with the FMM.

In the future, the author plans to embed the FMM method into the JPEG process thus combining the positive and desired effects of both methods. The plan is to discover a new class of quantization matrices that will quantize the DCT coefficients with minimal degradation.

The author also investigated the effect of the quantization matrix on the signal to noise ratio. For this test the Cameraman test image was chosen. The quantization matrix was varied between 1 and 100 (all qualities), and for each one the signal to noise ratio was calculated. The results of this test are shown in Figure 8.

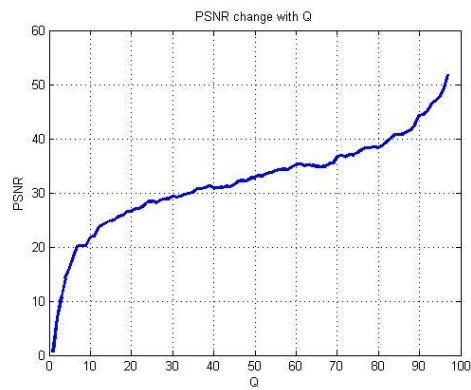


Figure 8. PSNR as a function of quantization matrix

REFERENCES

- [1] Michael P. Ekstrom: "*Digital Image Processing Techniques*", Academic Press, Inc., Orlando, FL.
- [2] M. Salapura, Diplomski rad, Fakultet tehničkih nauka, Novi Sad, 1996.
- [3] Željen Trpovski, Vladimir Crnojević, Mikloš Pot: Kompresija Slike Rastavljanjem na Bitske Nivoe, DOGS 2000.
- [4] Firass Jassim, Hind Qassim: Five modulus method for image compression, Signal Processing : An International Journal (SIPIJ), 2012.

Effect of Temperature on Low Frequency Noise Emission from Modern Lamps

Dr. Istók Róbert,

Óbuda University, Kálmán Kandó Faculty of Electrical Engineering Power System Department, Bécsi út 94-96/a 1034 Budapest, Hungary, istok.robert@kvk.uni-obuda.hu,

Abstract: The increased usage of modern lighting lamps produces increased electromagnetic emissions. From the frequency point of view the conducted electromagnetic emissions are divided into two groups: low frequency emissions and high frequency emissions. The electronic devices, which contain single phase rectifiers, have significant harmonics emissions. Modern lamps are driving by electronic ballast, which contains single phase rectifiers. The modern lamps are nonlinear loads and introduce harmonic distortions in power supply lines comparison to incandescent lamp which has no harmonics emission. Lighting is highly sensitive to rms voltage changes; even a slight deviation (of the order of 0.25%) is perceptible to the human eye in some types of lamps. Superimposed interharmonic voltages in the supply voltage are a significant cause of light flicker in both incandescent and fluorescent lamps [1]. Power Factor PF and Total Harmonic Distortion THD provide a quantitative measure of the power quality in an electrical system. The THD emission of a lamp could be influenced by temperature. The amount of useful power being consumed by an electrical system is predominantly decided by the PF of the system [2].

Keywords: keyword1; keyword2; keyword3; etc. 9 pt Justify Power Factor; Total Harmonic Distortion; electronic ballast; modern lighting

1 Introduction

Replacing of the incandescent bulbs are doing continuously. The main reason of replacing is the low efficiency of the incandescent bulbs. Using of modern lamps conduct to a decrease of energy consumption in lighting field. The energy saving is an important thing, which the modern lighting try to fulfil, but the apparition of modern lamps determines new questions. One of them is electromagnetic compatibility – EMC [3]. All the modern lamps: compact fluorescent lamps, induction lamps, LED, are driven by electronic ballasts. It is well known that the functionality of the electronic ballast is accompanied by noise emissions. This noise emission has low and high frequencies. The spreading path of

electromagnetic noise are next: conducted through power and signal cable and radiated. The conducted emission is divided in two groups: low frequency conducted emission as harmonic and flicker emission. The low frequency conducted emissions are noise emissions up to 9 kHz. The high frequency conducted emissions are noise emissions between 9 kHz-30 MHz. In case of modern lighting the low frequency, noise is mean typically the harmonic emission. The flicker emission does not represent a problem in case of lighting lamps.

2 Harmonic and total harmonic distortion

If a non-linear load is connected to the power system, it draws a current that is not sinusoidal. The current waveform can become quite complex, depending on the type of load and its interaction with other components of the system. The current waveform is described with the help of Fourier series analysis [3]. It is divided into a series of simple sinusoids, which start at the power system fundamental frequency and occur at integer multiples of the fundamental frequency.

The voltage from power source is distorted by current harmonics due to source impedance. If the voltage source has small source impedance, the current harmonics will cause only small voltage harmonics. This is the case when voltage harmonics are small compared to current harmonics. It is typically for lighting electronic ballast.

Total Harmonic Distortion (THD) is a measurement of the level of harmonic distortion present in power systems. Total harmonic distortion can be related to either current harmonics or voltage harmonics, and it is defined as the ratio of total harmonics to the value at fundamental frequency times 100% [4].

$$THD_V = \frac{\sqrt{V_2^2 + V_3^2 + \Lambda + V_n^2}}{V_1} \cdot 100\% = \frac{\sqrt{\sum_{k=2}^n V_k^2}}{V_1} \cdot 100\% , \quad (1)$$

$$THD_I = \frac{\sqrt{I_2^2 + I_3^2 + \Lambda + I_n^2}}{I_1} \cdot 100\% = \frac{\sqrt{\sum_{k=2}^n I_k^2}}{I_1} \cdot 100\% , \quad (2)$$

where V_n is the RMS voltage of k-th voltage harmonic; I_n is the RMS current of the k-th current harmonic; k=1 fundamental frequency.

3 Effects of harmonics

Motors and generators

The voltage and current harmonics in motors and generators increase heating due to iron and copper losses at the harmonic frequencies, and affects the efficiency and developed torque as well. The harmonic currents in a motor can raise the audible noise emission, and produce a resultant flux distribution in the air gap. The fifth and seventh harmonics can create mechanical oscillation in a turbine-generator combination or in a motor load system.

Transformers

Current harmonics cause an increase in copper losses and stray flux losses. Voltage harmonics cause an increase in iron losses. The result is transformer heating increases. The losses increase with frequency. The higher frequency harmonic components are more important than the lower frequency component. Another effect of harmonics is increasing audible noises.

Power cables

If cables take part in a resonance system, the cables could be affected by voltage stress and corona, which can produce dielectric failure.

Capacitors

The reactance of a capacitor bank decreases with frequency, and the bank acts as a sink for higher harmonic currents. This effect increases the heating and dielectric stresses.

Electronic equipment

Electronic devices, which are sensitive to the zero-crossing point of the voltage waveform, can be affected by harmonic distortion. Harmonics can shift the voltage zero crossing or the point at which one phase-to-phase voltage becomes greater than another phase-to-phase voltage.

Other types of electronic devices can be affected by transmission of ac supply harmonics through the equipment power supply or by magnetic coupling of harmonics, which can produce malfunctions of device. The harmonic voltage

distortion factor has to be no more than 5% and the largest single harmonic no more than 3% [5].

4 Measurement system

IEC 61000-3-2 is the standard, which describes the harmonic measurements method for lighting equipment. The measurement system is presented in *Fig 1*.

The power supply of the measurement system has to be a ‘clean supply’ with a stable voltage, frequency and poor harmonic emission.

The voltage of power supply has to be the same as the rated voltage of the device under test. In the case of 220V – 240V voltage range, the test voltage has to be 230 V. The variation of test voltage has to be within $\pm 2.0\%$ and the frequency within $\pm 0.5\%$ of the nominal value.

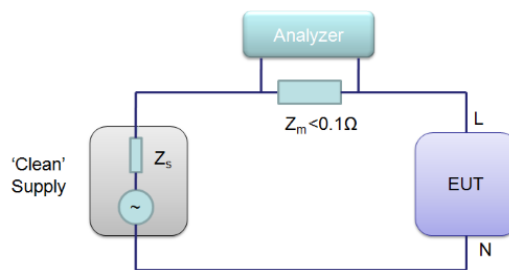


Fig. 1. Harmonic emission measurement system

The harmonic emissions must not exceeded the next values:

- 0.9 % for harmonic of order 3;
- 0.4 % for harmonic of order 5;
- 0.3 % for harmonic of order 7;
- 0.2 % for harmonic of order 9;
- 0.2 % for even harmonics of order from 2 to 10;
- 0.1 % for harmonics of order from 11 to 40.

The peak value of the test voltage shall be within 1.40 and 1.42 times its RMS value and shall be reached within 87° to 93° after the zero crossing [6]. The EUT (equipment under test) in this case is a lighting lamp.

5 Low frequency noise emission

The standards, which refer to harmonic emission, require measurements of only one device, but what is happening when the devices are working in a network. One idea is that the increase of the number of the lamps results in noise emission increase. In Fig. 2 the typical circuit diagram of electronic ballast is presented. The AC line input voltage, typically 220-240 VAC 50/60 Hz, an EMI filter to block the noise emission, a rectifier with smoothing capacitor, a half-bridge inverter for DC to AC conversion, and the resonant circuit to ignite and run the lamp. The main source of low frequency harmonics is the rectifier stage [7].

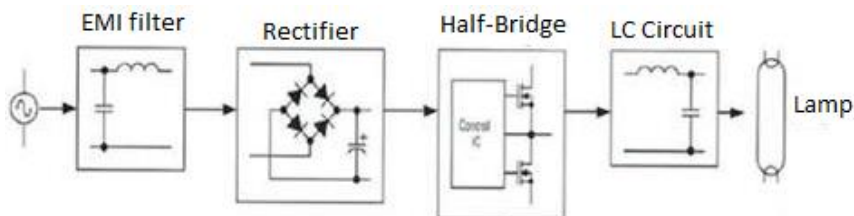


Fig. 2. Circuit diagram of electronic ballast

In Fig. 3 the voltage and current wave form of a 11 W compact fluorescent lamp is presented. The measurement result of a 23 W induction lamps is presented in Fig. 4. In both cases the current consumption is not sinusoidal, which means that the harmonic current emission is high. The amount of harmonic emission is higher if the current waveform starts to increase later than voltage wave form. Important is that current has to start flowing before 60° [6]. From measurement results it can be seen (Fig. 3 and Fig. 4) that the harmonic emission of induction compact fluorescent lamp is higher than the emission of compact fluorescent lamp.

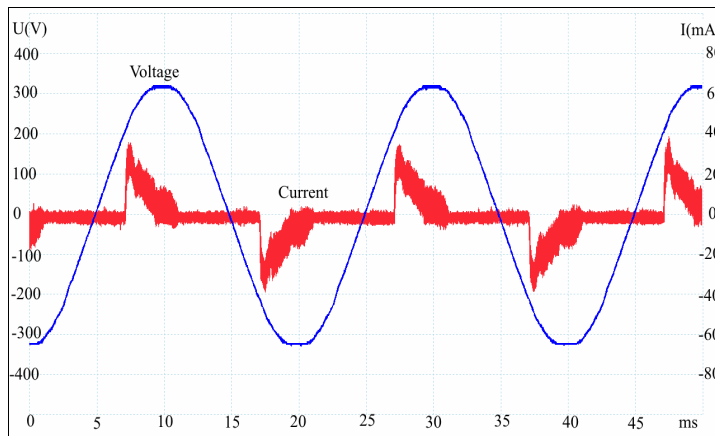


Fig 3. Voltage and current wave form of a compact fluorescent lamp

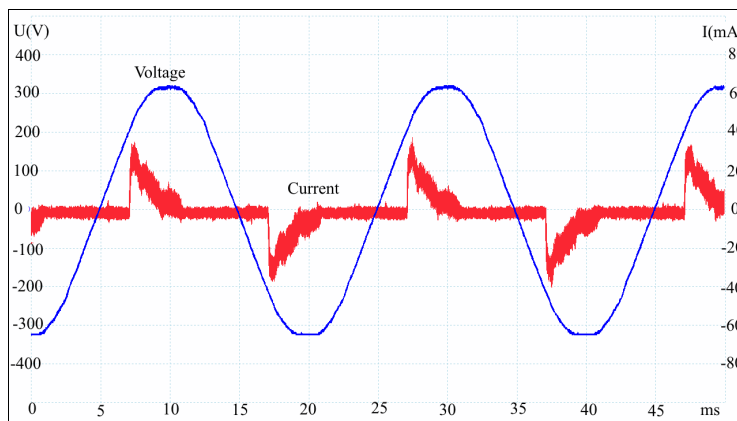


Fig 4. Voltage and current wave form of an induction lamp

Power Factor PF and Total Harmonic Distortion THD provide a quantitative measure of the power quality in an electrical system. The amount of useful power being consumed by an electrical system is predominantly decided by the PF of the system [2].

In case of cheap LEDs and compact fluorescent lamps the power factor correction is done with inductors which are used on DC side or AC side, Fig. 5 and Fig. 6.

C_i - capacitor could improve the power factor.

Typically, in case of LED lamps the harmonic emission is lower than in case of CFL lamps [8][9]. The reason is that the electronic ballast of LED contains active power factor correction circuits. In Fig. 7 is presented the wave forms of current and voltage of a 9W LED

and a 7W LED lamp. It could be seen that the current wave form of 7W LED is close to sinusoidal shape what is mean the harmonics emissions are on a low level. The current wave form of 9W LED lamp has spike form, what is mean this lamp has a high harmonic emission. Unfortunately, not all LEDs have a good power factor correction.

For higher quality LED lamps a better power factor is achieved with active power factor correction circuits[8]. In Fig. 8 is presented the measurement results for a 15W LED with good power factor correction and a 15W LED with poor factor correction. The voltage wave forms are the same. In case of modern lightings, the voltage total harmonic distortion is very low. The current wave forms are different. The LED with low power factor correction has a spike current wave form which is similar with current wave form of compact florescent lamps. In Fig. 9 is presented the measurement results of a 23W and a 22W compact florescent lamps. The current wave form are similar, but the in case of 23W lamp the current start to increase earlier than the 22W lamp, that is mean the harmonic emission of first lamp is lower. The second observation is that the current of second lamp is much lower, that is mean the wattage of the lamp is lower than the wattage specified on the lamp. In table 1 is presented the total current harmonic distortion and power factors of different compact florescent LED and induction lamps. The total harmonic distortion emission of LED lamp with a good power factor correction is more than 3 times lower than in case of LED with poor power factor correction.

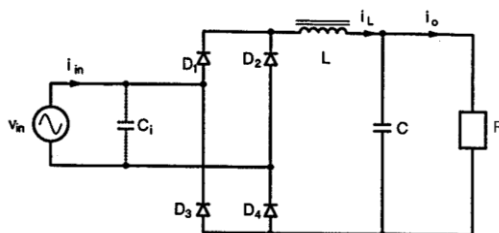


Figure 5. Full-wave rectifier with LC filter dc-side inductor

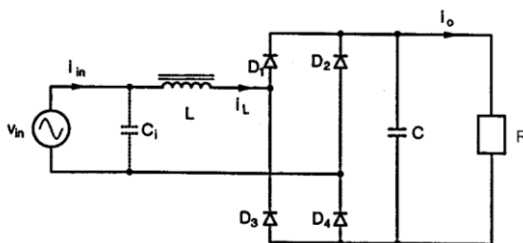


Figure 6. Full-wave rectifier with LC filter ac-side inductor

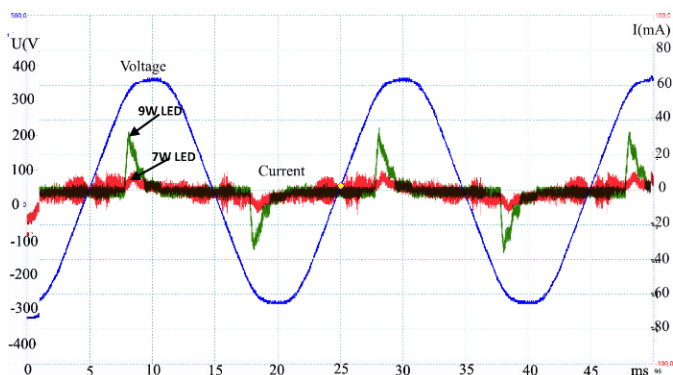


Figure 7. Current and voltage wave form of a 9W LED and a 7W LED

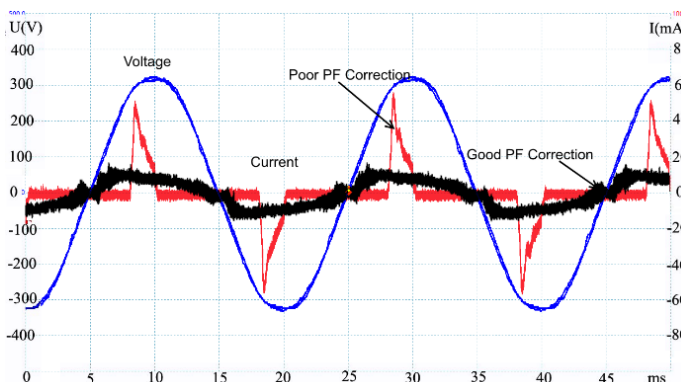


Figure 8. Current and voltage wave form of a 15W LED with good PF correction and a 15W LED with poor PF correction

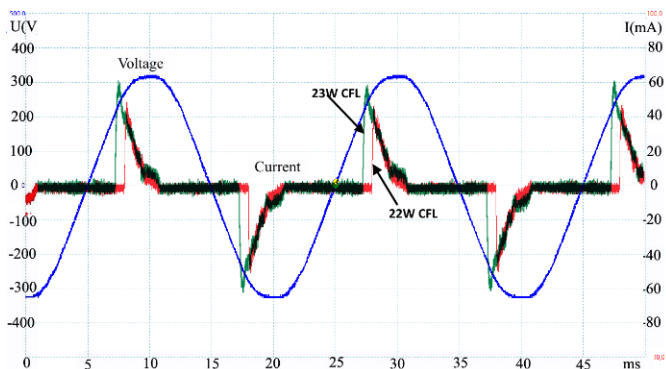


Figure 9. Current and voltage wave form of a 23W and 22W compact fluorescent lamps

6 Measurement results of lighting networks

As mentioned before, the standard measurement are required only one lamp to be measured, but in a office there are more than one lamp. In figure 10 can be seen the variation of noise emission function of CFL lamps number variation.

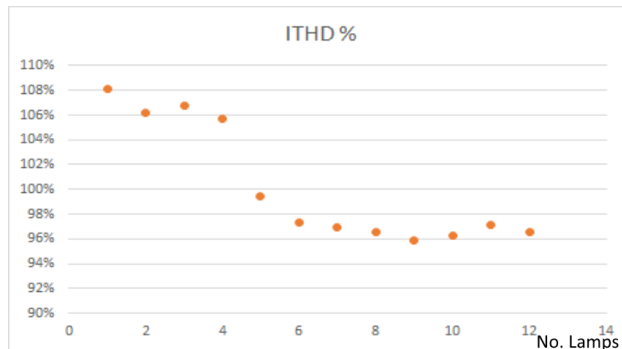


Figure 10. THD emission for different number of compact fluorescent lamps

The measurement results show that, increasing of number of CFL lamps, determine the noise emission decreasing from 108% to 96%. As the diagram show, if the number of lamps is higher than 8 the level of noise remain around of 96%. As a conclusion the emission of a CFL lamps network is lower than emission of one CFL lamp.

In figure 11. the noise emission was measured at different ambient temperature. The measurements were done with cold lamp, that is mean the lamps were switchen on and after 30 seconds the measurement was done. Variation of temperature determine a variation of noise emission too. During the measurements the lamps network contained 6 LED lamps.

In figure 12 is presented the noise emission variation function of working temperature variation. The noise emission of lamps depend by working temperature of lamps. After switching on the lamps the the noise emission should be higher than usual noise emission level.

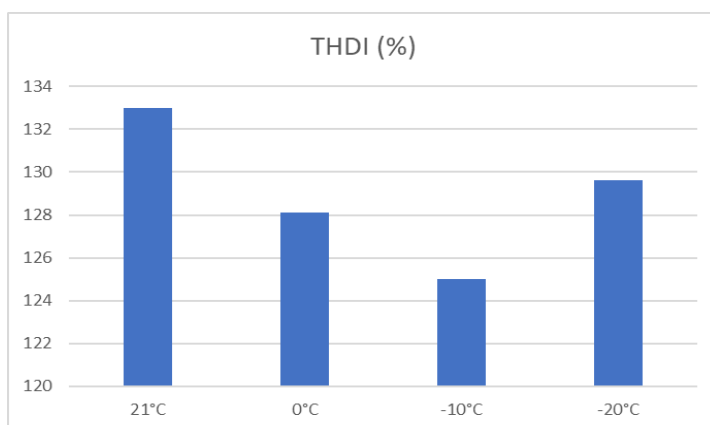


Figure 11. Variation of noise emission with variation of temperature

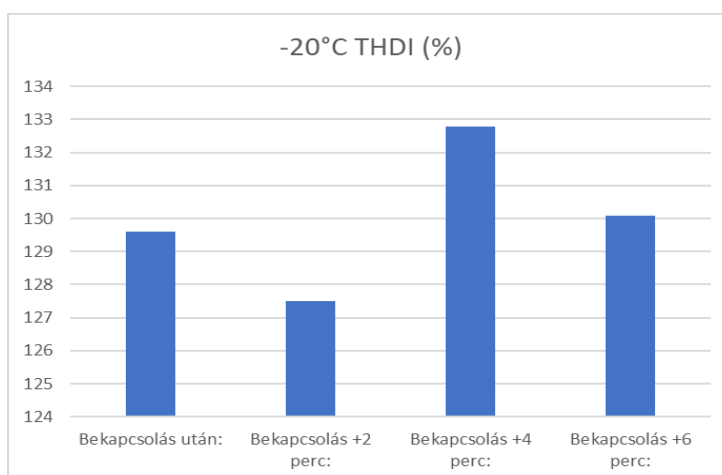


Figure 12. Variation of noise emission with variation of lamps working temperature

Conclusions

Some of modern lamps type have an important harmonic emission. Harmonic emission of some cheaper LED lamps could be higher than emission of compact fluorescent lamps. The differences between noise emissions in case of different compact fluorescent lamps are significantly, but the differences are not so high than in case of LED lamps. If the lamps are measured in a network, the noise emission is lower than in case of a single lamp. In case of CFL lamps this phenomena is more stronger than in case of LED lamps.

References

- [1] Electromagnetic compatibility (EMC) - Part 3-2: Limis - Limits for harmonic current emissions (equipment input current ≤ 16 A per phase), IEC 61000-3-2: 2014,
- [2] A. Gil-de-Castro ; S. Rönnberg ; M. H. J. Bollen ; A. Moreno-Muñoz ; V. Pallres-Lopez, “Harmonics from a domestic customer with different lamp technologies”, 2012 IEEE 15th International Conference on Harmonics and Quality of Power , Hong Kong 17-20 June 2012, pp. 585 – 590
- [3] Azcarate, J.J. Gutierrez, A. Lazkano, P. Saiz, K. Redondo, L.A. Leturiondo, “Experimental study of the response of efficient lighting technologies to complex voltage fluctuations”, International Journal of Electrical Power and Energy Systems, Vol. 63, 2014, pp. 499- 506.
- [4] Domagk M., Zyabkina O., Meyer J., Schegner P. Trend identification in power quality measurements, 2015 Australasian Universities Power Engineering Conference, Wollongong, Australia 27-30 September 2015, pp. 1–6.
- [5] IEEE Std 519, IEEE recommended practices and requirements for harmonic control in electrical power systems, 2014.
- [6] IEC 61000-3-2, Electromagnetic compatibility (EMC) - Part 3-2, Limits for harmonic current emissions (equipment input current ≤ 16 A per phase), 2014.
- [7] Koponen P., Hansen H., Bollen M. Inter-harmonics and light flicker, International Conference on Electricity Distribution, Lyon, France, 15-18 June 2015, paper 1100.
- [8] S. K. Rönnberg, M. Wahlberg and M. H. J. Bollen, “Harmonic emission before and after changing to LED lamps — Field measurements for an urban area”, 2012 IEEE 15th International Conference on Harmonics and Quality of Power, Hong Kong, 17-20 June 2012, pp. 552-557.
- [9] “Power Factor Correction (PFC) basics, Fairchild Semiconductor”, Application note 42047, 2004.
- [10] Power Factor Correction (PFC) basics, Fairchild Semiconductor, 2004, Application note, 42047.

Multiphysical Analysis of High Torque Density Propulsion Motors for E-mobility Applications

Sándor HORVÁTH, Kristóf KISS, István VAJDA

Széchenyi István University, Győr, Hungary
Electromobility Research Center
e-mail: sandor.horvath@pm.me

E-mobility is one the most demanding applications for rotating electrical machines in our present days. A typical duty includes not only non-periodic load and speed variations, but frequent overloads and changeovers between motoring and regenerative braking as well. To achieve competitiveness, an integrated electric powertrain has to face strict technical-economic requirements. These can only be fulfilled by applying high torque density propulsion motors. The utilization of a given electrical machine is generally expressed by its Torque per Rotor Volume (TRV) ratio. In order to protect the insulation system from overheating and thus lifetime reduction or critical failure, the maximum permissible value for TRV very much depends on the intensity of cooling. Further design aspects like mechanical stresses and deformations, envelope dimensions, efficiency requirements, limited weight of active and inactive parts also influence the achievable or allowable utilization. Software packages for industrial purposes provide great functionality with ease of use. However, for academic and research interests, often more flexible and transparent modeling and evaluation techniques are needed. At the Electromobility Research Center, Authors are developing a software tool to perform rapid multiphysical analysis on various propulsion motor types, equipped with different liquid-cooling methods. This Paper introduces the modeling and simulation processes, which have been implemented for sinusoidal supply machines with radial fluxpath and inner rotor so far.

Keywords: *electric propulsion, multiphysics, self-developed software, co-simulation*

1 Electromagnetic Topology Analysis

1.1 Software Concept and Implementation

Throughout various fields of engineering, topology optimization is a novel approach for problems of distributing a limited amount of material in a design space, by satisfying predefined objectives and constraints. To obtain practical solutions,

with regards to manufacturability, advanced methods are being recently implemented for different types of rotating electrical machines [1], [2].

The Electromagnetic Topology Analyser (EMTA), presented in this Paper, is a self-developed software tool for automated characterization of propulsion motor alternatives, like Squirrel Cage Induction Machine, Permanent Magnet Synchronous Machine, Switched Reluctance Machine and Synchronous Reluctance Machine. Topology refers to the combination of core geometry, material properties and winding scheme, being a simplified numerical representation of the physical machine. Operation of EMTA is based on a connection between a finite element software – capable of field simulation – and a high-level control environment. Block diagram of EMTA, indicating the software components, is shown in Fig. 1.1.

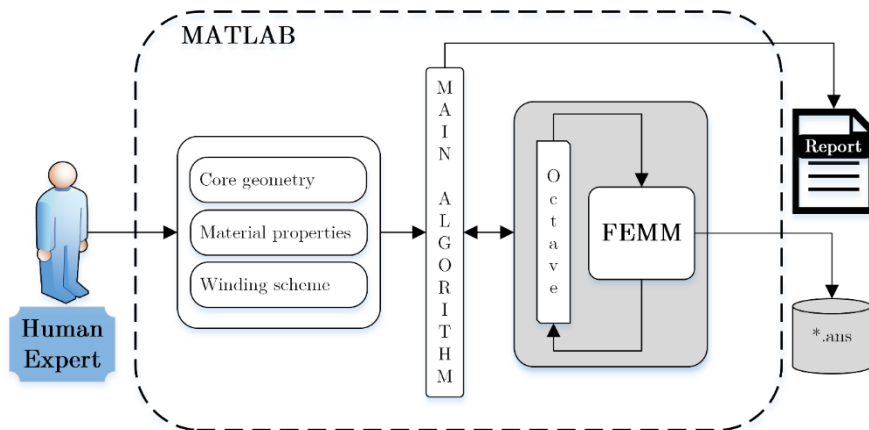


Fig. 1.1. System diagram of Electromagnetic Topology Analyser and the selected components

According to Fig. 1.1., the high-level control was implemented in MATLAB 8.5 environment, while FEMM v4.2 was chosen as the finite element software.

FEMM is a suite of programs for solving low frequency electromagnetic problems on two-dimensional planar and axisymmetric domains. The v4.2 addresses linear/nonlinear magnetostatic problems, linear/nonlinear time harmonic magnetic problems, linear electrostatic problems, and steady-state heat flow problems [3]. Octave is practically an interface, which enables the automation of FEMM via a predefined set of MATLAB-functions. The syntax of an Octave program is similar to that of FEMM's Lua scripting language, but is more powerful due to the matrix-oriented nature of MATLAB. Octave distribution is installed with FEMM v4.2 [4].

At the beginning of a new topology analysis process, the Human Expert has to choose between available machine types and enter the corresponding input data, based on physical dimensions. Main Algorithm is a complex MATLAB routine,

with separate modules for different machine types, which were design to be interchangeable. Topological similarities can be exploited due to this modular structure. While the Human Expert is an organic component of this system, to eliminate time-consuming repetitive human work and interaction, numerous automatisms were implemented:

- definition of the EM problem, boundary and symmetry conditions;
- model assembly (geometry + material properties + winding scheme);
- control of spatial discretization and solver algorithms;
- effective utilization of computational resources;
- raw data management and post-processing;
- extracting and storing useful information, visualization, data sharing.

FEMM is capable of certain post-processing tasks, which are also controlled and extended by the Main Algorithm. By default, all *.ans result files are stored, giving the possibility of additional data extraction in future. At the end of a topology analysis sequence, results get summarized for the Human Expert in a *.pdf Report file. FEMM was chosen as the core software component for EMTA because of its simple usability and detailed documentation for automation. A similar application, with a coupling between MATLAB and FEMM, is mentioned in [6] for SynRM.

1.2 Modeling and Simulation

To demonstrate analysis capabilities, an embedded-type PMSM was designed with a reasonable TRV ratio, approximately 85% of Nissan Leaf's peak torque density [5]. The specification includes the following requirements and constraints:

- Configuration: radial flux path, inner rotor, no field-weakening mode
- Total volume: 5 litres (SOD=240 mm and L=110 mm)
- Peak TRV $\approx 120 \text{ kNm/m}^3 \rightarrow \text{SID}=170 \text{ mm}$, stator with 48 slots
- Hypothetical operating temperature: 110 °C ; Ambient temperature: 20 °C
- Winding: 16 poles, max. 50% effective slot fill factor
- Core material: M350-50A
- PM material: N41UH ($H_c = -906 \text{ kA/m}$; $B_r = 1.17 \text{ T}$ at 110 °C)

As one may notice, a relatively commercial core material was selected, in order to obtain practical solutions. The rare-earth PM material was chosen to provide a competitive energy-product, yet capable of withstanding ultra high temperature. No field-weakening mode is required, meaning that a horizontal PM arrangement is suitable for the embedded-type rotor. Neither bridges and ribs in the rotor lamination, nor PM dimensions were optimized in the reference design.

For geometrical modeling of a given topology, point with Cartesian-coordinates are assigned to certain points of the lamination layout. This way, geometry can be easily manipulated. By increasing the number of these reference points, we have the possibility to create complex geometries with various transitions (chamfers, fillets). Time demand of simulation increases due to geometrical complexity.

During a topology analysis, often hundreds of individual electromagnetic problems must be solved. In case of a synchronous machine, e.g. to obtain detailed torque characteristics, a locked-rotor test is simulated at different positions (at their corresponding load-angles) for a current source feeding, via magnetostatic analysis. The Main Algorithm organizes these individual problems into a sequence.

For meshing, i.e. discretization of the solution region by thousands of simple shapes, *triangle.exe* is applied by default. Mesh density, i.e. the number of nodes and their size, is crucial in terms of calculation accuracy and time demand. In a region of high gradients, like the airgap of rotating machines, mesh should be set properly dense. Applied mesh density for the reference design can be seen in Fig. 1.1. below.

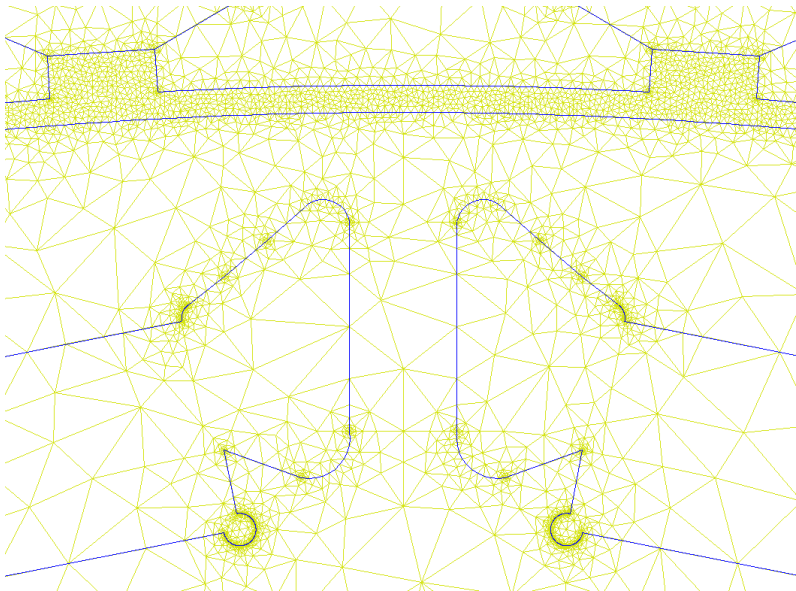


Fig. 1.2. Applied mesh density in the vicinity of air gap, before PM insertion

Effective utilization of computational resources was carried out by a multithreaded programming technique, via the parallelization of solver instances. By applying this MATLAB feature, the time demand of an analysis sequence can be significantly reduced for magnetostatic problems, as linear function of physical processor cores.

The relevant partial differential equations for all nodes are solved by fkern.exe. Both triangle.exe and fkern.exe are integrated components of FEMM v4.2.

According to the electromagnetic finite element calculation, the required peak TRV ratio ($\approx 120 \text{ kNm/m}^3$) can be reached by applying an electrical overload.

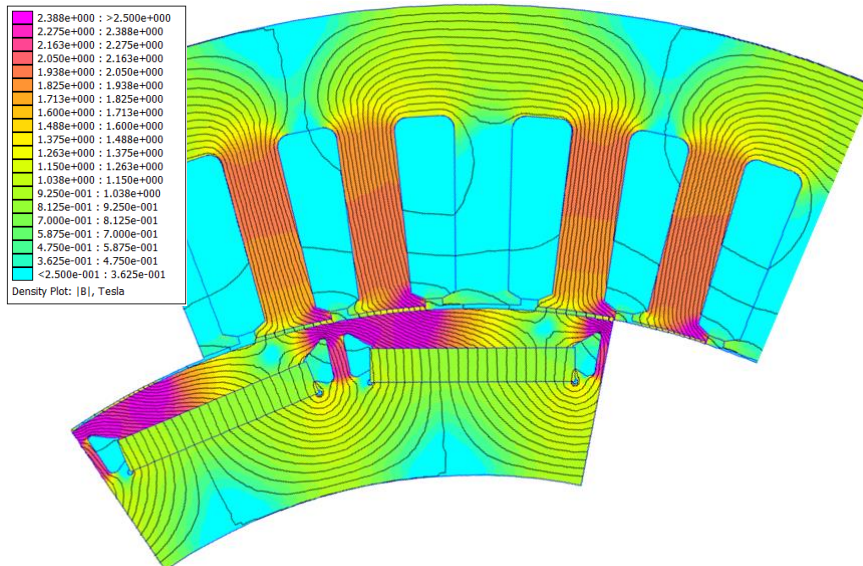


Fig. 13. Full-load flux-density plot for the modeled fraction

The reference design produces 300 Nm air gap torque at 120 kArms/m linear current density. Current density in the conductors is 22.5 A/mm^2 .

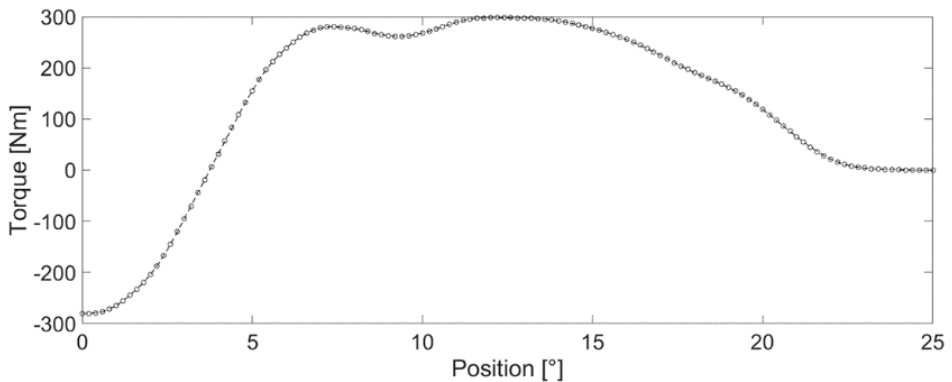


Fig. 14. Full-load torque-characteristics

Input geometry, loads and losses are then transferred to the thermal analysis modul.

2 Transient Thermal Topology Analysis

2.1 Software Concept and Implementation

A thermal model based on Beuken's RC-analogy was built in Matlab. The model is capable of calculating the temperature distribution of the stator when geometrical, cooling and load parameters are given.

The program starts with loading the model settings and parameters of the input geometry. Model settings define the chosen node density of the model, while the input geometry contains the dimensions of the stator. Then a test program is loaded, which defines the load characteristics in time. In the recent software version, only constant load is supported.

After storing the needed geometry, the list of materials used in the model are loaded. The geometry, the materials and their properties are contained in Matlab structures, 'structs' on the global workspace. For example the electrical steel is contained under the name of 'Iron', with the following properties:

- Specific heat
- Mass density
- Electrical conductivity
- Thermal conductivity in d,q and h directions
- Thermal coefficient of losses
- Hysteresis coefficient for loss calculation

As a lumped parameter thermal model requires the thermal nodes to be homogenous or quasi-homogenous, node size would need to be greatly reduced for the slot, for it contains a multitude of materials. Another approach we followed is to create an equivalent slot material based on the Hashin-Shtrikman approximation. [7] Although the approximation is described for a two-component system, we used a weighted average to calculate the equivalent insulation parameters (λ_p, c_p), and then, the equivalent slot parameters (λ_e, c_e) using the following formulae:

$$\lambda_e = \lambda_p \frac{(1 + v_c)\lambda_c + (1 - v_c)\lambda_p}{(1 - v_c)\lambda_c + (1 + v_c)\lambda_p} \quad [2](1)$$

$$c_e = \frac{v_c(\rho_c c_c - \rho_p c_p) + \rho_p c_p}{v_c(\rho_c - \rho_p) + \rho_p} \quad 2$$

Where v_c is the copper fill factor, ρ_p, ρ_c are the insulation and copper mass densities, respectively. The equivalent conductivity λ_e is valid in d and q (radial and tangential) directions. The axial conductivity is considerably higher – as there is continuous copper winding to conduct heat – it was chosen to be equal to the

conductivity of copper multiplied by the fill factor. This induces a negligible error because of the difference between material conductivities. [8]

The method for creating a quasi-homogenous material is erroneous when calculating with higher fill factors, showing a higher equivalent conductivity than numerical simulations and measurements of [7] showed. It is also computes a higher conductivity value when there is considerable difference between the conductivity values of the different insulating materials. It is, however, more accurate in calculating heat capacity than numerical models.

Once material properties are defined, a thermal network is to be created. For defining a thermal network, the object needs to be separated to finite volumes with simple geometries. In case of rotating machines, the simplest geometry is a cylindrical section, shown by Fig. 2.1. These simple geometries are called thermal cells [8] or nodes [9], and they also need to be homogenous, as mentioned before.

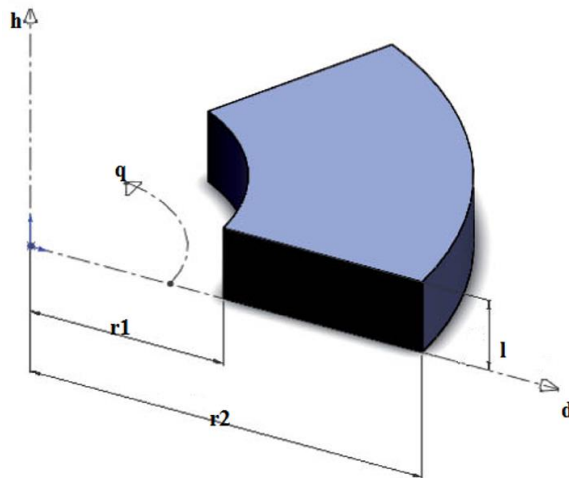


Fig. 2.1. Thermal cell definition for a simple cylindrical section

When these requirements are fulfilled, the thermal properties of these nodes can be calculated. This is the point where the advantages of lumped parameter models are noticeable: even with higher node count, the computation remains fast. This is because the simple geometries allow one to use a linear system of equations based on the result of the differential equation of heat transfer, rather than needing to solve the differential equation itself. One obvious disadvantage is also noticeable: it is tedious to create certain geometries, models often require simplifications.

The basic solution for the thermal conductivity of a cylindrical body:

$$K_D = \frac{\lambda_d \cdot q}{\log\left(\frac{r_2}{r_1}\right)}; \quad K_Q = \frac{\lambda_q \cdot \log\left(\frac{r_2}{r_1}\right)}{q}; \quad K_H = \frac{\lambda_h \cdot (r_2^2 - r_1^2) \cdot q \cdot \frac{\pi}{2}}{l} \quad [2](3)$$

In addition to conductivity values between two nodes, the heat capacities and nodal losses also need to be defined. Heat capacity is calculated by multiplying specific heat capacity and mass density values of materials by node volume.

External temperature and surface heat transfer coefficient can be set arbitrarily.

2.2 Importing Losses from 2D Electromagnetic Analysis

Nodal losses are gained by summing all losses inside their finite volume. For this reason it is advantageous to define specific losses as well. A specific loss value for copper losses is given as follows:

$$p_{Cu} = J^2 \cdot \frac{ff_{Cu}}{\sigma_{Cu}} \cdot k_R \quad [2](4)$$

Where J is the current density flowing in the copper conductor, ff_{Cu} the fill factor of copper in slot, σ_{Cu} is the electrical conductivity of copper, and k_R is a coefficient describing increased losses due to alternating current (depending on material parameters, slot geometry and supply frequency). [9] With this method, the geometrical and material input values are defined. The current density, as electrical load comes from the 2D electromagnetic solution. Copper loss for each node can be calculated by multiplying p_{Cu} with the node volume.

A similar approach is used with iron losses, where the source is, once again, the electromagnetic solution. This time the relevant source is the flux density map and the supply frequency. When multiple time steps are calculated, the time function of average flux density is extracted for each node. With the time functions and base frequency available, a Fourier transform is performed and the following expressions are evaluated to obtain $p_{Fe,EC}$ eddy current and $p_{Fe,Hy}$ hysteresis loss.

$$p_{Fe,EC} = \frac{\pi^2}{6} \cdot \sigma_{Fe} \cdot f^2 \cdot d^2 \cdot \sum_{n=1}^{\infty} n^2 B_n^2 \quad [2](5)$$

$$p_{Fe,Hy} = C_{Hy} \cdot \frac{f}{\rho_{Fe}} \cdot \sum_{n=1}^{\infty} n^2 B_n^2 \quad [2](6)$$

Where σ_{Fe} , ρ_{Fe} , C_{Hy} are the electric conductivity, mass density and hysteresis coefficient of lamination material, d is lamination thickness and f is base frequency of supply, respectively. [9] The specific iron losses are to be multiplied by node volume to acquire nodal losses – with the difference of even specific iron losses being differentiated node by node.

An easier solution is importing a single flux density solution, sweeping it by the radius and collecting the highest flux density absolute value for each specific radius. Then, assuming a sinusoidal flux distribution the losses are calculated with the above mentioned [2](5)-[2](6) equations. This assumption greatly decreases computational requirements, but reduces accuracy at the same time.

2.3 Modeling and Simulation

Correctly defining the finite volumes of the machine and creating a thermal conductance matrix is the most time-consuming part of creating a lumped parameter model. For every new topology the method requires a new matrix, in other words, a completely new model. Our goal was to create a system where building a model is as fast as possible. Using Matlab structures, thermal nodes are built. The input of a builder function for a cylindrical element requires the outer and inner radius, length and angle of the cylindrical section, the material and the loss flag to be used. Loss flags guide the program on which loss equation to use later. The structure of a machine part consists of the following elements:

- Heat Transfer Matrix
- Vector containing Volume of nodes
- Vector containing Heat capacity of nodes
- Vector containing Loss flag of nodes
- Vector containing Cooled flag of nodes
- Vector containing Cooling direction flag of nodes
- 6 Vectors containing conductivity values towards neighboring machine parts or the environment (one for each spatial dimension and direction)
- 6 Vectors containing the list of nodes that are connected with the environment
- 4 Vectors containing Surface area of nodes
- A struct containing geometry of nodes

A heat transfer matrix describes thermal connections between nodes of a model. If the i -th and j -th node are directly thermally connected, the matrix will contain the thermal conductivity value between them with a negative sign in its ij and ji elements. [3] The main diagonal is empty at this point.

After the basic structures are defined, they are to be joined, in order to create more complex geometries. Joining two structures means concatenating their matrices and vectors, as well as completing the thermal conductivity matrix by new elements, which describe connections between the two structs. If during joining some nodes have their material property described as 'coolant', they will not appear in the heat transfer matrix, the neighboring nodes will have their 'cooled' flag enabled instead.

Fig. 2.2.(a) shows the heat transfer matrix and the modeled part of the machine it represents. The model is built from 800 nodes and 3088 thermal connections are defined. The coloring of Fig. 2.2.(b) represents loss flags: blue for no loss, green for iron loss and yellow for copper loss.

Once the whole model is built, the losses are calculated for each node and the main diagonal of the heat transfer is filled according to the following rule:

$$K_{ii} = K_{i,0} - \sum_{k=1}^n K_{i,k} - \beta_i \cdot P_i \quad [2](7)$$

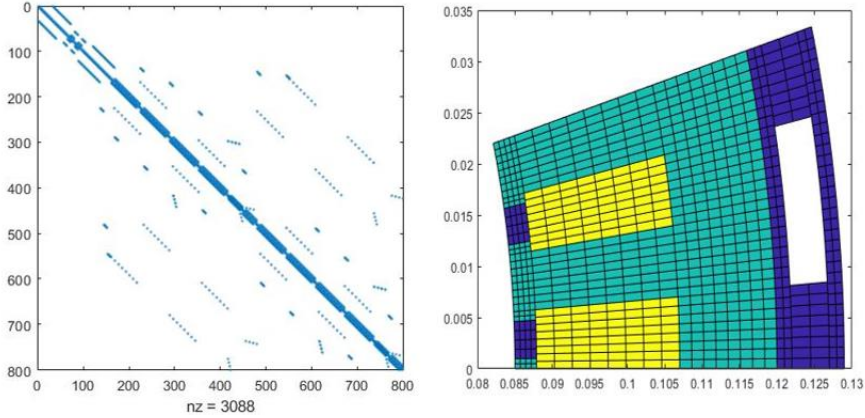


Fig. 2.2. (a) Heat transfer matrix ; (b) Modeled machine fraction, indicating losses

Where $K_{i,l}$ is the thermal conductivity towards the coolant or environment, if there is any, $\sum_{k=1}^n K_{i,k}$ is the sum of conductivity values between the i -th node and other nodes. $\beta_i * P_i$ is a correction factor for temperature-dependent losses (β_i is the temperature coefficient of loss and P_i is the loss in the i -th node).

Specific losses were calculated in the previously discussed manner for the reference design, at a low speed, maximum torque operating point. See Fig. 2.3. for details.

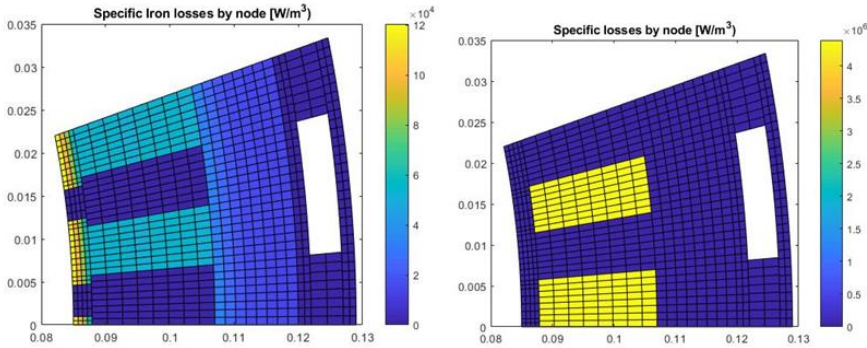


Fig. 2.3. (a) Specific iron losses ; (b) Specific copper losses

With the heat transfer matrix complete and the vector containing the losses ready the linear equation for thermal transients can be solved.

$$\vec{T}_{\tau+1} = \left(\frac{2 * \text{diag}\{\vec{C}\}}{\Delta\tau} + \mathbf{K} \right) \setminus \left\{ \vec{P}_{loss} \left(1 + \vec{\beta}(\vec{T}_{\tau} - T_{\beta}) \right) + \vec{K}_0 \vec{T}_{amb} + \frac{2\vec{C}}{\Delta\tau} \vec{T}_{\tau} \right\} \quad [2](8)$$

Where \vec{T} is the Vector of nodal temperatures, \vec{C} is the Vector of nodal heat capacitances, \mathbf{K} is the Heat transfer matrix, $\Delta\tau$ is the time step of choice, \vec{P}_{loss} is the Vector containing the nodal losses, $\vec{\beta}$ is the Temperature dependence vector of losses, \vec{T}_{amb} ambient temperature and \vec{K}_0 is heat transfer towards the environment.

The solution for the hot-spot temperature is seen on Fig. 2.4.(a). The steady-state temperature is much higher than acceptable – the electromagnetic load is greater than what cooling capabilities would allow in continuous operation. (The calculated operating point was a forced, peak torque transient-state). It should also be noted, that the end winding, which has usually weaker cooling [10], was not modeled.

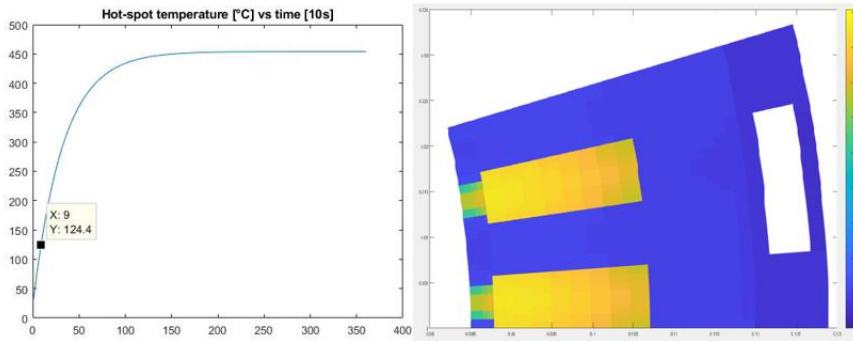


Fig. 2.4. (a) Hot-spot temperature: 124.4 °C after 90 sec ; (b) Temperature distribution after 80 seconds

The hypothetically allowed 110°C hot-spot temperature for the discussed reference design, under the given conditions, was reached in approximately 80 seconds.

4 Conclusion

The presented software tool is capable of performing a rapid and computationally efficient coupled analysis, considering electromagnetic and thermal domains with one-way data transfer. A more sophisticated multiphysical approach would use two-way data sharing, in order to take the changing material properties during a forced transient operation into account. In the recent software version, only stator losses are mapped to the thermal domain, meaning that so far the application is limited to permanent magnet synchronous and various kind of reluctance machines. Further development plans includes not only total validation, but extending capabilities to squirrel cage induction machine analysis as well. From the user's point of view, a graphical user interface should also be implemented in the future.

Development of a Multiphysical Topology Optimizer tool is a long-term goal for the Authors, e.g. to improve torque characteristics of prospering synchronous reluctance machines, similarly to [11]. However, practical improvements can only be made after detailed validation of presented methods.

5 Acknowledgement

Authors would like to express their gratitude to the Electromobility Research Center at Széchenyi István University, for supporting their ambitions and interest related to novel electric powertrain and propulsion motor development.

References

- [1] Sato, T. ; Watanabe, K. ; Igarashi, H.
Multimaterial Topology Optimization of Electric Machines Based on Normalized Gaussian Network
IEEE Transactions On Magnetics, 51(3): 7202604, 2015
- [2] Jung, S-W. ; Ro, J-S. ; Jung, H-K.
A Hybrid Algorithm Using Shape and Topology Optimization for the Design of Electric Machines
IEEE Transactions On Magnetics, 54(3): 8102604, 2018
- [3] Meeker, D.
Finite Element Method Magnetics v4.2 : User's Manual
<http://www.femm.info/Archives/doc/manual.pdf>, 2015
- [4] Meeker, D.
Finite Element Method Magnetics – OctaveFEMM v1.2 : User's Manual
<http://www.femm.info/Archives/doc/octavefemm.pdf>, 2010
- [5] Staton, D. ; Goss, J.
Open Source Electric Motor Models for Commercial EV & Hybrid Traction
https://www.coilwindingexpo.com/berlin/__media/pages/Tutorial-1-D--Staton-&-J--Goss-MDL.PDF , CWIEME 2017
- [6] Pellegrino, G. ; Cupertino, F. ; Gerada, C.
Automatic Design of Synchronous Reluctance Motors Focusing on Barrier Shape Optimization
IEEE Transactions On Industry Applications, 51(2): 15000375, 2015
- [7] Imre, L.
Villamos gépek és eszközök melegedése és hűtése
Műszaki Könyvkiadó, Budapest, 1982
- [8] Pyrhonen, J. ; Jokinen, T. ; Hrabovcova, V.
Design of Rotating Electrical Machines 2nd Ed.
Wiley, 2013

- [9] Krings, A.
Iron Losses in Electrical Machines – Influence of Material Properties,
Manufacturing Processes, and Inverter Operation
KTH Stockholm, 2014

- [10] Simpson, N. ; Wrobel, R. ; Mellor, P.H. ;
Estimation of Equivalent Thermal Parameters of Impregnated Electrical
Windings
IEEE Transactions On Industry Applications, 49(6): 13914355, 2013

- [11] Okamoto, Y. et al.
Improvement of Torque Characteristics For a Synchronous Reluctance
Motor Using MMA-based Topology Optimization Method
IEEE Transactions On Magnetics, 54(3): 7203104, 2018

Industry 4.0 laboratory of the University of Pannonia Nagykanizsa Campus

Sz. Jaskó, T. Holczinger, A. Skrop

Department of Applied Informatics, University of Pannonia, Zrínyi utca 18., 8800, Nagykanizsa, Hungary, jasko.szilárd@uni-pen.hu, holczinger.tibor@uni-pen.hu, skrop.adrienn@uni-pen.hu

Abstract: Digitization and the technologies provided by the Industry 4.0 strategy has changed the manufacturing industry significantly. This implies that stakeholders — universities, students, industrial partners — need to acquire new competences. In order to meet these needs the University of Pannonia Nagykanizsa Campus started to establish a fully automatized industrial laboratory. In this paper the architecture of the Industry 4.0 laboratory is presented.

Keywords: industry 4.0; digital factory; digitization.

1 Introduction

Digitization, the deployment of information technology and automation have great impact in manufacturing industry and manufacturing companies. The operation of manufacturing companies has changed significantly, it is switched from mass production to customized products and production. Industry 4.0 strategy includes several key technologies to digitize production flow or even the whole supply chain. The University of Pannonia Nagykanizsa Campus is establishing an Industry 4.0 laboratory. The goal of the laboratory is to cover most areas of factory digitalization.

Not only the production but the entire supply chain, i.e. from acquisition to customer services, will be modelled in the laboratory. It requires the integration of different research areas and technologies e.g. adaptive systems, data mining, machine learning, optimization, protocol technology, sensor and computer networks. These key technologies may provide to model the main elements of the fully automated industrial processes that leads to efficiency gains and allows to produce highly customized product at small lot size.

In this paper the idea and the structure of the laboratory is introduced. The paper is organized as follows. Section 2 describes Industry 4.0 concept. In Section 3 problem statement is presented. Section 4 presents the proposed system plan of the laboratory. Section 5 concludes the paper and suggests ideas for future work.

2 Industry 4.0 and learning factories

The innovation of technologies in industrial production leads the German government to start to promote the computerization of manufacturing the so-called fourth industrial revolution (Industry 4.0). This concept and the advancement of information technology strengthen each other. The continuous development of Cyber-Physical Systems (CPS), Internet of Things (IoT), Internet of Services (IoS), robotics, cloud- and cognitive computing, big data and augmented reality (AR) results significant change in production systems [1,2]. The Industry 4.0 term is specific mainly in Europe but the computerization of manufacturing system are not only restricted to the EU. In China the “Made-in-China 2025” concept, based on modern IT [3], is introduced to increase the efficiency and competitiveness of the production industry [4-6]. In the US, the “reindustrialization” of the manufacturing industry has started to reinvigorate it. Japan has introduced the “New Robot Strategy” to become the center of development and production of cooperative robots. Moreover, there are different strategies of different countries (e.g. France - New Industrial France, UK - high-value manufacturing, South Korea - advanced innovators’ strategy) but all of them based on the same goals [7]. All aforementioned strategies try to integrated the supply chains and the production systems which can help to make fully customized products [8].

All manufacturing firms should be prepared for the changes of Industry 4.0 taking into account the technology and the human perspectives. Most models are mainly focused on technology part [9-11] but the human operators also are important part of a manufacturing system [12-15]. With the newest IoT devices there is a chance to design machines which can replace human minds [16]. A research in US shows that about 47% of all employment will be at a risk of automatization/computerization by 2030 [17].

The Industry 4.0 is a widely researched area, systematic literature reviews are frequently published [4,18-20]. There are numerous learning factories which have focus on Industry 4.0. They look differently, they are used for different purpose and demonstrate different implementation aspects [21-25]. Some reviews represent the existing approaches of learning factories which are available in academia or in industry [26-29].

3 Problem statement

Nowadays, the technology changes too fast in our environment. Naturally, this process has advantages and disadvantage too. The complexity and the capability of these systems stand on incredible level. The knowledge that needs to create, update or operate these kinds of solution is also high. The fact is, the humanity has a big chance with this to do something really good. Probably, this will bring essential changes in all areas of our lives. But we can only use this opportunity if we can prepare ourselves in time.

Our goal is to create a multipurpose laboratory in the area of Industry 4.0. This solution will be able to use in the followings:

- The infrastructure of the laboratory will support the teaching of modern industrial processes. The students can learn about the structure and the interoperation of this modular architecture i.e. students can learn the functions, working flows and the place of the main units / components / elements / entities of the industry 4.0. In addition, they can understand the whole system and the relationship between each unit. Another very important goal is to maintain the motivation of students and their possibility to develop new capabilities of the system.
- The laboratory may serve as an infrastructural basis for useful industrial researches, which in the future can contribute to the development of the industry's 4.0 concept and its newer versions.
- It can become a cooperation and collaboration environment between the university and the industrial partners. The laboratory can demonstrate the possibilities of this new technology in practice. Moreover this environment makes it possible on the one hand to introduce and on the other hand to develop and test new technologies before industrial deployment.

An important design aspect is to develop the laboratory with modular structure. This property is important in many cases. One from these is that the capabilities of the laboratory can be expanded or modified with the help of minor improvements.

4 System plan

Our system will include all main components of a modern, fully automated industrial solution. This is necessary to reach the multipurpose operational area. Note that we want to model this process from the ordering of a customized product - through the production - to the customer's service. This activity requires coordinated work of numerous research areas. There are some dominant areas as example adaptive systems, data mining, machine learning, optimization, protocol technology, and sensor and computer networks. Figure 1 shows the logical structure of the system, where the tasks of each element are the followings:

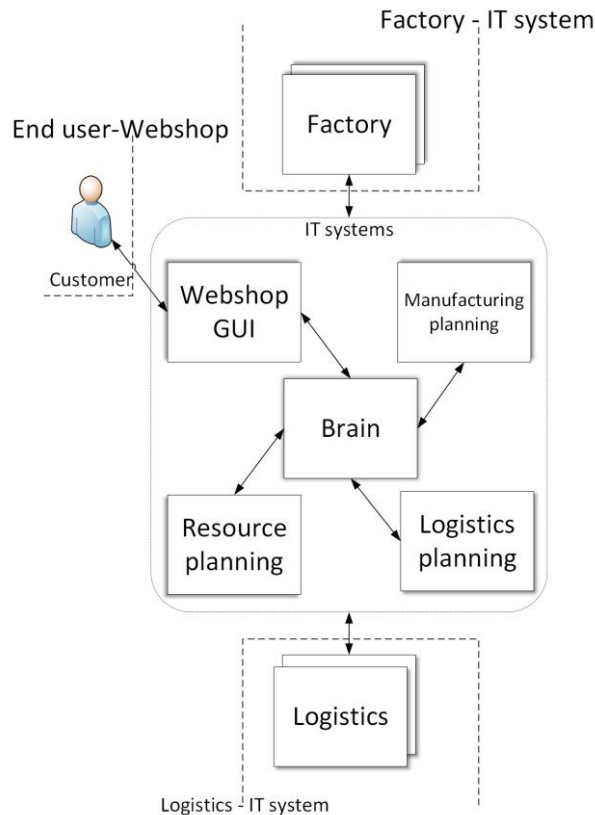


Figure 1

The logical structure of the system

- Customer: This entity indicates the manufacturing process. Note that this means the factory will only produce the ordered products.
- Webshop: The customer can manage (buy, modify, get information) his/her order with the help of this unit. This subsystem communicates with the brain unit.
- Brain: This is a central unit and the main functions of it are process controlling and information management: collection and transmission of information.
- Manufacturing planning: This unit determines the production scheduling and the raw material requirements based on the order.
- Logistics planning: This unit determines the scheduling of logistics for the manufacturing process based on the order.
- Resource planning: This unit selects the specific factory and logistics partner involved in the manufacturing process based on the availability information and manufacturing parameters.
- Logistics: This unit is responsible for transportation that provides information on its activities.
- Factory: The task of this unit is the physical production. It provides information on its activities.

It is important to note that the Web shop, the Brain, the Manufacturing planning, the Logistics planning and the Resource Planning are IT systems / services that work together in the process.

Because of its complexity, the system will be implemented in several phases. Therefore, the individual functions will be integrated step by step into the system. In the first phase, the Brain, the Factory, and the user platform will be developed in detail, while the other features will only appear with minimal functionality. Before the second phase, the operational experiences and the implemented industrial tasks will be analyzed and the exact specification of the second phase will be determined based on this research.

Figure 2 shows a block diagram of the Factory subsystem. The Brain subsystem communicates with the production support system and its controller communicates with the other external and internal subsystems of the Factory. The internal subsystems are responsible for the operation of the factory, including for example robots, conveyor belts, and machining units. Note that the important information from each subunit is processed and stored in an OPC / data collection system.

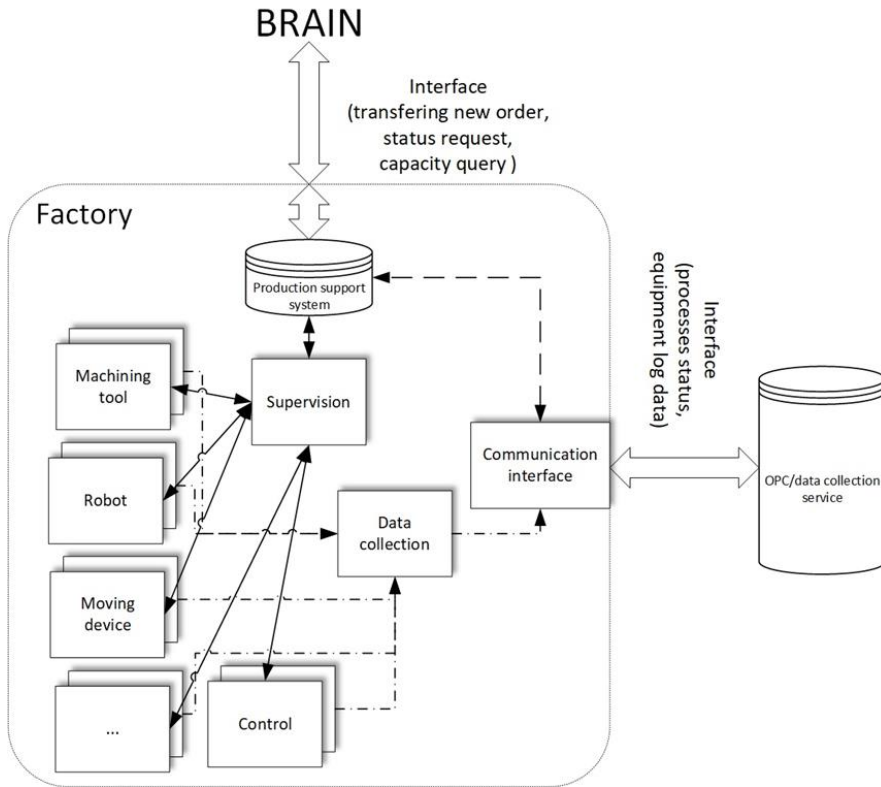


Figure 2

The factory subsystem

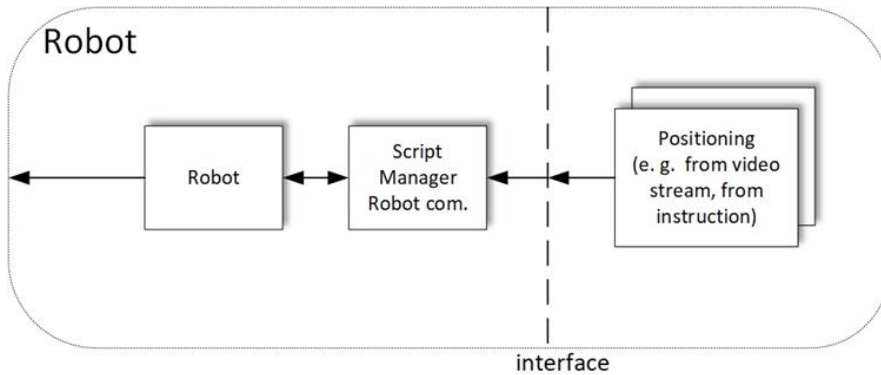


Figure 3

Block diagram of the robot element in the factory subsystem

In the case of the robot subsystem, as shown in Figure 3, a special interface has to be defined for the standardized data flow. Furthermore, a preprocessing unit must be developed to enable adaptive programming of the robot. Note that, most of the physical devices in the laboratory will belong to the factory subsystem.

Conclusions

The paper is represented the model of an Industry 4.0 based laboratory which is currently under construction in University of Pannonia Nagykanizsa Campus. The aims of the laboratory are teaching university students, making research in the field of Industry 4.0 and implementing industrial flows in small scale. The system mainly focuses on the information technology part of the automatization but the physical components of production systems also appear. The model of the laboratory is modular which enables to extend it later according to the industrial and academic needs.

The first phase of the realization is in progress. Most of the hardware are available on site and the development of interfaces of the first phase are close to finish. The next step will be a demonstration for a flexible production system with two customizable products.

Acknowledgement

This work was supported by the Széchenyi 2020 program under grant number EFOP-3.6.1-16-2016-00015.

References

- [1] Schmidt, R.; Möhring, M.; Härting, R.C.; Reichstein, C.; Neumaier, P.; Jozinovi'c, P. Industry 4.0-potentials for creating smart products: Empirical research results. In *International Conference on Business Information Systems*; Springer: Cham, Germany, 2015; Volume 12, pp. 16–27.
- [2] Pereira, A.; Romero, F. A review of the meanings and the implications of the Industry 4.0 concept. *Procedia Manuf.* 2017, 13, 1206–1214.
- [3] Wang, S.; Wan, J.; Zhang, D.; Li, D.; Zhang, C. Towards smart factory for industry 4.0: A self-organized multi-agent system with big data based feedback and coordination. *Comput. Netw.* 2016, 101, 158–168.
- [4] Xu, L.D.; Xu, E.L.; Li, L. Industry 4.0: State of the art and future trends. *Int. J. Prod. Res.* 2018, 56, 2941–2962.
- [5] Martin, K. Innovative Competition with Chinese Characteristics. The Case of 'Made in China 2025' in Relation to the German Industry. Bachelor's Thesis, 2018. Available online: <https://openaccess.leidenuniv.nl/handle/1887/63733> (accessed on 7 September 2018).

-
- [6] Shubin, T.; Zhi, P. “Made in China 2025” and “Industrie 4.0”—In Motion Together. In *The Internet of Things*; Springer: New York, NY, USA, 2018; pp. 87–113.
- [7] Huimin, M.; Wu, X.; Yan, L.; Huang, H.; Wu, H.; Xiong, J.; Zhang, J. Strategic Plan of “Made in China 2025” and Its Implementation. In *Analyzing the Impacts of Industry 4.0 in Modern Business Environments*; IGI Global: Derry Township, PA, USA, 2018; Volume 23, pp. 1–23.
- [8] Ford, S.; Despeisse, M. Additive manufacturing and sustainability: An exploratory study of the advantages and challenges. *J. Clean. Prod.* 2016, 137, 1573–1587.
- [9] Lanza, G.; Nyhuis, P.; Ansari, S.M.; Kuprat, T.; Liebrecht, C. Befähigungs- und Einführungsstrategien für Industrie 4.0. *ZWF Zeitschrift Wirtschaftlichen Fabrikbetrieb* 2016, 111, 76–79.
- [10] Lictblau, K.; Stich, V.; Bertenrath, R.; Blum, M.; Bleider, M.; Millack, A.; Schmitt, K.; Schmitz, E.; Schroter, M. *Industrie 4.0 Readiness*. Impuls-Stiftung des VDMA Aachen-Köln 2015, 52, 1–77.
- [11] Schumacher, A.; Erol, S.; Sihm, W. A maturity model for assessing industry 4.0 readiness and maturity of manufacturing enterprises. *Procedia CIRP* 2016, 52, 161–166.
- [12] Munir, S.; Stankovic, J.A.; Liang, C.J.M.; Lin, S. Cyber Physical System Challenges for Human-in-the-Loop Control. In *Proceedings of the Presented as part of the 8th International Workshop on Feedback Computing, USENIX, San Jose, CA, USA, 24–28 June 2013*; Volume 4, pp. 1–4.
- [13] Hancock, P.A.; Jagacinski, R.J.; Parasuraman, R.; Wickens, C.D.; Wilson, G.F.; Kaber, D.B. Human-automation interaction research: Past, present, and future. *Ergon. Des.* 2013, 21, 9–14.
- [14] Bidanda, B.; Ariyawongrat, P.; Needy, K.L.; Norman, B.A.; Tharmmaphornphilas, W. Human related issues in manufacturing cell design, implementation, and operation: A review and survey. *Comput. Ind. Eng.* 2005, 48, 507–523.
- [15] Roitberg, A.; Perzylo, A.; Somani, N.; Giuliani, M.; Rickert, M.; Knoll, A. Human activity recognition in the context of industrial human-robot interaction. In *Proceedings of the Signal and Information Processing Association Annual Summit and Conference (APSIPA), Siem Reap, Cambodia, 9–12 December 2014*; Volume 10, pp. 1–10.
- [16] Hawksworth, J.; Berriman, R.; Goel, S. Will Robots Really Steal Our Jobs? An International Analysis of the Potential Long Term Impact of Automation. Available online: http://pwc.blogs.com/economics_in_business/2018/02/will-robots-really-steal-our-jobs.html (accessed on 20 July 2018).
-

- [17] Frey, C.B.; Osborne, M. The Future of Employment: How Susceptible Are Jobs to Computerisation. Available online: <https://www.oxfordmartin.ox.ac.uk/publications/view/1314> (accessed on 15 November 2018).
- [18] Liao, Y.; Deschamps, F.; de Freitas Rocha Loures, E.; Ramos, L.F.P. Past, present and future of Industry 4.0—A systematic literature review and research agenda proposal. *Int. J. Prod. Res.* 2017, *55*, 3609–3629.
- [19] Monostori, L. Cyber-physical production systems: Roots, expectations and R&D challenges. *Procedia CIRP* 2014, *17*, 9–13.
- [20] Zhou, K.; Liu, T.; Zhou, L. Industry 4.0: Towards future industrial opportunities and challenges. In *Proceedings of the 2015 12th International Conference on Fuzzy Systems and Knowledge Discovery (FSKD)*, Zhangjiajie, China, 15–17 August 2015; pp. 2147–2152.
- [21] Reuter, M.; Oberc, H.; Wannöffel, M.; Kreimeier, D.; Klippert, J.; Pawlicki, P.; Kuhlenkötter, B. Learning factories' trainings as an enabler of proactive workers' participation regarding Industrie 4.0, *Procedia Manufacturing*, 9 (2017) 354–360.
- [22] Erol, S.; Jaeger, A.; Hold, P.; Ott, K.; Sihm, W. Tangible Industry 4.0: a scenario-based approach to learning for the future production, *Procedia CIRP*, 54 (2016) 113–118.
- [23] Prinz, C.; Morlock, F.; Freith, S.; Kreggenfiels, N.; Kreimeier, D.; Kuhlenkoetter, B. Learning factory modules for smart factories in Industrie 4.0, *Procedia CIRP*, 54 (2016) 7–12.
- [24] Simons, S.; Abé, P.; Nesper, S. Learning in the AutFab – the fully automated Industrie 4.0 learning factory of the University of Applied Sciences Darmstadt, *Procedia Manufacturing* 2017, *9*, 81–88.
- [25] Elbestawi, M.; Centea D.; Singh, I.; Wanyama, T. SEPT Learning Factory for Industry 4.0 Education and Applied Research, *Procedia Manufacturing* 2018, *23*, 249–254.
- [26] Abele, E.; Chryssolouris, G.; Sihm, W.; Metternich, J.; ElMaraghy, H.; Seliger, G.; Sivard, G.; ElMaraghy, W.; Hummel, V.; Tisch, M.; Seifermann, S. Learning factories for future oriented research and education in manufacturing, *CIRP Annals*, 66(2) 803–826.
- [27] Tisch, M.; Hertle, C.; Cachay, J.; Abele, E.; Metternich, J.; Tenberg, R. A systematic approach on developing action-oriented, competency-based learning factories, *Procedia CIRP*, 7 (2013) 580–585.
- [28] Mavrikios, D.; Sipsas, K.; Smparounis, K.; Rentzos, L.; Chryssolouris, G. A Web-based application for classifying teaching and learning factories, *Procedia Manufacturing*, 9 (2017) 222–228.

- [29] Tisch, M.; Metternich, J. Potentials and limits of learning factories in research, innovation transfer, education, and training, *Procedia Manufacturing*, 9 (2017) 89–96.

Measurement of Electric Fields Emitted by Household Appliances

Vanja Mandrić Radivojević

Faculty of Electrical Engineering, Computer Science and Information Technology
Osijek, Kneza Trpimira 2B, 31000, Osijek, Croatia, vanja.mandric@ferit.hr

Slavko Rupčić

Faculty of Electrical Engineering, Computer Science and Information Technology
Osijek, Kneza Trpimira 2B, 31000, Osijek, Croatia, slavko.rupcic@ferit.hr

Ante Lijović

Faculty of Electrical Engineering, Computer Science and Information Technology
Osijek, Kneza Trpimira 2B, 31000, Osijek, Croatia, ante.lijovic@etfos.hr

Abstract: Each electric device emits electromagnetic (EM) energy. If the radiated energy exceeds the safety level, it may affect the performance of other electrical devices. This influence of the device whose radiation is observed manifests in a way that degrades or even disables the operation of other devices. It is important to note that the radiated energy can be harmful to the health of living organisms near the radiating devices. In order to have such values of electric field strength controlled, the field amounts must be standardized. The radiation of household appliances is standardized by HRN EN 55014, which defines the limit values for different groups of devices. When measuring the EMI of a device, it is necessary to define the measurement requirements, identify the device, check the feasibility of the measurement, define the activity, and plan the measurement. Several types of household appliances have been reported in the paper, the application of the rules, regulations and instructions contained in the standard is presented. Measurements included the strength of the electric field of household appliances most commonly used in households: hair dryers, air styler, handheld blenders, hand mixers, cordless drill and hammer drill. The purpose of this paper is to determine the amount of electric field strengths that radiate frequently used home appliances and to check whether radiation is within the limits permitted by HRN EN 55014. The results of the measurement from the point of view of the prescribed boundary levels were analyzed at the end of the paper.

Keywords: EM radiation; Household Appliances; Standard; Electric Field Limits

1 Introduction

Each electric device radiates EM energy and in this way is interacting with other electrical devices. If the values of the radiated energy are high, signal degradation of the surrounding devices may be possible or functioning of the devices could be disabled. This is not the only manifestation of electrical devices radiation. For the same reason, the effects on the health of living organisms are also possible. From all of the above and preventive, the amount of energy emitted by such devices must be standardized [1].

Electromagnetic Interference (EMI) is an electromagnetic radiation from a device or system that interacts with other devices and systems in a normal (daily) operation. Radio-frequency Interference (RFI) is often referred to EMI in the texts as well.

Since each Device Under Test (DUT) is different, it is crucial to have good and quality EMI signal detection devices. Spectral Analyzer is a measuring device that measures the amplitude of the signal in the frequency domain within the defined frequency band and as such is one of the most commonly used EMI measurement devices.

The Croatian standard, which prescribes the limits of the permitted calculated strengths of the electric field of household appliances (and refers to the emission) is HRN EN 55014:1 [1]. If the immunity of a particular household appliance to radiation from the environment is observed, the standard for which measurements are made and the results are analyzed is HRN EN 55014: 2 [2].

The standard HRN EN 55014:1 is described below, a complete EM radiation measurement system has been analyzed - EM devices, antenna, cables, and home appliances whose radiation is important are used.

One of the most commonly used household appliances is a hair dryer, and this paper shows how significant contributions of the radiated EM energy are. This paper analyzes more hair dryers (different manufacturers and features), air styler, handheld blenders, hand mixer, cordless drill and hammer drill. The same chapter presents and analyze the measurement results achieved in a partially EM isolated room. Those results are compared with the permitted values of the electric field strengths specified in [1].

1.1 Croatian Standard HRN EN 55014:1 and Standards for Measurement EM Radiation of Household Appliances

The Croatian Standards Institute (at the proposal of the Technical Committee HZN / TO E500) has accepted the European standard EN 55014-1:2017 as the Croatian standard in the original English language, so the European standard EN 55014-1:2017 has the status of Croatian standard. The Croatian standard HRN EN 55014-1 refers to electromagnetic compatibility - requirements for household appliances, electrical tools and similar devices - Part 1: Emission [1]. The standard specifies (by the International Special Committee on Radio Interference CISPR 14-1: 2016) the requirements applicable to RF emissions in the frequency range of

9 kHz to 400 GHz of household appliances, electrical tools and similar devices. The International Standard CISPR 14-1 was prepared by the International Electrotechnical Commission (IEC). Also, IEC 61000-4-22:2010 defines Electromagnetic Compatibility (EMC): device emission and immunity measurement in Fully Anechoic Room (FAR) [3]. According to the above standard, Table 1 shows the limits of the permitted values of the radiated strengths electrical fields in the frequency range of 30 MHz to 1000 MHz.

Table 1

Permitted values of the electrical field intensity and the test methods in the 30 MHz – 1000 MHz frequency range (by the standard HRN EN 55014:1 [1])

Test method	Standard	Frequency, MHz	Permitted values, dB μ V/m	Comment
OATS or SAC	CISPR 16-2-3	30 to 230 230 to 1000	30 37	10 m distance measurement
FAR	CISPR 16-2-3	30 to 230 230 to 1000	42 to 35 42	3 m distance measurement
FAR	IEC 61000-4-22	30 to 230 230 to 1000	42 to 35 42	3 m distance measurement
TEM Waveguide	IEC 61000-4-22	30 to 230 230 to 1000	30 37	-

Where test methods are:

OATS: Open Area Test Site

SAC: Semi Anechoic Chamber

FAR: Fully Anechoic Room

TEM: Transferzal EM Waveguide

This paper describes the measurement of EM radiation of six different hair dryers (different characteristics and manufacturers), one air styler, two handheld blender, one hand mixer, one cordless drill and one hammer drill according to [1], in Open Area (OATS), but at a distance of 3 m (the explanation below).

2 Measurement Settings and Measurement Results

2.1 Defining of the Household Appliances

Selected household devices (DUT) that were tested - are six different hair dryers (Figures 1 - 6); one air styler (Figure 7), two handheld blenders (Figure 8 and 9), one hand mixer (Figure 10), one cordless drill (Figure 11) and one hammer drill (Figure 12) of the following manufacturers and power characteristics:

- DUT 1: hair dryer Remington ac 8000 (max 2200 W);
- DUT 2: hair dryer Grundig hd 6080 (max 2200 W);
- DUT 3: hair dryer Rowenta cv 1220 (max 1400 W);
- DUT 4: hair dryer Rowenta cv 5062 (max 2300 W);
- DUT 5: hair dryer Grundig hd 6760 (max 2000 W);
- DUT 6: hair dryer Sencor shd 108 vt (max 2000 W);
- DUT 7: air styler Remington as 8090 (max 700 W);
- DUT 8: handheld blender Clatronic sms 3190 (max 200 W);
- DUT 9: handheld blender Tefal dd 1000 (max 350 W);
- DUT 10: hand mixer Severin hm 3817 (max 250 W);
- DUT 11: cordless drill Einhell th-cd 12-2 li (max 1.3 W);
- DUT 12: hammer drill Bosch psb 500 re (max 500W).



Figure 1

Hair dryer Remington ac 8000



Figure 2

Hair dryer Grundig hd 6080



Figure 3

Hair dryer Rowenta cv 1220



Figure 4

Hair dryer Rowenta cv 5062



Figure 5

Hair dryer Grundig hd 6760



Figure 6

Hair dryer Sencor shd 108 vt



Figure 7

Air styler Remington as 8090



Figure 8

Handheld blender Clatronic sms 3190



Figure 9

Handheld blender Tefal dd 1000



Figure 10

Hand mixer Severin hm 3817



Figure 11

Cordless drill Einhell th-cd 12-2 li



Figure 12

Hammer drill Bosch psb 500 re

Most hair dryers work in three temperature modes (1 – cold, 2 – semi hot and 3 - hot) and two speed modes (except hair dryer Rowenta cv 1220 which has one temperature mode and two speed modes). handheld blender Clatronic sms 3190 works in one mode, cordless drill Einhell th-cd 12-2 li has two speed modes, handheld blender Tefal dd 1000 works in one mode, Remington as 8090 works in two temperature modes, hand hand mixer Severin hm 3817 can work in five speed modes and finally, hammer drill Bosch psb 500 re works in one mode.

All listed devices emit the EM field in their environment and could be able to affect operation others electrical devices.

2.2 Measurement Procedure and Plan for Measurement Measurement of Electric Fields Emitted by Household Appliances

The HRN EN 55014-1 standard prescribes the measurement settings as follows:

- The measurement should be performed in the range of frequencies between 30 MHz and 1000 MHz;
- Measurements should be carried out at a distance of 10 m;
- Setting up a device that measures DUT on nonconductive substrate 0.8 m from the ground (in a laboratory where there is an EM echo);
- To set RX antenna to measure the electrical field strength at a certain height from the ground;
- The RX antenna is connected to the device that measures electrical field strength;
- To set the selected mode of operation of the DUT (with the selection of maximum heat and speed).

2.3 Measurement and Measurement Results of EM Radiation of Household Appliances

Most of the settings and measurement parameters were met as stated and prescribed in standard, with the addition of measurements – the electric field strength without the DUT included and the included DUT was measured. These two values have been subtracted in order to achieve the value of electric field strength of the each DUT. Then, the radiation of all DUTs was measured in all possible combinations of modes - heat and speed (this is difference from the standard). The antenna distance and the DUT measured was 3 m.

The decision on the measurement at 3 m from the DUT was made because the measurers were limited by the space in which the measurement was performed and the equipment could not be set at 10 m distance. For this reason, the values in

Tables 2 – 5 are values of electrical fields obtained after computation for a distance of 3 m to 10 m. The conversion principle of dB μ V/m at 3 m to dB μ V/m at 10 m is based on the basic formula that links the strength of the electric field and the power of the transmitter antenna:

$$E = \frac{\sqrt{30 \cdot P \cdot G}}{r} \quad (2-1)$$

where:

P – is power of the transmitter antenna,

E – electrical field strength emitted by antenna,

r – measurement distance (3 m),

G – antenna gain.

The conversion procedure is as follows:

$$E, dB\mu V / m_{10m} = 20 \log \left(10^{\frac{E, dB\mu V / m_{3m}}{20}} \cdot \frac{3}{10} \right) \quad (2-2)$$

This approach to electrical field strength measurements is the result of many years of engineering practice in the area of measuring high frequency fields. Standard HRN EN 55014-1 prescribes the measurements of the activated DUT - a combination of maximum heat and speed mode. Therefore, measurements of all possible combinations of the modes of operation of the certain device is an additional decision and procedure of the accredited Laboratory for HF Measurements at the Faculty of Electrical Engineering, Computer Science and Information Technology Osijek, and provides a more detailed approach to the stated norms and measurements in general.

Instruments and devices used in radiated electrical field measurements DUT 1 - 12 (Figure 13) are:

- RX antenna: conical dipole PCD 8250;
- Rotator and tripod (1.5 m height) to which the antenna is mounted;
- Spectrum Analyzer (SA HMS-X Rhode Schwarz) connected to RX antenna;
- The coaxial cables used to connect the antenna and rotator, as well as rotator and spectrum analyzer are RG 178 and RG 400, respectively.

Figure 13 shows all the instruments, antenna, cables and DUT involved in measuring procedure.

Since measurement is performed in an EMI (Electromagnetic Interference) area, the signals from three groups of radio systems will appear in the defined range of 30 MHz to 1000 MHz (Figure 14) [4]:

- 88 MHz - 108 MHz → FM broadcasting;
- 470 - 821 MHz → TV Broadcasting and LTE;
- 880 - 915 and 925 - 960 MHz → GSM900 (GSM) and UMTS900,

and those amplitudes is desirable to eliminate as much as possible in order to obtain information on the DUT itself [5]. All measurement results are shown in Tables 2 - 5.

Measurement method used for HF fields measurements is ADD3D method. This method uses an omnidirectional broadband antenna – conical dipole PCD 8250 of

a frequency range of 80 MHz to 2500 MHz. Using this antenna – effective field strength can be determined by three orthogonal orientation (x, y and z) voltage measurements. Effective field strength is obtained by using the relation:

$$E_{eff} = \sqrt{E_x^2 + E_y^2 + E_z^2} = \sqrt{U_x^2 + U_y^2 + U_z^2} \cdot AF \tag{2-3}$$

Spectrum Analyzer (SA HMS-X Rhode Schwarz) measures the voltage V_{emi} and it is proportional to the permissible E of Table 1:

$$V_{emi}(dB\mu V) = E(dB\mu V/m) - AF(dB/m) + Gain(dB) - Loss(dB) \tag{2-4}$$

Assuming that the antenna gain equals the sum of antenna factor AF and losses in cables $Loss$, equation (2-4) can be written:

$$V_{emi}(dB\mu V) = E(dB\mu V/m) \tag{2-5}$$

and E (dB μ V/m) is the measured value in Tables 2 – 5 (2-5).

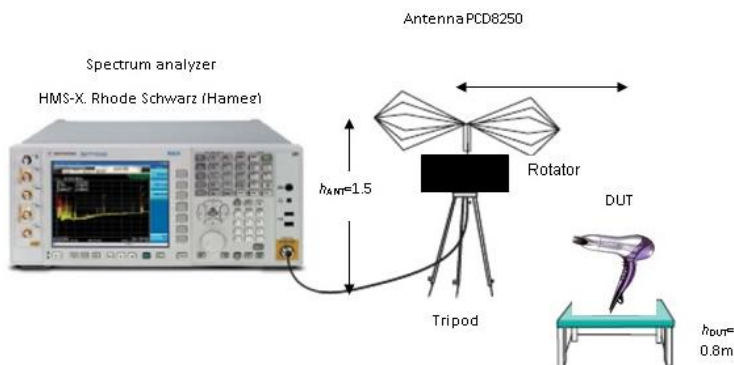


Figure 13

Measurement scheme of the household appliance radiation according to HRN EN 55014-1

After setting all the parameters of EM radiation measurement of DUT and done measurements, all results are processed and presented in Tables 2 - 5. The values of measured and calculated fields are compared with the permissible values in Table 1 and prescribed by the Croatian standard HRN EN 55014:1. The reference values used for comparison are in the first row of Table 1.

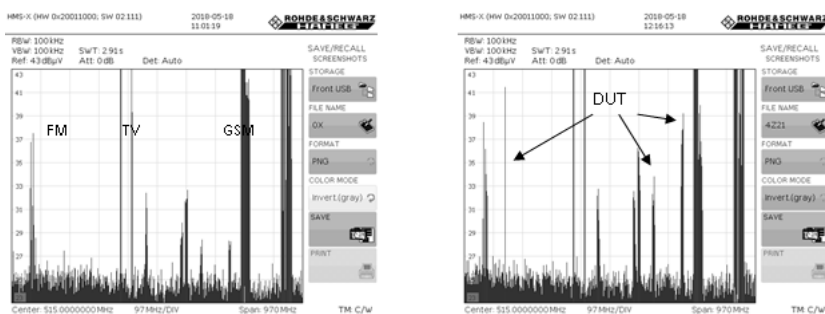


Figure 14

RF spectrum without and with activated DUT (measured at 3m distance from RX antenna)

Table 2

The measured electric field strength of the DUT (different types of hair dryer) at a distance of 3 m, and after the conversion to the value at a distance of 10 m

Mode DUT	Heat 1 Speed 1	Heat 1 Speed 2	Heat 2 Speed 1	Heat 2 Speed 2
	$E_{uk \max}$, dB μ V/ m< 230 MHz	$E_{uk \max}$, dB μ V/ m> 230 MHz	$E_{uk \max}$, dB μ V/ m< 230 MHz	$E_{uk \max}$, dB μ V/ m> 230 MHz
Remington AC 8000	-0.26	18.85	3.79	23.46
Grundig hd 6080	-1.25	28.66	5.34	11.54
Rowenta cv 1220	5.51	9.47	-0.43	13.04
Rowenta cv 5062	1.70	24.95	-1.77	9.94
Grundig hd 6760	4.14	23.46	3.52	18.44
Sencor shd 108vt	6.41	23.69	11.52	17.54

Table 2 - continued

DUT \ Mode	Heat 3	Speed 1	Heat 3	Speed 2
	E_{uk} max, dB μ V/ m< 230 MHz	E_{uk} max, dB μ V/ m> 230 MHz	E_{uk} max, dB μ V/ m< 230 MHz	E_{uk} max, dB μ V/ m> 230 MHz
Remington AC 8000	-0.58	9.23	-1.75	27.01
Grundig hd 6080	-1.74	29.13	8.42	19.09
Rowenta cv 1220	No mode	No mode	No mode	No mode
Rowenta cv 5062	-1.14	-1.14	-1.14	-1.14
Grundig hd 6760	-0.08	17.17	3.22	30.77
Sencor shd 108vt	1.02	17.86	7.43	24.88

Table 3

The measured electric field strength of the DUT (two handheld blenders, cordless drill and hammer drill) at a distance of 3 m, and after the conversion to the value at a distance of 10 m

DUT \ Mode: On	E_{uk} max, dB μ V/m< 230 MHz	E_{uk} max, dB μ V/m> 230 MHz
Clatronic sms 3190	3.02	28.27
Tefal HB100138	-0.38	31.44
Einhell th- cd 12-2 li	6.74	8.90
Bosch psb 500 re	0.13	23.37

Table 4
The measured electric field strength of the DUT (air styler) at a distance of 3 m, and after the conversion to the value at a distance of 10 m

Mode DUT	Cold		Heat 1		Heat 2	
	$E_{uk\ max}$, dB μ V/ m< 230 MHz	$E_{uk\ max}$, dB μ V/ m> 230 MHz	$E_{uk\ max}$, dB μ V/ m< 230 MHz	$E_{uk\ max}$, dB μ V/ m> 230 MHz	$E_{uk\ max}$, dB μ V/ m< 230 MHz	$E_{uk\ max}$, dB μ V/ m> 230 MHz
Remington AS 8090	4.67	2.77	3.34	23.95	3.25	30.52

Table 5
The measured electric field strength of the DUT (hand mixer) at a distance of 3 m, and after the conversion to the value at a distance of 10 m

Mode DUT	Speed 1		Speed 2		Speed 3		Speed 4	
	$E_{uk\ max}$, dB μ V/ m< 230 MHz	$E_{uk\ max}$, dB μ V/ m> 230 MHz	$E_{uk\ max}$, dB μ V/ m< 230 MHz	$E_{uk\ max}$, dB μ V/ m> 230 MHz	$E_{uk\ max}$, dB μ V/ m< 230 MHz	$E_{uk\ max}$, dB μ V/ m> 230 MHz	$E_{uk\ max}$, dB μ V/ m< 230 MHz	$E_{uk\ max}$, dB μ V/ m> 230 MHz
Severin hm 3817	1.04	33.72	2.59	23.71	0.47	11.88	0.86	3.71

Table 5 - continued

Mode DUT	Speed 5	
	$E_{uk\ max}$, dB μ V/m <230 MHz	$E_{uk\ max}$, dB μ V/m >230 MHz
Severin hm 3817	0.47	26.48

Conclusions

The testing of electromagnetic compatibility of each device (DUT) is necessary for the purpose of its safe operation in the environment where other devices are present. Testing refers to the measurement and verification of the calculated electrical field strength of the DUT, to make sure that the el. fields are in the prescribed permissible limits.

Regulatory bodies such as IEC and CISPR, and the norm HRN EN 55014-1 under their jurisdiction, prescribe the maximum values that can be emitted by household appliances.

This paper describes the procedure for measuring and processing the EM radiation results of several different hair dryers, air styler, handheld blenders, hand mixer, cordless drill and hammer drill. Thus, DUT emits a certain amount of EM energy in the spectrum of interest (30 MHz to 1000 MHz). The HRN EN 55014-1 standard prescribes the measurement method and permitted electric field values. Measurements have shown (Tables 2 to 5) a significant contribution of these type of devices in the range of 30 MHz to 1000 MHz (up to several dozen dB μ V/m).

The measured values of the electric field strength radiated by all DUTs ranges from:

- In the area below 230 MHz the minimum value is -2.12 dB μ V/m and the maximum value is 28.27 dB μ V/m,
- In the area above 230 MHz the minimum value is 2.77 dB μ V/m and the maximum value is 34.57 dB μ V/m.

After comparing all measured values with OATS condition (30 dB μ V/m up to 230 MHz and 37 dB μ V/m above 230 MHz), it can be concluded that none of the devices exceeds permitted values of the electric field strengths set by HRN EN 55014-1, but all measured DUTs contributes significantly to the total EM power spectrum. Devices are safe to use.

References

- [1] HRN EN 55014:1 Electromagnetic compatibility - Requirements for household appliances, electric tools and similar apparatus - Part 1: Emission, may 2017.
- [2] HRN EN 55014:2 Requirements for household appliances, electric tools and similar apparatus - Part 2: Immunity, april 2015.
- [3] http://www.iec.ch/emc/basic_emc/basic_emc_immunity.htm
- [4] <http://www.hakom.hr/UserDocsImages/dokumenti/Baza%20radiofrekvencijaskog%20spektra%20za%20javne%20pokretne%20komunikacijske%20mre%20C5%BE%20GSM-UMTS.pdf>
- [5] S. Rupčić: Predavanja iz kolegija EMC, Fakultet elektrotehnike, računarstva i informacijskih tehnologija Osijek, 2016/2017.

Security issues in healthcare IT systems

Zsolt Szabó

Óbuda University, Doctoral School on Safety and Security Sciences, Népszínház
utca 8., H-1081, Budapest, Hungary

Abstract: Nowadays IT systems are essential for the safe, efficient and reliable operation of organizations. Health information technology (e-Health) increasingly becomes an integral part of the services. Doctors, nurses, and other therapists spend more and more time on the computer, using family medicine, specialist care, or integrated hospital systems. Today, it is difficult to imagine health care or the operation of the insurance system without the proper records and computer tools, but modern diagnostic tools can also be considered IT tools with a little exaggeration. The purpose of the article is to highlight the security problems and shortcomings of health IT systems, and medical equipment. We also seek solutions for protection and examine their applicability using international and national regulations (GDPR, Act L of 2013, Act CLXVI. of 2012), recommendations and standards related to the operation of health information systems (CEN, MITS, HL7, IHE, HS).

Keywords: e-Health; data protection and information protection; Advanced Persistent Threat (APT), GDPR

1 Introduction

Health information technology (e-Health) increasingly becomes an integral part of the services (Fig. 1). Today, it is difficult to imagine health care or the operation of the insurance system without the proper records and computer tools, but modern diagnostic tools can also be considered IT tools with a little exaggeration [1]. Doctors, nurses, and other therapists spend more and more time on the computer, using family medicine, specialist care, or integrated hospital systems. Data handled during health care activities mostly belong to the category of special data, whose handling is governed by strict rules [2]. Below, we focus on the problems of health information technology we deem most important. We think that a solution to these problems provides a sound foundation for the creation of a high level of IT background necessary for a high standard of health care. We detail the issues of protecting health care data and Hungarian specialities. It is not easy to find one's way in the maze of laws, regulations and guides. Not knowing them, however, does not absolve anyone of responsibility. This study summarises the most important information in international recommendations, standards, and

laws, and provides useful practical advice for the safe and lawful handling of health care data.

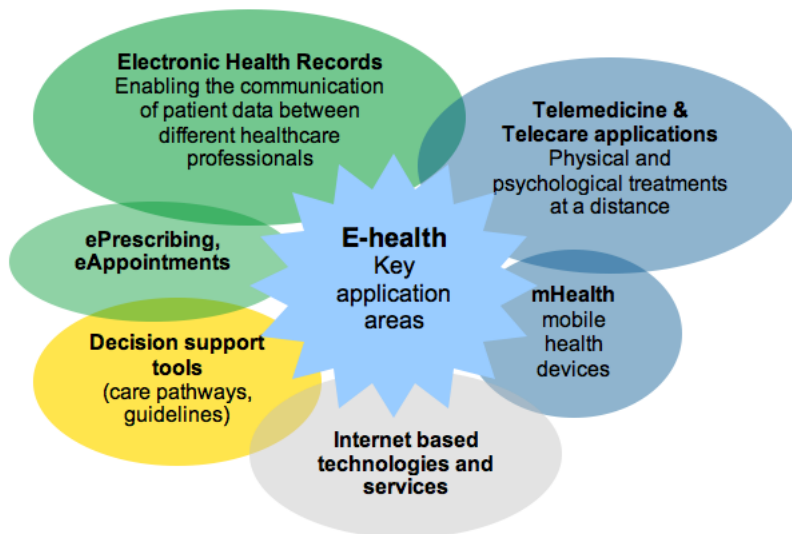


Figure 1
e-Health application areas

2 Attacks against health information services

A cyberattack is an offensive or defensive operation whose expected outcome is personal injury or death, or material loss or destruction [3]. A cyberattack was launched against the British health care system on Friday 12 May, 2017. According to the report of the British National Health Service (NHS Digital), some hospitals in 19 areas, including London, Blackburn, Nottingham, Liverpool and Manchester were attacked, but the media reported similar problems in 40 different areas. In most of the hospitals affected, the telephone service and computer systems faltered. In these hospitals they suspended accepting patients with non-emergency problems [4]. According to NHS Digital, it was a ransomware attack: the writers of the virus demanded money from the hospitals to return access to files the virus encrypted. Some hospitals reported that messages appeared on the infected computers demanding 300 dollars' worth of bitcoin, a cryptocurrency. NHS Digital's investigations revealed that it was probably the Wanna Decryptor virus variant. Many hospitals stopped their own IT systems to protect their databases themselves from attacks. Many GPs reported that they could not access the electronically stored data of their patients, including test

results. According to the NHS, there were no signs that the attackers were able to access personal data of patients. The Portuguese National Commission for Data Protection (Comissão Nacional de Proteção de Dados, CNPD) fined the Barreiro hospital in Portugal for allowing illegal access to patient data, reported the Portuguese Publico on 22 October, 2018 [5]. CNPD started the investigation in the middle of July, as a result of which they decided on a fine of 400 ezer Euros. The fine consists of several parts as various sections of the General Data Protection Regulation of the EU (GDPR) [6] were violated. The Portuguese hospital stored the data of the patients in its own system but did not handle access properly according to the CNPD. As a result, at least nine persons gained access to the data, who had no medical qualification whatsoever, such as social workers. Also, a total of 985 users registered as registered medical doctors in the system, when there are only 296 doctors in the hospital. In addition, the hospital did not separate its own patient data properly from the archived data of other hospitals, and authentication during access to the was not adequate. The CNPD stated that the hospital did not do anything to stop unauthorised access, and did not differentiate between groups, who, for example were only allowed access to the data under certain conditions. The further 100 thousand Euro fine was imposed because according to the CNPD, the data handler cannot guarantee integrity and confidentiality within its system in general.

3 Data and information protection solutions

The use of IT in health care (Fig. 2) became a factor of medicine. Medical informatics emerged as a special area and became an essential factor of medical services. A knowledge of the regulation of and ways of implementing information security is important, since the unprofessional handling of medical data can lead to serious problems [2]. The General Data Protection Regulation (GDRP) of the EU came into force in May 2016 [6]. It updated data protection regulation after more than two decades. The regulation started to be enforced after a grace period of two years, on 25 May, 2018. Its purpose is to unite the fragmented data protection regulation existing earlier, therefore it is directly enforced in every member state, including Hungary. The goal is to give people more control over their data and provide stronger protection of data against not only cybercriminals but also companies and intitutions handling the data. Attacks are basically directed to data, which is surrounded by system elements and handled by processes [7]. Cyberthreats threaten data and data handling processes through a chain of system elements. Protection does not only mean implementing a system of tools but the complete system of protection of a system from designing to implementation, including the physical (operation), logic (password generation, cryptography methods, compatibility matrix etc.) administrative (regulation background) and human resources [8]. One of the most important assets of the economy and society

is information. Information is essential for every economic entity, whether it be public or private. There is no development without information; without it nothing can be planned, which results in falling behind [9].

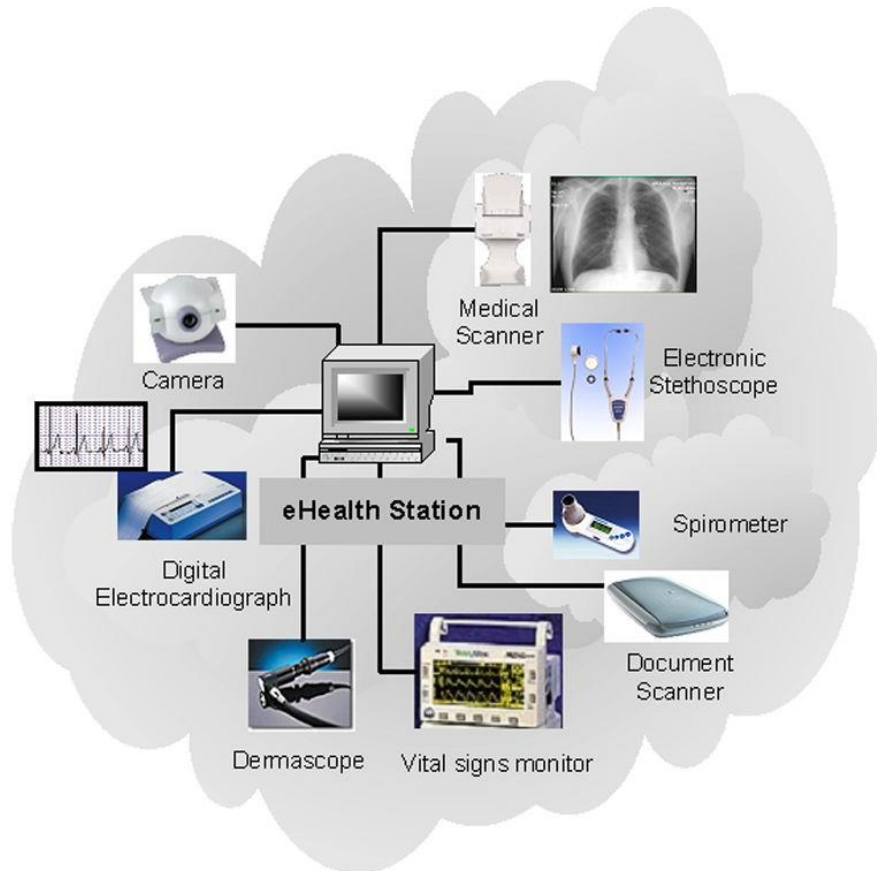


Figure 2
e-Health station

Information security means that the IT components of organisational activities are maintained in an adequate state [10]. Security is an essential element of the operation of an organisation [11], and in the case of health IT systems, it is as important as organisational conditions. Organisational security is a complex concept—the individual subfields are closely related and depend on each other. The following areas need to be taken into account in planning and design: physical security; object protection; data and information security; business security; human security; incident handling and business continuity. Taking into account the above, security has to be closed, comprehensive, proportional to the risks and continuous [12]. The security management of an organisation should be

centralised, uniform, clear, supported by IT tools, and as automated as possible, leaving as little possibility for human error as possible. The information security law [13] requires that the IT systems of state organisations have to be able to detect, log and automatically handle critical security events of hardware and software that is essential for the operation of the organisation. When the security management of a state organisation is designed, it is also important that the security system reflects the security policy of the organisation. The security management should organically include network, user, and firewall management, content filtering and virus protection of the mailing system and other IT systems.

4 Targeted attack of health IT systems

Nowadays the state and its organisations and citizens depend on very complex electronic information systems (Fig. 3) in Hungary’s cyberspace, without which the state cannot operate, and services cannot be provided and used. Society is not prepared to operate without this infrastructure, these tools and services therefore they need to be protected. Also, the information and data generated and used during their operation constitute considerable wealth.

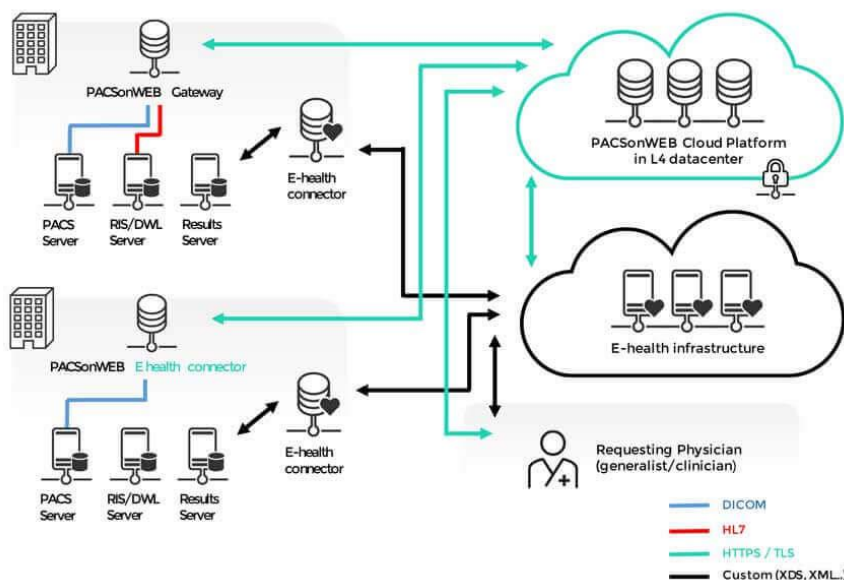


Figure 3
e-Health integration

Based on the above, a possible definition of critical infrastructure is the following: a network of connected and interactive (mutually depending on each other) infrastructure elements, facilities, services, systems and processes, which are essential for the operation of a country and have a fundamental role in providing a minimum level of security, economic operability, public health and environment as expected by society [14]. Targeted Attacks are threats specially directed against a given person or organisation. As opposed to computer viruses, the creator of the malware does not wish to spread the malware as widely as possible, but intends to install it on the devices of the target. Targeted attacks are combinations of simpler attacks (attacks through the web or mail, the attack of a system) but require very deep knowledge of IT systems, since they have to be invisible as well, and also, they are usually directed against systems which are well-protected.

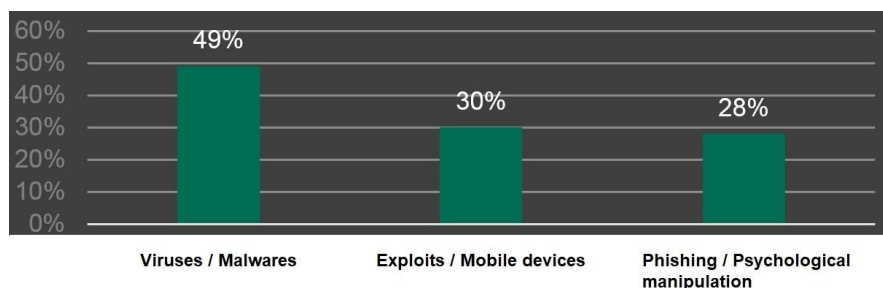


Figure 4

Main methods of Advanced Persistent Threats

Advanced Persistent Threats (APT) require very great expertise. They are usually carried out by professionals, mostly employed by intelligence agencies or criminal organisations. They are also directed to one target, and steal data from it [15]. Advanced Persistent Threats differ from normal cyberattacks in the selection of the target, the duration of the attack and the initial inactivity period. These attacks use Social Engineering (psychological) attacks. Advanced Persistent Threats have been growing in number in the past few years and the tendency seems to be continuous. APTNotes, a data bank created and maintained by GitHub (<https://github.com/kbandla/APTnotes>) has been collecting published reports about APTs since 2008. Fig. 5 shows that the number of these attacks has increased considerably in the past few years. However, these were only the reported incidents - there have probably been a great number of undiscovered attacks as well. In August 2015, they collected a total of 291 APTs against companies, institutions and governments. Of these, 72 were observed in 2015, which is more than twice the amount in the same period in 2014, and similar to the amount experienced in the second half of 2014. Most APTs are directed against financial and business organisations but sometimes political motivations can also be suspected. A worrying trend is the increasing number of attacks against medical data. Nowadays most IT attacks are experienced at the application level.

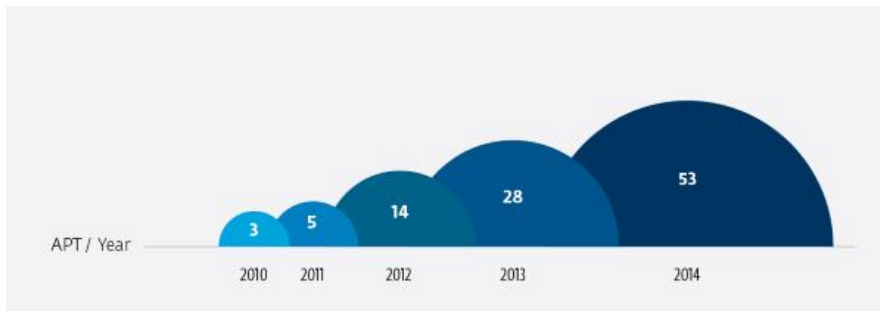


Figure 5
Reports of APTs

At the lower levels of Fig. 3, sophisticated defence solutions are available which protect against attacks effectively but not necessarily fully. Among applications, services accessible through the web are most popular. Nowadays this affects certain portal engines but some tools are already available which detect vulnerabilities of web services. The above-mentioned international incidents indicate that such attacks may also be directed against Hungary's health information systems in the future, and therefore they need to be prepared for with the help of national and international standards (CEN, MITS, HL7, IHE, HS), recommendations and good practices, and reinforce IT systems [16].

Conclusions

We presented two important data and information security issues of health information systems, focusing on international comparison and tasks in Hungary. We could not strive for comprehensiveness in the framework of this article as each subfield would require independent analysis and strategic planning. In our opinion, the most important tasks are:

- Grading the systems used in the management of institutions and in providing health care.
- Applying the standards for the storage and transmission of medical data.
- Ensuring that the central databases are authentic and up-to-date.
- Electronic identification of patients and doctors/medical staff.
- Publishing a collection of medical data and information protection regulations, and providing information security awareness training for users.

References

- [1] P. Racsó, Health Informatics abroad and in Hungary. *Health Economics Review* 6/2008, pp. 26-31

-
- [2] J. Ködmön, E. Z. Csajbók, Information Security in Healthcare, *Medical Weekly*, 2015, 156(27), pp. 1075–1080
- [3] Tallinn Manual on the International Law Applicable to Cyber Operations, General editor Michael N. Schmitt, US Naval War College, Cambridge University Press 2013, rule 30, pp. 1-255
- [4] The Guardian Massive ransomware cyber-attack hits nearly 100 countries around the world, Last accessed September 2018. [Online]. Available: <https://www.theguardian.com/technology/2017/may/12/global-cyber-attack-ransomware-nsa-uk-nhs>
- [5] Publico Hospital do Barreiro contesta judicialmente coima de 400 mil euros de Comissão de Dados, Last accessed October 2018. [Online]. Available: <https://www.publico.pt/2018/10/22/sociedade/noticia/hospital-barreiro-contesta-judicialmente-coima-400-mil-euros-comissao-dados-1848479>
- [6] Regulation (EU) 2016/679 of the European Parliament and of the Council of 27 April 2016 on the protection of natural persons with regard to the processing of personal data and on the free movement of such data, and repealing Directive 95/46/EC (General Data Protection Regulation) (Text with EEA relevance). Brussels, Official Journal of the European Union 119/1 05/04/2016. (EN) pp. 1-88
- [7] Z. Nyikes, Z. Németh, A. Kerti, "The electronic information security aspects of the administration system," 2016 IEEE 11th International Symposium on Applied Computational Intelligence and Informatics (SACI), Timisoara, DOI:10.1109/SACI.2016.7507395, 2016, pp. 327-332
- [8] Zs. Szabó, Cybersecurity issues of pension payments, Anikó Szakál (ed.) IEEE 15th International Symposium on Intelligent Systems and Informatics: SISY 2017. Szabadka, Szerbia, 14-16/09/2017, New York: IEEE, 2017. pp. 289-292
- [9] Á. Csiszárík - Kocsir, J. Varga, Crisis - Project - Risk: According to the Opinions of Hungarian SMES', Project Management Development - Practice and Perspectives: Sixth International Scientific Conference on Project Management in the Baltic Countries.2017. pp. 60-70
- [10] P. Michelberger, Cs. Lábodi, After Information Security – Before a Paradigm Change: A complex Enterprise Security Model, *Acta Polytechnica Hungarica* 9:(4), 2012, pp. 101-116
- [11] D. Csubák, K. Szücs, P. Vörös, A. Kiss, Big Data Testbed for Network Attack Detection, *Acta Polytechnica Hungarica* Volume 13 Issue Number 2 2016. DOI: 10.12700/APH.13.2.2016.2.3. pp. 47-57
- [12] Zs. Szabó, Options of micro-simulation in the modelling of the pension system and the intelligent IT security system, Computational Intelligence and Informatics (CINTI), 2016 IEEE 17th International Symposium on

- Óbudai University 17-19. Nov. 2016, Conference book, DOI: 10.1109/CINTI.2016.7846421. 2017, pp. 295 -298
- [13] Act LX of 2013 on the Safety of Electronic Information Systems of Public and Local Government Offices (Ibtv.). Hungarian Bulletin No 68 of 2013, pp. 50241-50255
- [14] Z. Rajnai, B. Puskas, Requirements of the Installation of the Critical Informational Infrastructure and its Management, Interdisciplinary Description of Complex Systems 13: (1) pp. 48-56
- [15] Zs. Szabó, Cybersecurity issues in industrial control systems, Anikó Szakál (ed.) IEEE 16th International Symposium on Intelligent Systems and Informatics: SISY 2018. Szabadka, Szerbia, 13-15/09/2018, Budapest: IEEE Hungary Section, 2018. pp. 231-234
- [16] P. Simon, Information management theory and practice in health care, Semmelweis University 2014, Last accessed November 2018. [Online]. Available:
https://www.tankonyvtar.hu/hu/tartalom/tamop412A/2011_0015_informaciokezeles_elmelet/html/block-11714-page-2.html